

**Investigating the intermittency route of chaos to order
transition in laminar and turbulent thermoacoustic
systems**

A Project Report

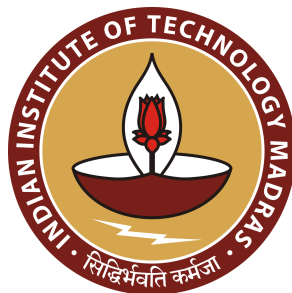
submitted by

SHRUTI TANDON

*in partial fulfilment of the requirements
for the award of the*

DUAL DEGREE

(Bachelor of Technology and Master of Technology)



**DEPARTMENT OF AEROSPACE ENGINEERING
INDIAN INSTITUTE OF TECHNOLOGY MADRAS**

JUNE 2021

CERTIFICATE

This is to certify that the project report titled **INVESTIGATING THE INTERMITTENCY ROUTE OF CHAOS TO ORDER TRANSITION IN LAMINAR AND TURBULENT THERMOACOUSTIC SYSTEMS**, submitted by **Shruti Tandon**, to the Indian Institute of Technology Madras, for the award of the degree of **Bachelor of Technology and Master of Technology**, is a bona fide record of the research work done by her under our supervision. The contents of this project report, in full or in parts, have not been submitted to any other Institute or University for the award of any degree or diploma.

Place: Chennai

Date: June 30, 2021

Prof. R. I. Sujith

Research Guide

D Srinivasan Chair Professor

Dept. of Aerospace Engineering

IIT Madras, 600 036

ACKNOWLEDGEMENTS

My thesis is not my work alone, it is the manifestation of the guidance, love and support that I have received from several people.

I would like to express my faith and regards towards the great God for paving my path into research.

I wish to extend my heartfelt gratitude to my guide Prof. R. I. Sujith for supporting and guiding me in this research work. He is not only my mentor, but also my true inspiration. His perseverance and hard work fills me with enthusiasm and motivates me to push my boundaries. Prof. Sujith has a special power to pump motivation and enthusiasm into his students. Under his supervision I have indeed learnt several nuances of the subject (thermoacoustic instability), but more importantly I have learnt how to learn and how to approach a subject. Through our talks during short walks or while cycling from lab to Gajendra Circle, I have also gained some deep spiritual insight to life and its mysterious ways. I am very grateful to Prof. Sujith for placing his belief in me and nurturing me as a whole. I aspire to instill in myself the kind of dedication with which Prof. Sujith drives himself and his whole research group.

I would like to express my regards to my professors from the Department of Aerospace Engineering, Prof. Bhaskar, Prof. Luoyi Tao, Prof. H. S. N. Murthy, Prof. M. Ramakrishna, Prof. Sameen, Prof. Sunetra Sarkar, Prof. Rajesh, Prof. Manikandan Mathur, Prof. Santanu Ghosh, Prof. Amit Kumar, Prof. Nagabhushana Rao, Prof. Sriram, and my faculty advisor Prof. Senthil Murugan. I would also like to express my gratitude to Prof. Suresh Govindarajan, Prof. Arul Lakshminarayan, Prof. Pattabiraman and Prof. Manoj Gopalakrishnan from the Department of Physics. Their in and out of class support, guidance and motivation has fostered me in the past five years.

For me, an important source of learning and inspiration came from my seniors and colleagues. I would like to thank Dr. Samadhan Pawar, Dr. Abin Krishnan and Dr.

Vishnu Unni for their valuable insights and for help with paper writing. Also, I express my gratitude to Praveen, Induja, Amitesh, Manikandan, Vedasri, Alan and Premraj and appreciate the time and efforts they spent in our healthy discussions that helped me with this research. I would like to thank Subham Banerjee and Dr. Samadhan Pawar for their help with experiments in the Rijke tube set-up. Further, I acknowledge Dr. Vishnu Unni and Dr. Samadhan Pawar for providing the experimental data from bluff-body and swirl stabilized turbulent combustors, and low-turbulence spray combustor.

I acknowledge the financial support for this project from the Office of Naval Research Global and Contract Monitor Dr. R. Kolar (Grant No. N62909-14-1-N299). I am also obliged to the Department of Science and Technology, Government of India for providing financial support to Prof. R. I. Sujith under grant Nos. DST/SF/1(EC)/2006 (Swarnajayanti Fellowship) and JCB/2018/000034/SSC (JC Bose Fellowship).

Finally, most heartfelt regards to my dear Nanaji Naniji (grandparents), my beloved parents and my affectionate brother. I draw my faith and will power from their love, and their encouragement forms the backbone of my life. Special thanks to dearest Gaurav for bringing hope and support into my life.

ABSTRACT

KEYWORDS: Thermoacoustic Instability; Intermittency; Phenomenological model; Bursts; Amplitude-modulated bursting; Complex networks; Cycle networks; Phase space topology; Phase transition; Bose-Einstein condensation; Chaos to order.

Combustion engines in rockets or gas turbine engines exhibit complex dynamics and are susceptible to a catastrophic phenomenon, namely thermoacoustic instability. The transition from stable (combustion noise) to unstable state (thermoacoustic instability) of operation in combustors was conventionally viewed as a transition from a stable fixed point to stable limit cycle oscillations. However, recent studies have shown that combustion noise is essentially high-dimensional chaos. With increase in the Reynolds number, order emerges amidst chaos. First, the dynamics exhibits intermittent bursts of periodicity and then subsequently transitions to high amplitude periodic oscillations. These high amplitude periodic oscillations are self-sustained due to the positive feedback established between the heat release and acoustic fluctuations in the combustor, and are referred to as thermoacoustic instability. Such high-amplitude periodic oscillations can be ruinous and may disrupt the functioning of a combustor, can cause structural damage to the internal mechanism of the combustor, or even cause the guidance system of rockets to malfunction leading to mission failures. It is therefore essential to identify the onset of such oscillatory dynamics, and characterize the emergence of order from chaos in thermoacoustic systems.

In this study, we endeavour to develop a fundamental understanding of the phenomena that lead to the occurrence of intermittency prior to the onset of orderly dynamics in combustors. The state of intermittency is characterized by the occurrence of bursts of high-amplitude periodic oscillations (active state) amidst epochs of low-amplitude aperiodic fluctuations (rest state). Recent studies have shown that the transition from

combustion noise to thermoacoustic instability via the route of intermittency occurs in several disparate thermoacoustic systems such as laminar multiple flame combustor, low-turbulence spray combustor, turbulent bluff body as well as swirl stabilized combustors. While the underlying physical mechanisms of these systems is distinct, the transition from chaos to order via the route of intermittency is a common feature. In this thesis, we study the complex dynamics observed in both laminar as well as turbulent combustors.

Several model-based studies conjectured that bursting arises due to the underlying turbulence in the system. However, such intermittent bursts occur even in laminar and low-turbulence combustors, which cannot be explained by models based on turbulence. We assert that bursting in such combustors may arise due to the existence of subsystems with varying timescales of oscillations; thus, forming slow-fast systems. Experiments were performed on a horizontal Rijke tube and the effect of slow-fast oscillations was studied by externally introducing low-frequency sinusoidal modulations in the control parameter. Further, we develop a phenomenological model for the interaction between different subsystems of a thermoacoustic system by either coupling the slow and fast subsystems, or by introducing noise in the absence of slow oscillations of the control parameter. We show that bursting in laminar and low-turbulence systems occurs predominantly due to the interdependence between slow and fast oscillations; while bursting in high-turbulence systems is predominantly influenced by the underlying turbulence.

The occurrence of intermittency during the transition from chaos to order delineates the spontaneous emergence of order amidst chaos. It is, thus, very essential to characterize the intermittency route of chaos to order transitions in distinct feedback-driven systems. While tools from dynamical systems and complex networks have been utilized to study such transitions, the understanding of emergence of order from chaos in turbulent systems is far from complete. We attempt to fill the gap by studying the transformations in the topology of the phase space using complex networks derived from the phase space cycles. To that end, we study the transition of dynamics in two distinct turbulent thermoacoustic systems, namely bluff-body and swirl stabilized turbulent combustors. Using unweighted complex networks built from phase space cycles

of the acoustic pressure oscillations, we characterize the topology of the phase space during various dynamical states in these combustors. We propose the use of network centrality measures derived from cycle networks as a novel means to characterize the number and stability of periodic orbits in the phase space. We also study the topological transformations in the phase space during the emergence of order from chaos in the combustors using these network measures.

Finally, we propose that the onset of oscillatory instabilities in turbulent systems is analogous to Bose-Einstein condensation transition observed for Bosons. By defining the phase space cycles as particles and the periodic orbits as energy levels, we show that the onset of oscillatory instabilities is essentially the onset of a condensation transition.

TABLE OF CONTENTS

	Page
ACKNOWLEDGEMENTS	i
ABSTRACT	iii
LIST OF FIGURES	xiii
ABBREVIATIONS	xiv
NOTATION	xv
CHAPTER 1: Introduction	1
1.1 Thermoacoustic systems and thermoacoustic instability	1
1.2 Distinct perspectives to study the transition from stable to unstable operation in thermoacoustic systems	3
1.3 The occurrence of intermittency state en route to thermoacoustic instability in various combustors	6
CHAPTER 2: Experiments in various thermoacoustic systems	10
2.1 Experiments in laminar Rijke tube set-up	10
2.2 Various dynamical states observed during experiments in turbulent combustors	11
CHAPTER 3: Phenomenological model for the occurrence of intermittency in laminar and turbulent systems	14
3.1 Introduction	14
3.2 Rijke tube experiments designed to study the slow-fast hypothesis	19
3.3 Model based on the normal form of subcritical Hopf bifurcation	20
3.3.1 Governing Equations	20
3.4 Results and discussion	24
3.4.1 Bifurcation diagram	24

Table of Contents (continued)		Page
3.4.2	Effect of slow oscillations in the control parameter on the transition to thermoacoustic instability	26
3.4.3	Delayed bifurcation due to slow oscillations across a subcritical Hopf bifurcation	29
3.4.4	Factors effecting the delayed bifurcation	32
3.5	Delayed bifurcation due to slow oscillations across a supercritical Hopf bifurcation	34
3.6	Investigating the interdependence of slow and fast subsystems using model	36
3.6.1	Effect of coupling the slow and fast subsystems	37
3.6.2	Effect of additive and multiplicative noise	39
3.7	Summary	43
CHAPTER 4: Preliminary concepts: Complex networks		45
4.1	History: Complex networks as a tool to analyse real-world systems	45
4.2	Basic definitions	47
4.2.1	Centrality measures	48
CHAPTER 5: The onset of thermoacoustic instability via the route of intermittency as a phase transition similar to Bose-Einstein Condensation.		51
5.1	Introduction	51
5.1.1	Emergence of order from chaos in various turbulent systems	51
5.1.2	A new perspective: Emergence of order from chaos in the phase space as a condensation transition	53
5.1.3	Potential contributions of the new perspective	56
5.2	Converting time series of acoustic pressure to cycle network	58
5.3	Identifying the onset of thermoacoustic instability via network centrality measures	62
5.4	Deriving the phase space topology from the degree distribution of cycle networks	67
5.4.1	2D Degree Distribution	67
5.4.2	Quantifying the peaks in the 2D degree distribution: <i>VND</i>	71
5.5	Analogy with Bose-Einstein Condensation	74

5.6 Summary	78
CHAPTER 6: Conclusions and Scope of the study	80
6.1 Conclusions	80
6.2 Scope for future work	83
APPENDIX A: Appendix for Chapter 3.	85
A.1 Detection of the onset of the active state of burst in the parameter space	85
APPENDIX B: Appendix for Chapter 5.	87
B.1 Variation of centrality measures as a function of \bar{u} for different correlation thresholds	87
B.2 Effect of the range of correlation threshold on the 2D degree distribution	88
REFERENCES	97
LIST OF PUBLICATIONS.	98

LIST OF FIGURES

Figure	Title	Page
1.1	Schematic diagram showing the interaction of various subsystems of a thermoacoustic system.	2
2.1	The schematic of the experimental setup of the horizontal Rijke tube and a cross-section of the Rijke tube duct showing the position of the heater in the system.	11
2.2	Schematic diagram of (a) the experimental set-up of a turbulent combustor, and two types of flame stabilizing mechanisms: (b) a circular bluff-body and (c) a swirler. The figure has been reproduced from the doctoral thesis of Dr. Pawar (Pawar (Indian Institute of Technology Madras, 2018)), with the kind permission of the author.	12
3.1	The time series of the acoustic pressure oscillations during the state of intermittency observed prior to thermoacoustic instability obtained from studies involving different classes of thermoacoustic systems, such as (a, b) a turbulent gas-fired combustor with a bluff-body and a swirl stabilizer (Nair <i>et al.</i> (2014)), respectively, (c) a turbulent gas-fired swirl combustor (Ebi <i>et al.</i> (2018)), (d) a low turbulence laboratory spray combustor (Pawar <i>et al.</i> (2016)), (e) a laminar multiple flame matrix burner (Kasthuri <i>et al.</i> (2019b)), and (f) a Rijke-type laminar flame burner (Weng <i>et al.</i> (2016)). These plots are reproduced with permission from (a, b) <i>J. Fluid Mech.</i> 756, 470-487 (2014), Cambridge University Press, (c) <i>J. Eng. Gas Turb. Power</i> 140, 061504 (2018), ASME, (d) <i>J. Eng. Gas Turb. Power</i> 138, 041505 (2016), ASME, (e) <i>Chaos</i> 29, 043117 (2019), AIP, (f) <i>Combust. Flame</i> 166, 181-191 (2016), Elsevier.	16
3.2	The bifurcation diagram of the acoustic pressure fluctuations (p') with respect to (a) K_h , the heater power (W) or heater voltage (V) from experiments in the Rijke tube and (b) non-dimensional parameter c_1 from the standard model, when $\sigma_a = 0.0001$, $\sigma_m = 0$ in Eq. (3.9), $c_3 = c_5 = 1$ in equation (7). Points F and H represent the fold and the Hopf point, respectively, while a , b , c and d are reference points.	25

3.3	Comparison of the time series of acoustic pressure (p') obtained from experiments (I) and from the model (II) for slow-scale oscillations in the control parameter about a mean value. For experiments, the mean value of K_h is varied from (a) to (d) as 1.8 V (306 W), 2.1 V (365 W), 2.2 V (428 W), and 2.56 V (568 W), respectively, where the amplitude and frequency of oscillations of K_h are fixed at 0.5 V and 0.05 Hz throughout. In the model, the parameter c_1 oscillates with amplitude $B = 0.4$ and frequency $f = 0.17$ Hz when its mean value is increased from (e) to (h) as $A = 0.2, 0.6, 0.75$ and 0.95 , respectively. The noise intensity in the model is $\sigma_a = 0.0001$	27
3.4	(a) Transformed phase portrait of acoustic pressure oscillations (p') obtained from the standard model superposed on the bifurcation diagram of acoustic pressure (p'_{max}) obtained from quasi-static variation of c_1 . (b) The overlapped time series of the control parameter oscillations (c_1) and the acoustic pressure oscillations (p') during a state of bursting in the system, obtained from the model. Here, p'_{maxR} and p'_{maxF} refer to the reverse and the forward paths of quasi-static variation of c_1 . The point demarcated as A represents the mean value of c_1	29
3.5	(I) Transformed phase diagrams and (II) the corresponding overlapped time series of the control parameter oscillations and the acoustic pressure oscillations obtained from the model, for the cases shown in (a), (b) with different mean values A_I and A_{II} while B and f are fixed, (c), (d) with different frequencies f_I and f_{II} , while A and B are fixed, and (e), (f) with different amplitudes B_I and B_{II} while A and f are fixed. The point demarcated as A represents the mean value of c_1	33
3.6	(a) Transformed phase portrait of acoustic pressure oscillations obtained from the standard model for supercritical bifurcation superposed on the bifurcation diagram of acoustic pressure (p'_{max}) obtained from quasi-static variation of c_1 . (b) The overlapped time series of the control parameter oscillations (c_1) and the acoustic pressure oscillations (p') during a state of bursting in the system.	35
3.7	Schematic representation of the simultaneous evolution of the acoustic pressure (p' , in blue) and the control parameter (c_1 , in red) oscillations obtained through the modified model. The dotted line represents the chosen threshold of $p'_{th} = 25$ Pa (which is around 15% of the maximum amplitude); if $p'_{env} < p'_{th}$, frequency of the control parameter (c_1) oscillation is $f = 0.17$ Hz; if $p'_{env} > p'_{th}$, then $f = 15 \times 0.17$ Hz. The frequency of the acoustic pressure oscillations is 170 Hz. The noise intensities are $\sigma_a = 0.0001$, $\sigma_m = 0$	38

3.8	Time series of the acoustic pressure oscillations and corresponding amplitude spectrum observed during the state of intermittency prior to thermoacoustic instability in (a) spray combustor (Pawar <i>et al.</i> (2016)) ($Re \approx 2.6 \times 10^3$) and (b) turbulent combustor (Nair <i>et al.</i> (2014)) ($Re \approx 1.4 \times 10^4$). The insets show small epochs of periodic oscillations during bursts where the inset of (a) shows regular amplitude modulations in the envelope and the inset of (b) highlights irregularly modulated envelope of the acoustic pressure oscillations	40
3.9	(a) The intermittency signal obtained from the modified model when the pressure threshold is set at $p'_{th} = 25$ Pa. If $p'_{env} < p'_{th}$, frequency of oscillating control parameter c_1 is $f = 0.17$ Hz, while if $p'_{env} > p'_{th}$, then $f = 8.5$ Hz with noise strengths $\sigma_a = 0.1$ and $\sigma_m = 0$. (b) The intermittency signal obtained from introducing additive and multiplicative noise of strengths $\sigma_a = 0.05$ and $\sigma_m = 0.2$, respectively, in the model. The amplitude spectrums corresponding to periodic oscillations of each time series shown in the insets are plotted in the right column.	42
5.1	Schematic diagram showing a sample realization of the trajectory around two unstable periodic orbits (UPOs) in the phase space.	54
5.2	The time series of acoustic pressure fluctuations (I), the corresponding normalised phase space (II) and cycle network (III) during distinct dynamical states namely, (a) combustion noise, (b) intermittency, and (c) weakly correlated and (d) strongly correlated limit cycle oscillations during thermoacoustic instability observed in a bluff-body stabilized turbulent combustor. The adjacent colorbar indicates the degree of nodes across the various dynamical states. The network is derived by setting $\rho_{th} = 0.92$	59
5.3	The variation in the average (a) closeness centrality ($\langle C_{close} \rangle$), (b) betweenness centrality ($\langle C_{BC} \rangle$) and (c) clustering coefficient ($\langle CC \rangle$) with the variation in the control parameter (\bar{u} and corresponding Re) of the bluff-body stabilized turbulent combustor, for the derived cycle networks with $\rho_{th} = 0.92$. The regions (I), (II) and (III) correspond to the different dynamical states observed that are combustion noise, intermittency and thermoacoustic instability, respectively (Pawar <i>et al.</i> (2017)).	64
5.4	The variation in the average (a) closeness centrality (C_{close}), (b) betweenness centrality (C_{BC}) and (c) clustering coefficient (CC) with the variation in \bar{u} (and corresponding Re) of a swirl-stabilized turbulent combustor for the derived cycle networks with $\rho_{th} = 0.94$. The regions (I), (II) and (III) correspond to the different dynamical states observed that are combustion noise, intermittency and thermoacoustic instability, respectively (Pawar <i>et al.</i> (2019)).	65

5.5	2D degree distribution showing the variation of the degree distribution of cycle networks obtained from the time series of acoustic pressure oscillations with the correlation threshold, during the states of (a) combustion noise, (b) intermittency, (c) weakly correlated and (d) strongly correlated limit cycle oscillations observed in a bluff-body stabilized turbulent combustor. Here, ρ_{th} is varied from 0.55 to 0.99 in steps of 0.001. Bins refer to degrees and count refers to the number of nodes having certain degree.	69
5.6	Variation of VND (variance of the normalized derivative) of the 2D degree distribution with the control parameter (\bar{u} and corresponding Re) for (a) bluff-body and (b) swirl stabilized turbulent combustors. The dynamical states of the combustor are demarcated by I-combustion noise, II-intermittency and III-thermoacoustic instability. Here, ρ_{th} is varied from 0.55 to 0.99 in steps of 0.001.	72
5.7	Distribution of nodes (particles) in energy levels whose energy is defined as $\varepsilon = 1 - k/k_{max}$ (where $k_{max} = N - 1$ and N is the number of nodes in the network), during different dynamical states of operation in a bluff-body stabilized turbulent combustor ($\rho_{th} = 0.92$). The dynamical states shown are combustion noise (blue), intermittency (brown), weakly correlated (green) and strongly correlated (red) limit cycle oscillations (LCO) during thermoacoustic instability.	75
5.8	The variation in the percentage of particles (nodes) which occupy energy levels less than (black) and more than (red) ε_0 with variation in \bar{u} (and corresponding Re) for (a) bluff-body and (b) swirl stabilized combustors, where $\varepsilon_0 = 0.003$ in both cases. The regions (I), (II) and (III) correspond to the different dynamical states observed in these combustors namely combustion noise, intermittency and thermoacoustic instability respectively.	77
A.1	(a) The variation of acoustic pressure oscillations (p') and (b) log of the amplitude envelope of these pressure oscillations (p'_e) as a function of the time-varying control parameter (c_1) during the growth of amplitude of the burst. The values of parameters are: $A = 0.8$, $B = 0.4$, $f = 0.17$ Hz and $\sigma_a = 0.0001$ while $\sigma_m = 0$	86
B.1	The variation in the average (a) closeness centrality ($\langle C_{close} \rangle$), (b) betweenness centrality ($\langle C_{BC} \rangle$) and (c) clustering coefficient ($\langle CC \rangle$) with the variation in the control parameter (\bar{u}) of a bluff-body stabilized turbulent combustor for the derived cycle networks with $\rho_{th} = 0.9$, 0.92, and 0.94. The regions (I), (II) and (III) correspond to the different dynamical states observed that are combustion noise, intermittency and thermoacoustic instability, respectively (Pawar <i>et al.</i> (2017)).	87

B.2	The variation in the average (a) closeness centrality ($\langle C_{close} \rangle$), (b) betweenness centrality ($\langle C_{BC} \rangle$) and (c) clustering coefficient ($\langle CC \rangle$) with the variation in the control parameter (\bar{u}) of a swirl-stabilized turbulent combustor for the derived cycle networks with $\rho_{th} = 0.9, 0.92,$ and 0.94 . The regions (I), (II) and (III) correspond to the different dynamical states observed that are combustion noise, intermittency and thermoacoustic instability, respectively (Pawar <i>et al.</i> (2017)).	88
B.3	The variation of VND with the control parameter for (a) bluff body stabilized and (b) swirl stabilized turbulent combustor for different choices of the range of ρ_{th} . Note that the crimson and the blue graphs overlap.	89

ABBREVIATIONS

SLPM	Standard litres per minute
LCO	Limit Cycle Oscillations
PS	Phase synchronized
GS	Generalized synchronized
UPO	Unstable Periodic Orbits
BEC	Bose-Einstein Condensation

NOTATION

English Symbols

Re	Reynolds number
\bar{u}	Mean flow velocity
D	Characteristic length - burner diameter
p'	Acoustic pressure fluctuations
u'	Acoustic velocity fluctuations
\dot{q}'	Heat release rate fluctuations
\dot{q}'_c	Coherent heat release rate fluctuations
\dot{q}'_{nc}	Non-coherent heat release rate fluctuations
M	Mach number
K_i	Degree of node i
C_{close}	Closeness centrality
C_{BC}	Betweenness centrality
CC	Clustering coefficient
VND	Variance of normalised derivative

Greek Symbols

γ	Ratio of specific heat capacities
η	Non-dimensional acoustic modes
ε	Damping coefficient
ω	Non-dimensional frequency
ξ	Noise term
δ	Delay-value in terms of control parameter
σ_a	Amplitude of additive noise
σ_m	Amplitude of multiplicative noise
ρ_{ij}	Correlation coefficient for correlation between time series i and j
ρ_{th}	Correlation threshold

Operators

$ x $	Absolute value of x
$\langle x \rangle$	Mean value of x
Σ	Summation
Cov	Covariance
var	Variance

CHAPTER 1

Introduction

1.1 Thermoacoustic systems and thermoacoustic instability

Continuous combustion is required in several applications for power generation, such as aero-engines, rocket propulsion and gas turbine engines. The operation and lifetime of combustors developed for such power generation are plagued by the phenomenon of thermoacoustic instability, also called combustion instability (Culick (2006); Sujith *et al.* (2016)). The unsteady combustion that occurs in the confined length of combustors drives the acoustic perturbation modes of the confinement. Moreover, the unsteady acoustic perturbations may disturb the surface of the flame stabilized in the combustor, by either bluff-body or swirler configurations, and lead to perturbations in the rate of heat release. In other systems, such as that involving fuel injection via spray, the heat release rate fluctuates due to the influence of acoustic pressure oscillations on the fuel injection rate. As a result, a positive feedback loop is established between the acoustic field perturbations and the rate of heat released due to combustion. The acoustic pressure waves are amplified due to the positive feedback of energy from heat released due to combustion. It is due to such coupling between the acoustic perturbations and the heat released from combustion that we obtain large amplitude self-sustained tonal sound waves during the occurrence of thermoacoustic instability (Strutt and Rayleigh (1945)).

Figure 1.1 shows a schematic diagram showing the different subsystems of a thermoacoustic system and their possible interactions with each other. The acoustic subsystem comprises perturbations in the acoustic pressure (p') and acoustic velocity (u'). The dynamics of the hydrodynamic subsystem includes vortex formation and impingement, and turbulent fluctuations for high Reynolds number flows. Also, the rate of

heat released by combustion is influenced by several factors such as oscillations in the flame surface, and variations in the fuel injection rate, burning rate and equivalence ratio. Further, the dynamics of each subsystem influences and is influenced by the dynamics of other subsystems. For example, acoustic pressure oscillations will vary the pressure difference between injection pressure and combustor pressure, as a result of which the fuel injection rate varies. Also, the size of fuel droplets, equivalence ratio and burning rate of fuel may vary. Further, vortex shedding occurs in the dump plane of a combustor or at the tip of flame-stabilizing bluff-body (Seshadri *et al.* (2016)). These vortices carry fuel which burns either when a certain vortex strength is reached or on impingement with combustor walls. Thus, the hydrodynamic flow field influences the rate of heat release due to combustion. Turbulent flow field may interact and influence the flame surface fluctuations which in turn control the rate of heat released. Acoustic perturbations also influence the flame surface fluctuations. As a result of such interactions between various subsystems, thermoacoustic systems are characterized by rich spatio-temporal dynamics and pattern formation (George *et al.* (2018)).

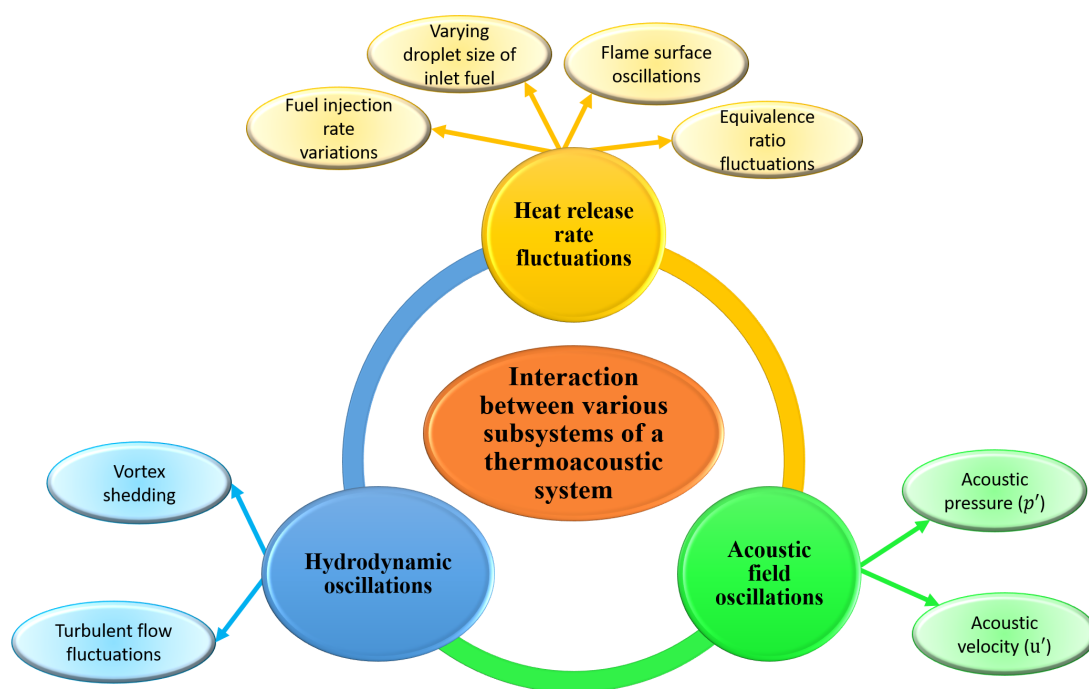


Fig. 1.1: Schematic diagram showing the interaction of various subsystems of a thermoacoustic system.

For low Reynolds number, thermoacoustic systems operate in a stable state in which

the acoustic pressure field is characterized by low-amplitude chaotic fluctuations in turbulent systems or noisy aperiodic fluctuations in laminar systems. The spatial dynamics exhibits incoherent heat release rate patterns and vortex shedding in the flow field (George *et al.* (2018); Unni *et al.* (2018); Krishnan *et al.* (2019)). In order to operate at a point of optimum combustion, we increase the inlet mass flow rate of air. As a result the Reynolds number increases and equivalence ratio decreases. On increasing the inlet mass flow rate, we observe intermittent dynamics in the acoustic pressure signal characterized by bursts of periodic oscillations interspersed by aperiodic (or chaotic) fluctuations (Pawar *et al.* (2016); Nair *et al.* (2014)). Also, in the flow field we observe periodic vortex shedding and spatial coherence in the heat release rate during epochs of periodicity, while incoherent dynamics persists during aperiodic pressure fluctuations (George *et al.* (2018)). On further increasing the inlet mass flow rate, we observe high-amplitude periodic oscillations in the acoustic pressure field characterizing thermoacoustic instability. Moreover, vortex shedding occurs periodically at acoustic frequency (Pawar *et al.* (2017)) and the heat release rate exhibits periodic spatial coherence (Unni *et al.* (2018); Krishnan *et al.* (2019)). Such periodic dynamics observed during the occurrence of thermoacoustic instability is as intriguing as detrimental it is to the system. Identification of dynamical routes that lead to thermoacoustic instability and developing measures for predicting or mitigating such a state has been a field of intense research recently (George *et al.* (2018); Juniper and Sujith (2018); Sujith and Unni (2020a)).

1.2 Distinct perspectives to study the transition from stable to unstable operation in thermoacoustic systems

Traditionally, the onset of thermoacoustic instability has been viewed as a sudden transition from stable operation to unstable operation of the system. In the purview of dynamical systems theory, this transition is referred to as Hopf bifurcation (Lieuwen (2002); Ananthkrishnan *et al.* (2005)) and the state of thermoacoustic instability is con-

sidered to be a stable limit cycle (Culick (1994)). However, this approach regards the stable state of operation as a fixed point rather than chaotic dynamics. Recently, the focus of the scientific community has shifted to characterizing the transition from chaos to order using bifurcation analysis motivated through the perspective of dynamical systems and complex systems theory (Sujith and Unni (2020b,c)). Nair *et al.* (2013) using Kaplan-Glass test and Tony *et al.* (2015) using a host of measures such as the Hurst exponent and surrogate analysis have shown that the state of combustion noise in a turbulent combustor is essentially high-dimensional deterministic chaos. Also, Nair and Sujith (2014) have discussed how the multifractal characteristics of the acoustic pressure fluctuations obtained during the stable state of operation differ significantly from signals that are obtained via stochastic random processes. Thus, as noted by Nair and Sujith (2014), the term ‘combustion noise’ used to describe chaotic dynamics during the stable state of operation in a thermoacoustic system is a misnomer and requires careful consideration.

Moreover, Nair *et al.* (2014) showed that the transition from stable operation (combustion noise) to unstable operation (thermoacoustic instability) in turbulent combustors is interspersed by a dynamical state called intermittency. Intermittency prior to thermoacoustic instability is a state consisting of bursts of high amplitude periodic oscillations interspersed amongst epochs of low amplitude aperiodic oscillations. In the intermittency signals, the epochs of periodicity increase as the system dynamics approaches the point of onset of thermoacoustic instability. Subsequently, several studies have reported the presence of intermittency prior to thermoacoustic instability in different combustors (Gotoda *et al.* (2014); Unni and Sujith (2017); Domen *et al.* (2015); Delage *et al.* (2017); Kheirkhah *et al.* (2017); Ebi *et al.* (2018)).

The transition of the system dynamics from chaos to order in turbulent combustors has also been characterized using the synchronization framework. Pawar *et al.* (2017, 2019) explain the various dynamical states observed in turbulent combustors by treating the acoustic pressure fluctuations p' and the heat release rate fluctuations \dot{q}' as oscillators. They model the chaotic dynamics observed during the state of combustion noise by assuming that p' and \dot{q}' are chaotic oscillators which are not synchronized. Further,

during the state of intermittency, Pawar *et al.* (2017) showed that p' and q' are synchronized during the intermittent epochs of periodic oscillations but remain asynchronous during the chaotic fluctuations in p' . Finally, Pawar *et al.* (2017) identified two distinct states during the occurrence of thermoacoustic instability, (a) phase synchronized limit cycle oscillations (PS state) during which p' and q' are periodic oscillators that are phase synchronized, and (b) generalized synchronized limit cycle oscillations (GS state) during which p' and q' are periodic oscillators that are in a functional relationship.

Another interesting and recent perspective views thermoacoustic phenomena as a complex system with interacting subsystems. Thermoacoustic systems exhibit various dynamical states that are manifestations of interaction between different subsystems such as oscillating flame and heat release due to combustion, hydrodynamic fluctuations and acoustic perturbations (Fig. 1.1). Complex networks provide a natural framework to study such interactions between components of a system and have been used effectively to characterize the complex dynamics in thermoacoustic systems.

Complex networks can be derived from the time series of system variables, such as acoustic pressure, obtained from experiments in several different ways (Gao *et al.* (2017)). Using visibility algorithm on the time series of acoustic pressure oscillations in a combustor, Murugesan and Sujith (2015) revealed that the chaotic dynamics observed during stable operation corresponds to a scale-free complex network. However, as the system transitions to the state of limit cycle oscillations, the structure of these complex networks becomes more ordered and its scale-free nature is lost. Further, Gotoda *et al.* (2017) have used constrained visibility graphs to characterize the different dynamical states and to predict the onset of blowout states in thermoacoustic systems. In a recent work, Godavarthi *et al.* (2017) studied the transition of dynamics in a thermoacoustic system as the variation in topology of ϵ -recurrence networks constructed from the acoustic pressure fluctuations in a turbulent combustor. Also, Kasthuri *et al.* (2019a) have identified the various dynamical states in a self-excited model liquid rocket-engine combustor using time series analysis on experimental data. They have proposed robust measures based on recurrence quantification analysis and multifractal theory to diagnose the onset of thermoacoustic instability in the system.

Further, Okuno *et al.* (2015) have used weighted complex networks constructed from phase space cycles to characterize the pseudo-periodicity observed during the occurrence of thermoacoustic instability. We note that a pseudo-periodic signal is defined as a combination of a periodic function along with a set of parameters that define the deviations of the process from true periodicity (Sethares (2001); Wong and Sethares (2004)), such as variations in the amplitude of periodic signal. Moreover, Kobayashi *et al.* (2019) have used complex networks approach to predict the occurrence of thermoacoustic instability in combustors by studying the transition patterns in ordinal partition transition networks using machine learning. Also, Hachijo *et al.* (2020) have used weighted cycle-networks to study the occurrence of oscillatory instabilities and identify the formation of noisy limit cycle oscillations during cascade flutter in a model low-pressure turbine for aircraft engines.

1.3 The occurrence of intermittency state en route to thermoacoustic instability in various combustors

Different type of combustors involve different types of underlying physical phenomena. However, all of these systems exhibit similar dynamical states and the transition between these states. We observe that, thermoacoustic systems operate in a stable state characterized by very low amplitude fluctuations in the acoustic pressure signal. As the control parameter (such as the Reynolds number) of the system is altered, we see that the system dynamics transitions to a state of unstable operation characterized by very high amplitude periodic oscillations in the acoustic field. This transition from stable operation, called combustion noise to a state of unstable operation, called thermoacoustic instability, occurs through the route of intermittency. The occurrence of intermittency has been reported in several types of combustors and is of great interest to the thermoacoustic community (Nair *et al.* (2014); Domen *et al.* (2015); Noiray and Schuermans (2013); Pawar *et al.* (2016)). Studying the state of intermittency prior to the onset of thermoacoustic instability allows us to identify and predict, and possibly mitigate, the occurrence of thermoacoustic instability. The objective of this study is to develop an

understanding of the occurrence of intermittency state and the transition route from combustion noise (chaos) to thermoacoustic instability (order) in laminar and turbulent combustors.

In a laminar thermoacoustic system consisting of a matrix burner, Kasthuri *et al.* (2019b) showed the presence of bursting oscillations (switching of oscillations between bursts of periodic oscillations and a nearly quiescent state) and mixed-mode oscillations (characterized by periodic oscillations switching between two different amplitudes) prior to the onset of limit cycle oscillations. In addition, Weng *et al.* (2016) showed the existence of self-sustained beating dynamics arising due to fluctuations in the flame location in a Rijke-type burner with a laminar premixed flame. Therefore, while intermittent bursts are observed in both laminar and turbulent combustors, the characteristic features of such bursts are different in these combustors due to the difference in the preceding stable state. In laminar combustors the intermittent bursts consist of periodic oscillations amidst epochs of quiescence, and hence referred to as ‘bursting oscillations’ (Kasthuri *et al.* (2019b)). However, in turbulent combustors, the intermittent oscillations consist of bursts of periodic oscillations interspersed by epochs of low-amplitude chaotic fluctuations; thus, referred to as ‘intermittency’ (Nair *et al.* (2014)) and not bursting oscillations.

While intermittency is observed in a wide range of combustors, the features of the intermittency state vary remarkably across the various systems. In laminar (Kasthuri *et al.* (2019b)) and low-turbulence combustors (Pawar *et al.* (2016)), we obtain distinct high amplitude periodic oscillations interspersed by almost quiescent state or aperiodic fluctuations of negligible amplitude. The bursts of periodic oscillations delineate amplitude modulation (Boudy *et al.* (2013); Pawar *et al.* (2016)) known as amplitude modulated bursting. On the other hand, in turbulent combustors, the bursts occurrence of intermittency prior to the onset of thermoacoustic instability is characterized by epochs of periodic oscillations interspersed by epochs of chaotic fluctuations. These bursts of periodicity are not necessarily amplitude modulated.

Several attempts have been made to characterize the state of intermittency in these combustors (Pawar *et al.* (2016); Seshadri *et al.* (2016); Noiray (2017); Lieuwen and

Banaszuk (2005)). However, previous studies have regarded turbulence and background noise as the cause of such bursting behavior observed during intermittency state. As a result, these models cannot explain the occurrence of the state of intermittency in laminar and low-turbulence combustors. In Chapter 3, we propose that intermittency occurs due to interplay between slow and fast timescales associated with various subsystems. We discuss synthetic experiments conducted to understand the dynamics resulting from control parameter modulations in a Rijke tube set up. Further, we develop a phenomenological model to explain the occurrence of bursting during the intermittency state observed en route to thermoacoustic instability in laminar and low-turbulence combustors. We use physical insight and base our model on the premise that the dynamics of a thermoacoustic system is influenced by the interaction of various subsystems, as discussed in Sec. 1.1 (Fig. 1.1). Our model introduces interactions between various subsystems and successfully replicates amplitude modulated bursting as observed in the experiments in practical low-turbulence combustors.

Also, as discussed earlier, complex systems approach has been used to identify the onset of thermoacoustic instability in various combustors. Using recurrence networks (Godavarthi *et al.* (2018, 2017)), visibility networks (Murugesan and Sujith (2015)) various information has been extracted about the onset of thermoacoustic instability. However, the understanding of the transition from chaos to order in turbulent combustors is far from complete. We analyse such a transition using complex networks constructed from phase space cycles, called cycle networks. Using network centrality measures derived from cycle networks we show how the topology of the phase space changes as the dynamics of the combustor transitions from chaos to order. We not only identify the onset of thermoacoustic instability but also identify the occurrence of the state of intermittency prior to the occurrence of thermoacoustic instability. In Chapter 5 we thus provide novel insight to the physical topology of the phase space during various dynamical states and also propose new early warning indicators for these states. Finally, we compare the transition from chaos to order in turbulent systems with the occurrence of Bose-Einstein condensation and show that these two are similar processes.

In Chapter 3 we discuss the Rijke-tube experiments and our phenomenological

model to explain the occurrence of intermittency en route to thermoacoustic instability. Further, we provide a brief overview of complex networks and basic definitions of measures derived from networks in Chapter 4. In 5, we discuss the transition from chaos to order in turbulent thermoacoustic systems. We conclude and summarize the future scope of our study in Chapter 6.

CHAPTER 2

Experiments in various thermoacoustic systems

2.1 Experiments in laminar Rijke tube set-up

The experimental setup of a horizontal Rijke tube [Fig. 2.1] consists of an aluminium duct that is 100 cm long with a square cross-section of $9.3 \times 9.3 \text{ cm}^2$. A decoupler is attached to the inlet of the duct. The decoupler eliminates the fluctuations of the incoming flow and maintains ambient pressure conditions at the attached side of the duct. The Rijke tube houses a stainless-steel wire gauge (henceforth, referred to as the heater), which is used as a concentrated heat source in the system. The heater is connected to a DC power supply (TDK-Lambda, GEN 8-400, 0-8 V, 0-400A) through two copper rods. The DC power supply is used to control the supplied voltage to the heater, which thus controls the amount of power supplied to the system. The heater voltage (i.e., the control parameter) is varied in a quasi-static manner such that the system dynamics transitions from the steady state to thermoacoustic instability (i.e., limit cycle oscillations) via a subcritical Hopf bifurcation. The airflow rate is maintained constant at $100 \pm 0.52 \text{ SLPM}$ (standard litres per minute), using an electronic mass flow controller (Alicat Scientific). The corresponding Reynolds number of the air flow in the Rijke tube is 1154 ± 6 .

The unsteady acoustic pressure oscillations generated in the Rijke tube are recorded using a pressure transducer (PCB103B02) which has an uncertainty of $\pm 0.2 \text{ Pa}$. The transducer is located at a distance of 31.5 cm from the inlet of the Rijke tube. The sampling frequency was fixed at 10 kHz. The acoustic pressure data were collected using a 16-bit data acquisition system DAQ (NI-USB 6343). To ensure repeatability of the experimental results, environmental factors such as temperature and relative humidity were maintained at $23 \pm 3^\circ\text{C}$ and $60 \pm 5\%$, respectively. The acoustic decay rate of the setup under cold flow conditions was always recorded to be between 12 ± 0.5

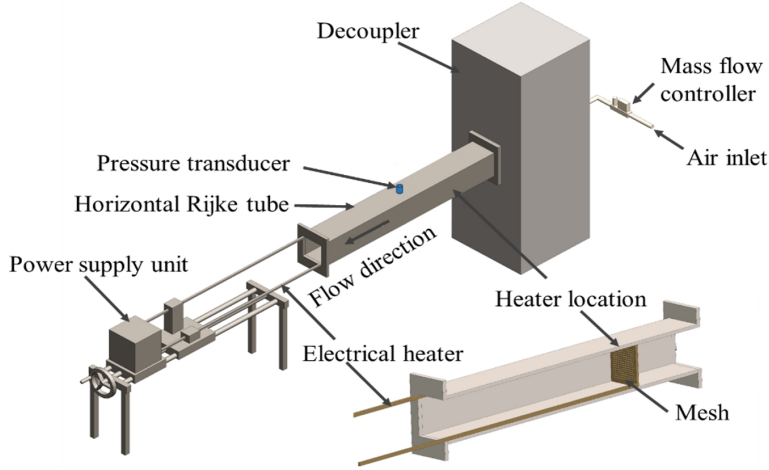


Fig. 2.1: The schematic of the experimental setup of the horizontal Rijke tube and a cross-section of the Rijke tube duct showing the position of the heater in the system.

s^{-1} . The acoustic damping is maintained within bounds to ensure repeatability of the experiments.

2.2 Various dynamical states observed during experiments in turbulent combustors

To study the emergence of order from chaos we consider the experiments performed in swirl-stabilized and bluff-body stabilized turbulent combustors. Figure 2.2 shows a schematic of a turbulent combustor and the two types of flame stabilizing mechanisms used, namely a bluff-body and a swirler. The dynamics of these combustors is studied as the control parameter, i.e. the mean velocity of the flow (\bar{u}) is varied. The Reynolds number is obtained around the location of the burner as $Re = \bar{u}D/\nu$, where ν is the kinematic viscosity of the fuel-air mixture at experimental conditions and D is the burner diameter. The fuel flow rate in the combustor is maintained at 25 SLPM (standard liter per minute), while the air flow rate is varied from a value of 400 SLPM to 940 SLPM. In turn, the mean flow velocity varies from 9.2 m/s to 18.1 m/s. Correspondingly, Re varies from 1.09×10^5 to 2.12×10^5 with uncertainties ranging from $\pm 1.97 \times 10^3$ to $\pm 2.71 \times 10^3$. Also, the equivalence ratio of the air-fuel mixture varies from 0.95 ± 0.02

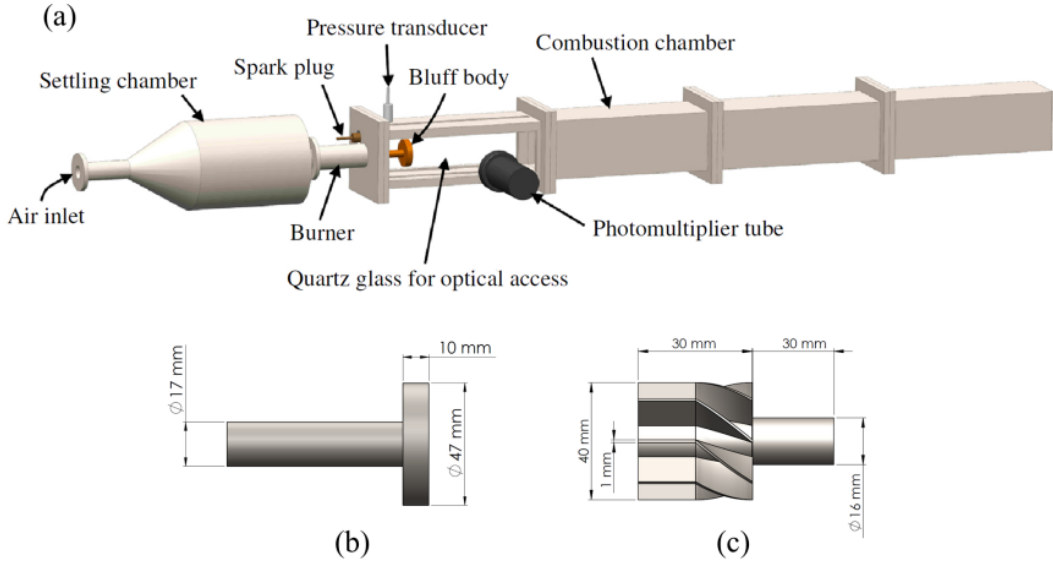


Fig. 2.2: Schematic diagram of (a) the experimental set-up of a turbulent combustor, and two types of flame stabilizing mechanisms: (b) a circular bluff-body and (c) a swirler. The figure has been reproduced from the doctoral thesis of Dr. Pawar (Pawar (Indian Institute of Technology Madras, 2018)), with the kind permission of the author.

to 0.46 ± 0.01 . The acoustic pressure oscillations are recorded using a piezoelectric transducer (PCB Piezotronics PCB103B02) with an uncertainty of ± 0.15 Pa. The signals from the transducer are recorded at a sampling rate of 10 kHz for 3 s. Further details of the experimental setup can be referred in Nair *et al.* (2014) and Pawar *et al.* (2017).

Similarly, we consider the dynamics for a swirl-stabilized turbulent combustor where the fuel flow rate is maintained at 21 SLPM, while the air flow rate is varied from a value of 330 SLPM to 700 SLPM. Correspondingly the mean flow velocity varies from 7.6 m/s to 15 m/s, while Re varies in the range of 9.04×10^4 to 1.75×10^5 with an uncertainty in the range of 1.81×10^3 to 2.42×10^3 . Further, this leads to the variation in the equivalence ratio of the air-fuel mixture from 1 ± 0.02 to 0.47 ± 0.01 . The acoustic pressure fluctuations are recorded at a sampling rate of 10 kHz for 3 s, using a piezoelectric transducer (PCB Piezotronics PCB103B02) having an uncertainty of ± 0.15 Pa. A detailed description of the experimental set-up can be found in Nair *et al.* (2014) and Pawar *et al.* (2019).

The resulting dynamics for the bluff-body and swirl stabilized combustors have been reported earlier by Nair *et al.* (2014) and recently investigated through the framework of synchronization by Pawar *et al.* (2017, 2019). Nair *et al.* (2014) have discussed the transition of the dynamics from a state of stable operation to thermoacoustic instability via the route of intermittency in both the turbulent combustors. Firstly, at low values of the mean flow velocity (\bar{u}), the acoustic pressure dynamics of the turbulent combustors exhibit low-amplitude chaotic fluctuations, referred to as combustion noise. With increase in the control parameter of the system (\bar{u}), the acoustic pressure delineates intermittent bursts of periodic oscillations interspersed by aperiodic fluctuations. On further increase in \bar{u} , the combustor dynamics exhibit self-sustained high-amplitude periodic oscillations, which is the state of thermoacoustic instability.

Using the synchronization framework, Pawar *et al.* (2017, 2019) have further identified two distinct states during the occurrence of thermoacoustic instability, namely the PS and the GS states (discussed in Sec. 5.1), in the bluff-body (Pawar *et al.* (2017)) and the swirl (Pawar *et al.* (2019)) stabilized turbulent combustors. We note that during the occurrence of the PS state in the bluff-body stabilized combustor, the p' signal exhibits high-amplitude periodic oscillations with distinct amplitude modulations that may be a signature of pseudo-periodicity. Whereas, the high-amplitude periodic oscillations in p' obtained during the occurrence of the GS state in the bluff-body stabilized combustor delineates almost constant amplitude. On the other hand, the acoustic pressure signal during the PS state obtained from experiments in the swirl-stabilized combustor delineates small amplitude modulations for only a short range of values of the control parameter. Pawar *et al.* (2017) have referred to such amplitude-modulated dynamics during the PS state in the acoustic pressure signal as weakly correlated limit cycle oscillations, while the acoustic pressure dynamics obtained during the GS state is referred to as strongly correlated limit cycle oscillations. Further, Godavarthi *et al.* (2018) have also identified the onset of the state of intermittency, and the PS and GS states observed in the bluff-body stabilized turbulent combustor using recurrence networks, for the same data set as reported by Pawar *et al.* (2017).

CHAPTER 3

Phenomenological model for the occurrence of intermittency in laminar and turbulent systems

3.1 Introduction

Thermoacoustic instability has detrimental effects on the lifetime of a combustor and is a plaguing problem in the gas-turbine and rocket industries. Large amplitude self-sustained oscillations in the acoustic field may arise due to positive feedback between the heat release rate and the pressure oscillations in a combustor, leading to thermoacoustic instability. Recently, studies in many systems have shown that such thermoacoustic oscillations are preceded by a state of intermittency (Chapter 1). In order to predict or mitigate these oscillations, it is essential to characterize the route to thermoacoustic instability and recognize its cause. During intermittency, bursts of high amplitude periodic oscillations occur amidst epochs of low amplitude aperiodic fluctuations. Such dynamical state has been observed across various combustors, but the features of these bursts are different in different combustors. The cause of intermittent bursting is usually attributed to turbulent fluctuations in the underlying flow. However, intermittent bursts are also observed in laminar and low-turbulence combustors, indicating a different physical cause.

There are several subsystems in a thermoacoustic systems such as the acoustics, flame dynamics and hydrodynamics (Fig. 1.1). In this chapter, we conjecture that the existence of the multiple timescales associated with the oscillations in these different subsystems in a thermoacoustic system is responsible for the occurrence of the bursts during intermittency, and the interaction between these oscillations determines the features of the bursts. To that end, we study the effect of multiple timescales on the occurrence of bursts in a prototypical thermoacoustic system, a horizontal Rijke tube.

Furthermore, we present a phenomenological model to explain the cause of bursting in laminar and low-turbulence combustors through the framework of slow-fast systems. We also investigate the effect of the interaction between various subsystems on the characteristics of bursts observed during intermittency.

In Chapter 1, we discussed various experimental studies that have highlighted the occurrence of intermittency en route to thermoacoustic instability in laminar and turbulent combustors. Recently, several attempts have been made to explain the transition from a state of stable operation to thermoacoustic instability via intermittency in various combustors. Using the framework of synchronization theory, Pawar *et al.* (2017) studied the coupling between the acoustic pressure and the heat release rate fields and showed that these fields undergo intermittent phase synchronization during the state of intermittency in thermoacoustic systems. Further, most studies attribute the occurrence of bursting during intermittency to the effects of the underlying turbulent fluctuations, which are modelled either as stochastic forcing terms in the heat release rate (Noiray (2017)) or stochasticity in velocities of the vortices that convect in a turbulent combustion chamber (Nair and Sujith (2015)). On the other hand, a deterministic approach was presented by Seshadri *et al.* (2016) to explain the cause of intermittency, which was based on the feedback between the acoustic waves generated due to the localized heat release and the vortex shedding in the system. Although some understanding has been developed on the occurrence of intermittency in turbulent combustors, the aforementioned studies could not explain the causes and characteristics of bursts in laminar and low-turbulence combustors.

The kind of bursting behaviour observed during intermittency prior to thermoacoustic instability in various combustors is remarkably different. Figure 3.1 shows the time series of such intermittent oscillations reported in some of the recent studies involving different type of combustors with varying levels of turbulence. For combustors having a high turbulence intensity [Figs. 3.1(a-c)] in the underlying flow field, the intermittent bursts are almost continuous in time with no distinct transition between epochs of periodic and aperiodic fluctuations. On the other hand, the intermittent oscillations observed in low-turbulence (Pawar *et al.* (2016)) [Fig. 3.1(d)] and laminar (Kasthuri *et al.*

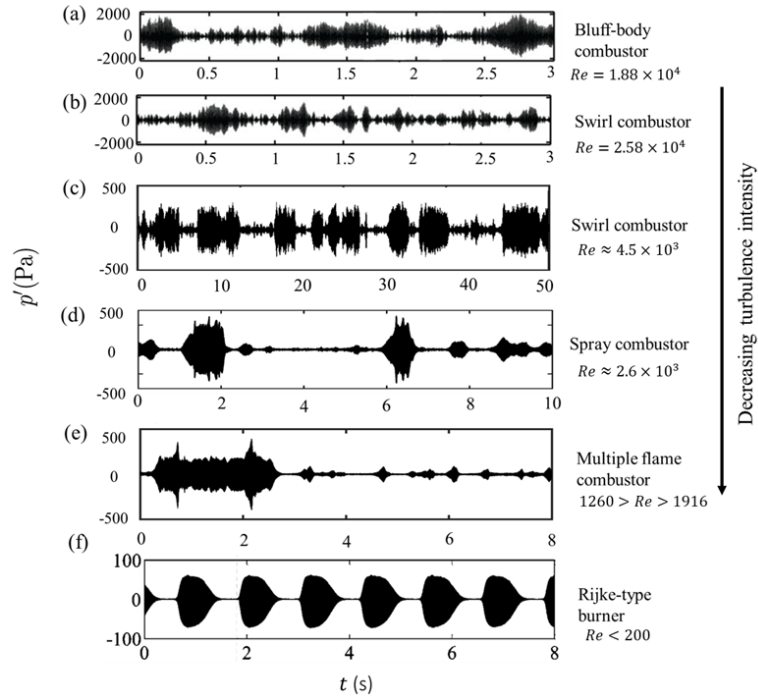


Fig. 3.1: The time series of the acoustic pressure oscillations during the state of intermittency observed prior to thermoacoustic instability obtained from studies involving different classes of thermoacoustic systems, such as (a, b) a turbulent gas-fired combustor with a bluff-body and a swirl stabilizer (Nair *et al.* (2014)), respectively, (c) a turbulent gas-fired swirl combustor (Ebi *et al.* (2018)), (d) a low turbulence laboratory spray combustor (Pawar *et al.* (2016)), (e) a laminar multiple flame matrix burner (Kasthuri *et al.* (2019b)), and (f) a Rijke-type laminar flame burner (Weng *et al.* (2016)).

These plots are reproduced with permission from (a, b) *J. Fluid Mech.* 756, 470-487 (2014), Cambridge University Press, (c) *J. Eng. Gas Turb. Power* 140, 061504 (2018), ASME, (d) *J. Eng. Gas Turb. Power* 138, 041505 (2016), ASME, (e) *Chaos* 29, 043117 (2019), AIP, (f) *Combust. Flame* 166, 181-191 (2016), Elsevier.

(2019b)) [Fig. 3.1(e)] combustors shows the occurrence of pronounced bursts of large amplitude as well as small amplitude periodic oscillations amidst very low amplitude (nearly quiescent) aperiodic fluctuations. The intermittent oscillations in these systems are characterized by relatively smooth and regular variation in the amplitude envelope with distinct occurrence of growth and decay pattern for the bursts. Further, [Fig. 3.1(f)] shows self-sustained beating dynamics in a Rijke-type laminar burner (Weng *et al.* (2016)), where the pressure oscillations show a regular transition between bursts of periodic oscillations and epochs of steady state. Clearly, the occurrence of intermittent bursts in the system shown in Fig. 3.1(d-f) is not turbulence-induced and, hence, cannot be explained by earlier models based on turbulence (Seshadri *et al.* (2016); Noiray (2017)). We endeavor to possibly fill this gap and provide a model to explain bursting behaviour observed in low-turbulence combustors through a different approach.

Intermittent bursts may arise as a result of turbulent fluctuations in the flow that affect the heat release rate fluctuations as well as the acoustic fluctuations just prior to the onset of thermoacoustic instability. However, in the absence of high-intensity turbulence in the combustor, such bursting behaviour is prone to arise due to interactions between the oscillations in the flow field, heat release rate, acoustics, etc. which have very distinct timescales. Recent experimental studies have provided insight into the interaction between the hydrodynamic and acoustic subsystems leading to bursting dynamics in thermoacoustic systems. Hong *et al.* (2008) have shown that control parameters such as the equivalence ratio oscillate at a timescale much slower than the acoustic timescale when the system is close to the onset of thermoacoustic instability. In addition, Nair *et al.* (2014) have conjectured that intermittent bursts in turbulent combustors can arise if the acoustic subsystem is modulated by the hydrodynamics over slow timescales. Premchand *et al.* (2019) have shown the presence of two dominant frequencies during the state of intermittency in a bluff body stabilized turbulent combustor. They showed that the low-frequency peak in the amplitude spectrum of velocity fluctuations corresponds to the slow hydrodynamic timescale, while the high-frequency peak in the amplitude spectrum of the pressure fluctuations corresponds to the fast acoustic timescale.

Kasthuri *et al.* (2019b) showed that the temperature close to the burner in a multiple flame combustor fluctuates at a slow timescale. They conjectured that the nonlinear interaction of the slow temperature oscillations and fast acoustic fluctuations gives birth to mixed-mode and bursting oscillations in their system. Further, Weng *et al.* (2016) conjectured that beating occurs in their system due to slow and fast timescales of the flame oscillations, where the slow timescale is around 100 to 1000 times the timescale of acoustic fluctuations induced in the system. Thus, all these studies provide an incentive to study the interaction of slow-fast dynamics in thermoacoustic systems, where the acoustic fluctuations are the fast subsystem while the slow subsystem is formed by the hydrodynamic oscillations or flame fluctuations. The hydrodynamic oscillations may further introduce slow oscillations in several other subsystems such as the heat release rate or the temperature, or in the control parameters such as the local equivalence ratio or the flow Reynolds number.

The occurrence of ‘bursts’ is a widely studied phenomenon across numerous fields such as neuroscience (Izhikevich (2000)), chemical systems (Bi (2010)) and fluid mechanics (Yalin (1992)). Across these numerous fields, bursting phenomena has been studied under the purview of coupling of slow and fast subsystems or multiple timescales associated with the system. Thus, bursting dynamics in thermoacoustic systems may also be studied in the purview of multiple timescales associated with the oscillations of various subsystems and control parameters. With the insight from experiments in thermoacoustic systems and studies from other fields as our motivation, we try to explain the cause of intermittency in low-turbulence systems using the slow-fast approach.

We conduct an experimental and theoretical investigation on a prototypical thermoacoustic system, known as the horizontal Rijke tube (Matveev (2003)). The horizontal Rijke tube inherently does not show intermittency or bursting behaviour prior to the onset of thermoacoustic instability (Matveev (2003); Mariappan and Sujith (2011); Gopalakrishnan and Sujith (2014)). We design the experiments so as to create bursting behaviour, and hence, to test the hypothesis of the occurrence of bursts due to multiple timescales in the Rijke tube. In pursuit of the same, we purposefully introduce sinusoidal oscillations in the control parameter (i.e., heater voltage) at a frequency which is

orders of magnitude lesser than the acoustic frequency. The mean value of this oscillatory control parameter is varied such that the system dynamics transitions from steady state to limit cycle oscillations.

We also develop a low order phenomenological model with a canonical form for subcritical Hopf bifurcation for heat release rate fluctuations, where low turbulence intensity is modelled using additive noise and interactions between various subsystems is modelled using multiplicative noise. Slow-fast dynamics is introduced in the model by the slow sinusoidal oscillation of the control parameter, in a similar manner as described for the experiments. Prior to thermoacoustic instability, we observe the occurrence of bursts of high amplitude periodic oscillations amidst low amplitude aperiodic oscillations in the acoustic pressure due to the slow modulations of the control parameter in the experiments on the Rijke tube as well as through our model. Finally, we study the interdependence of the various subsystems of a thermoacoustic system by two approaches in the model. In the first approach, we use the slow-fast systems approach and couple the oscillations of the slow and the fast subsystems. While in the second approach, we introduce multiplicative noise in the heat release rate term in the absence of slow oscillations in the control parameter. We show that a coupling between the slow and the fast subsystems induces regular amplitude modulations in the bursts of periodic oscillations, while the multiplicative noise introduces small and irregular modulations in the amplitude envelope of bursts.

3.2 Rijke tube experiments designed to study the slow-fast hypothesis

To test our hypothesis on the occurrence of bursts due to slow-fast oscillations in a thermoacoustic system, we use the Rijke tube setup described in section 2.1 in Chapter 2. We externally introduce slow timescale oscillations in the heater voltage. Such control parameter oscillations are introduced by generating a sinusoidal voltage signal using the SignalExpress™ software, which in turn, introduces sinusoidal oscillations

in the heater power. Throughout all the experiments in the Rijke tube, the sinusoidal oscillations of the voltage supplied to the heater are maintained at an amplitude of 0.5 V and a frequency of 50 mHz. The mean value of the heater voltage is varied in the range 1.5 to 2.75 V, corresponding to which the mean value of the heater power varies in the range 200 to 600 W. In order to obtain bursting behaviour in the system, we ensure that the frequency of the oscillations in the heater voltage is of the order of $1/1000^{th}$ of the natural frequency of the acoustic oscillations developed during thermoacoustic instability in the Rijke tube, which is around 162 Hz. We use such a low ratio in order to allow enough decay and growth time between consecutive bursts of periodic oscillations in the acoustic pressure dynamics. Thus, the heater power oscillations reflect the slow subsystem, while the unsteady acoustic pressure fluctuations developed inherently in the system comprise the fast subsystem.

3.3 Model based on the normal form of subcritical Hopf bifurcation

In general, any thermoacoustic system consists primarily of a source of unsteady heat release subjected to an acoustic field established in a confinement. If the premixed/diffusion flame inside the duct is restricted to a smaller length compared to the size of the duct, it can essentially be considered as a concentrated source of heat, just like the electrically heated wire mesh in the case of a horizontal Rijke tube. We, therefore, use a model similar to that discussed by Gopalakrishnan *et al.* (2016), which is a modified form of the nonlinear model developed by Balasubramanian and Sujith (2008), to obtain subcritical Hopf bifurcation through a generalized heat release rate function (Juniper (2012)).

3.3.1 Governing Equations

The linearized non-dimensional equations for momentum and energy in one-dimension, neglecting the effect of mean flow and temperature gradient, are as follows (Balasubra-

manian and Sujith (2008); Nicoud and Wieczorek (2009)),

$$\gamma M \frac{\partial u'}{\partial t} + \frac{\partial p'}{\partial x} = 0, \quad (3.1)$$

$$\frac{\partial p'}{\partial t} + \gamma M \frac{\partial u'}{\partial x} = (\gamma - 1) \dot{Q}' \delta(x - x_f), \quad (3.2)$$

where γ is the ratio of specific heat capacities, M is the mean flow Mach number, \dot{Q}' is the fluctuating heat release rate at the location of the heat source (x_f) in the system, while p' and u' are the fluctuations in the acoustic pressure and the acoustic velocity, respectively. Here, t denotes time and x denotes the distance along the axial direction of the duct. The set of partial differential Eqs. (5.1) and (3.2) are converted to a set of ordinary differential equations by using the method of modal expansion, also often called the Galerkin projection (Zinn and Lores (1971)). Accordingly, we expand the acoustic pressure and velocity fluctuations as a linear combination of basis functions that satisfy the boundary conditions associated with the Rijke tube duct, which is open at both ends. Since, at open ends, the acoustic pressure fluctuations are zero and the acoustic velocity fluctuations are maximum, sine and cosine functions are a natural choice as basis functions for the modal expansion of p' and u' , respectively. The pressure and velocity fluctuations are expressed in terms of time-varying modes η and $\dot{\eta}$ as follows,

$$u'(x, t) = \sum_{j=1}^{\infty} \eta_j(t) \cos(j\pi x) \quad (3.3)$$

and
$$p'(x, t) = - \sum_{j=1}^{\infty} \frac{\gamma M}{j\pi} \dot{\eta}_j(t) \sin(j\pi x).$$

Substituting the expressions from Eq. (3.3) into Eqs. (5.1), and (3.2) and projecting the resulting equation on the j^{th} mode of the basis function, we obtain the set of ordinary differential equations (ODEs) as given in Eqs. (3.4) and (3.5). Finally, we include the effect of damping in Eq. (3.2) by adding a damping term which is dependent on the frequency of the system (Matveev (2003)).

$$\frac{d\eta_j}{dt} = \dot{\eta}_j, \quad (3.4)$$

$$\frac{d\dot{\eta}_j}{dt} + 2\varepsilon_j\omega\dot{\eta}_j + \omega^2\eta_j = \dot{q}', \quad (3.5)$$

where ω is the non-dimensional angular frequency, \dot{q}' is the non-dimensional heat release rate term. Here, ε_j is the damping coefficient which is calculated according to the following equation, with $k_1 = 0.1$ and $k_2 = 0.06$.

$$\varepsilon_j = \frac{1}{2\pi} \left(k_1 \frac{\omega_j}{\omega_1} + k_2 \sqrt{\frac{\omega_1}{\omega_j}} \right) \quad (3.6)$$

where $\omega_j = j\pi$ for the j^{th} duct mode (Matveev (2003); Sterling (1993)).

For a horizontal Rijke tube, the model developed by Balasubramanian and Sujith (2008) uses a modified form of the King's law (King (1914); Heckl (1988)) to model the heat release rate term (\dot{Q}'). The King's law governs the heat release rate from the thin hot wire to the surrounding fluid, which is appropriate to describe the heat transfer from the electrically heated wire mesh to the air in the Rijke tube. However, for thermoacoustic systems in general, the King's law may not be the most general description of the heat source as it is for a Rijke tube with electric heater.

For the current study, the non-dimensional heat release rate fluctuations are decomposed into coherent and non-coherent components in Eq. (3.7), as suggested by Noiray (Noiray (2017)). The coherent fluctuations in the heat release rate (\dot{q}'_c) are due to the interaction of the acoustic field fluctuations with the flame, while the non-coherent heat release rate fluctuations (\dot{q}'_{nc}) occur due to the turbulence in the underlying flow field.

$$\dot{q}' = \dot{q}'_c + \dot{q}'_{nc}. \quad (3.7)$$

The non-coherent component of the heat release rate, \dot{q}'_{nc} , is modelled using the noise term $\xi(t)$ in Eq. (3.8). The coherent heat release rate \dot{q}'_c is considered to be a nonlinear function of the non-dimensional acoustic modes η and $\dot{\eta}$. For the current study, we use the canonical form of the subcritical Hopf bifurcation for \dot{q}'_c with a time delay coupling between η and $\dot{\eta}$, as motivated by Gopalakrishnan *et al.* (2016), which is given by Eq.

(3.8).

$$\dot{q}'_c = -c_1(\eta - \tau\dot{\eta}) - c_3(\eta - \tau\dot{\eta})^3 + c_5(\eta - \tau\dot{\eta})^5 \quad \text{and} \quad \dot{q}'_{nc} = \xi(t), \quad (3.8)$$

where c_1 , c_3 and c_5 are constants, and τ is the time delay term. As discussed by Gopalakrishnan *et al.* (2016), the time delay term ensures that the heat release rate responds to the velocity fluctuations at the location of the heating source with a certain time delay. Furthermore, the heat release rate introduces nonlinear feedback between the evolution of acoustic pressure and acoustic velocity fluctuations. The specific expression of \dot{q}'_c in Eq. (3.8) also ensures that a subcritical Hopf bifurcation [Fig. 3.2(b)] is obtained for the set of ODEs (3.4) and (3.5).

The term $\xi(t)$ is a combination of multiplicative and additive noise. A random term [ξ_a in Eq. (3.9)] is added at each iterative step to the acoustic pressure fluctuations, to effectuate additive noise (strength σ_a) in the system. Similarly, we generate multiplicative noise of strength σ_m by adding a random term [ξ_m in Eq. (3.9)] to the acoustic pressure oscillations at each step, where the strength of the random term is directly proportional to $\dot{\eta}$ as noted in Eq. (3.9). Both the random terms ξ_a and ξ_m are generated by the Weiner process and are white Gaussian noise terms. The non-dimensional strengths σ_a and σ_m are a fraction comparable to the maximum amplitude of the non-dimensional pressure variable $\dot{\eta}$, which is of the order of 1 ($\dot{\eta} \sim 1$). These non-dimensional strengths are varied to simulate the absence of turbulent fluctuations ($\sigma_a = 0.0001$) and also low or high levels of turbulence or perturbations from other subsystems (where σ_a and σ_m are of the order of 0.1). We choose such order of magnitude for the noise intensities, so that the ratio of amplitudes of periodic and aperiodic oscillations in the acoustic pressure signal obtained from the model is similar to that obtained from experiments.

$$\xi(t) = \sigma_a \xi_a + \sigma_m \dot{\eta}(t) \xi_m. \quad (3.9)$$

A slow-fast system is formed by the two-way interaction of both the slow and the fast subsystems. The evolution of each subsystem is, in general, dependent on the other. To study slow-fast oscillations in a thermoacoustic system where the pressure fluctua-

tions have a fast timescale, we introduce slow sinusoidal oscillations in the control parameter c_1 [Eq. (3.8)] centred at a mean value A , amplitude B , and frequency f . As stated earlier for the experiments, we maintain the value of the frequency of the control parameter in the model at an order of magnitude of $1/1000^{th}$ of the natural frequency of the acoustic fluctuations (fast timescale). The oscillations in the non-dimensional control parameter c_1 are governed by the following equation, Eq. (3.10).

$$c_1 = A + B \sin(2\pi ft). \quad (3.10)$$

The set of ordinary differential equations, Eqs. (3.4) and (3.5), are solved by the stochastic Runge-Kutta method (Burrage (1999)) for the heat release rate function given by Eqs. (3.7) and (3.8), subject to noise [as given in Eq. (3.9)] and control parameter oscillations of the form shown in Eq. (3.10). In the rest of the paper, we refer to the above model as the ‘standard model’. We also assume that the evolution of the control parameter (slow subsystem) stays independent of the dynamics of the acoustic field variables (fast subsystem), say p' in the system in Sec. 3.4. Further, we investigate the effect of the evolution of fast subsystem on the evolution of the slow subsystem by introducing an interdependence between the two subsystems, which is discussed in detail in Sec. 3.6.

3.4 Results and discussion

3.4.1 Bifurcation diagram

We plot the bifurcation diagram of the acoustic pressure oscillations obtained during the transition to thermoacoustic instability through experiments in the horizontal Rijke tube and the model. The bifurcation diagrams [Figs. 3.2(a,b)] show the variation of root mean square value (rms) of the acoustic pressure (p'_{rms}) with a quasi-static change in the heater power (or heater voltage) for the experiments and the non-dimensional parameter c_1 for the model, respectively. The non-dimensional acoustic pressure from

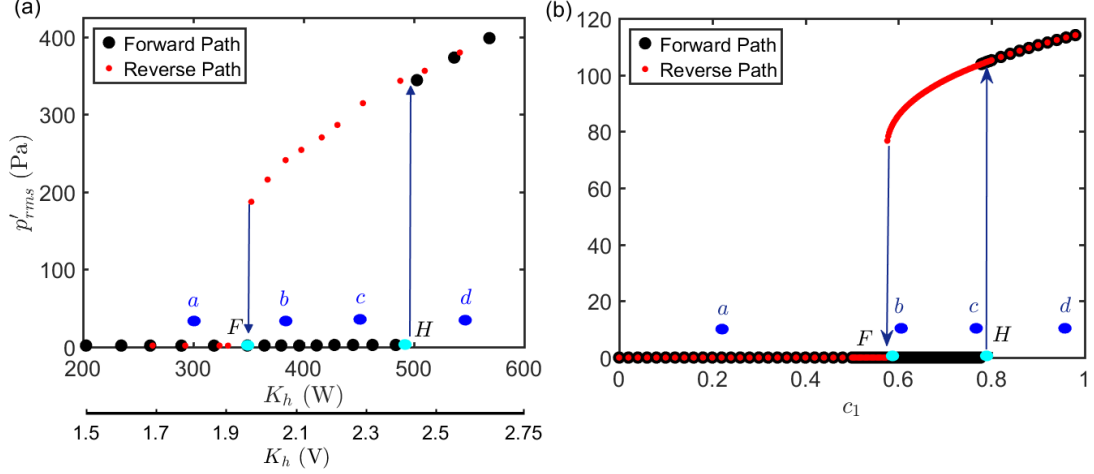


Fig. 3.2: The bifurcation diagram of the acoustic pressure fluctuations (p') with respect to (a) K_h , the heater power (W) or heater voltage (V) from experiments in the Rijke tube and (b) non-dimensional parameter c_1 from the standard model, when $\sigma_a = 0.0001$, $\sigma_m = 0$ in Eq. (3.9), $c_3 = c_5 = 1$ in equation (7). Points F and H represent the fold and the Hopf point, respectively, while a , b , c and d are reference points.

the model is converted to a dimensional form by multiplying it with the atmospheric mean pressure for the ease of comparison with the experimental results. Since this is a phenomenological model, we aim only for a qualitative match with the experiments. The bifurcation diagrams shown in Figs. 3.2(a,b) are for laminar flow ($Re = 1154 \pm 6$) conditions in the experiment and very low noise intensity in the model ($\sigma_a = 0.0001$ to account for inherent noise in real systems), respectively.

When the control parameter value is varied in a quasi-static manner in the forward direction (i.e., the value of control parameter is increased), we notice a sudden transition of the system behaviour from steady state to limit cycle oscillations at the Hopf bifurcation point H in Figs. 3.2(a,b). A further increase of the control parameter beyond the point H leads to a continuous increase in the amplitude of the limit cycle oscillations in the system. In the reverse direction, as the value of the control parameter is reduced, we notice a continuous decrease in the amplitude of limit cycle oscillations, along the same path as in the forward direction. However, the transition from limit cycle to stable equilibrium state in the reverse direction occurs at point F (i.e., fold point), which is well past the point H . Thus, the bifurcation diagram exhibits a hysteresis region, indicative of a subcritical Hopf bifurcation in the system dynamics. In experiments, the Hopf

bifurcation point is found to be at 2.45 V (483.6 W) and the fold point at 1.95 V (352.6 W). From the model, the Hopf and the fold point values for the non-dimensional parameter c_1 are 0.77 and 0.57, respectively, when we choose $\tau = 0.2$, $c_3 = c_5 = 1$. Also, the bifurcation diagram in Fig. 3.2 is marked with points a , b , c and d representing different dynamical states for reference in Fig. 3.3.

3.4.2 Effect of slow oscillations in the control parameter on the transition to thermoacoustic instability

In this section, we present the results of experiments on the horizontal Rijke tube, which were designed to investigate the occurrence of bursting oscillations induced due to the slow oscillations of the control parameter during the transition from steady state to limit cycle oscillations in the system. Figures 3.3-I and 3.3-II show the time series of acoustic pressure fluctuations from the experiments performed on the Rijke tube and from the model, respectively, for the reference points of the subcritical Hopf bifurcation shown in Fig. 3.2.

Column I in Fig. 3.3 shows results from the experiments in the Rijke tube when slow oscillations, with fixed amplitude (0.5 V) and frequency (0.05 Hz), are induced in the heater voltage (K_h). The mean value of the heater voltage is increased from point a to d [with reference to the bifurcation diagram in Fig. 3.2(a)] in Figs. 3.3(a-d), respectively. For oscillations about the mean value of K_h corresponding to a point in the steady state region, we observe only very low amplitude aperiodic fluctuations, which can be considered as a quiescent state. As the mean value of the control parameter is increased to a value around the fold point [point b in Fig. 3.2], we observe bursts of high amplitude periodic oscillations amidst nearly quiescent state, as seen in Fig. 3.3(b). We also obtain such bursting dynamics [Fig. 3.3(c)] when the mean value of the control parameter is in the bistable zone [point c in Fig. 3.2]. Comparing Fig. 3.3(b) and Fig. 3.3(c), we note that as the mean value of K_h is increased, the average epoch of the rest state reduces and the maximum amplitude achieved by periodic oscillations in the pressure signal increases. Finally, corresponding to control parameter oscillations about

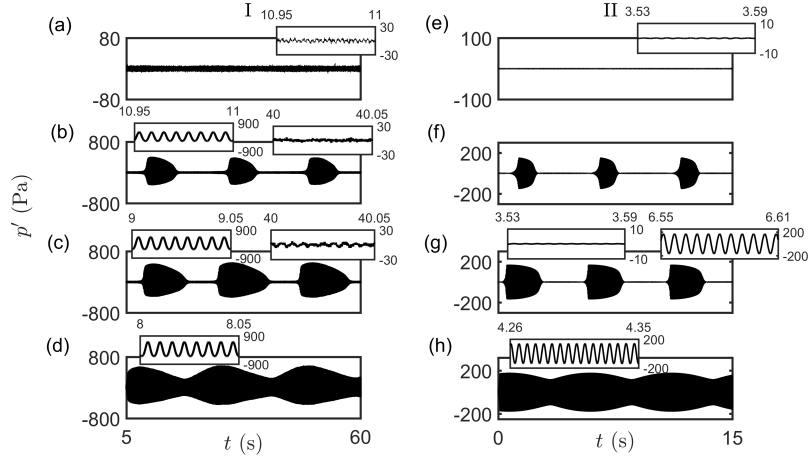


Fig. 3.3: Comparison of the time series of acoustic pressure (p') obtained from experiments (I) and from the model (II) for slow-scale oscillations in the control parameter about a mean value. For experiments, the mean value of K_h is varied from (a) to (d) as 1.8 V (306 W), 2.1 V (365 W), 2.2 V (428 W), and 2.56 V (568 W), respectively, where the amplitude and frequency of oscillations of K_h are fixed at 0.5 V and 0.05 Hz throughout. In the model, the parameter c_1 oscillates with amplitude $B = 0.4$ and frequency $f = 0.17$ Hz when its mean value is increased from (e) to (h) as $A = 0.2, 0.6, 0.75$ and 0.95 , respectively. The noise intensity in the model is $\sigma_a = 0.0001$.

a point far ahead of the Hopf bifurcation point in the limit cycle regime [point d in Fig. 3.2], we observe the occurrence of limit cycle oscillations with modulated amplitude envelope, as shown in Fig. 3.3(d). Such modulations in the amplitude envelope arise when the minimum value of the control parameter oscillations is more than or close to (if less than) the value of the control parameter at the fold point. That is, even though the control parameter oscillations may cross the fold point by a small margin, and transit to the steady state region, the acoustic pressure oscillations never achieve a quiescent state. This is because the acoustic pressure oscillations in the active state have insufficient time to decay to the rest state, when a lesser fraction of the oscillation cycle of the control parameter occurs in the steady state region of the bifurcation diagram.

In column II of Fig. 3.3, we show the time series of acoustic pressure fluctuations obtained from the standard model (discussed in Sec. 3.3) in the presence of slow timescale oscillations of the control parameter c_1 , as indicated by Eq. 3.10. The mean value (A) of the oscillating control parameter is increased in a quasi-static manner from point a to d [with reference to Fig. 3.2(b)] to obtain the dynamics shown in Fig. 3.3(e-

h). The model qualitatively captures all the features of bursting oscillations observed from experiments in the Rijke tube [Fig. 3.3-I]. The acoustic frequency of limit cycle oscillations obtained from the standard model is $f_a = 170$ Hz. In the absence of random perturbations, (i.e., for $\sigma_a = \sigma_m = 0$) in the model, when the control parameter oscillations are introduced, we observe bursting behaviour only when the mean value of the oscillating control parameter is greater than that at the Hopf bifurcation point. However, from the experiments in the Rijke tube, we observe bursting behaviour even when the control parameter oscillations are centred much before the Hopf bifurcation point (i.e., in the bistable zone), for example see Fig. 3.3(b). This is because noisy fluctuations are inherent to any real system; hence, we use very low noise intensity ($\sigma_a = 0.0001$) to mimic such a noise in real systems. As a result, we obtain bursting behaviour even when the control parameter is centred around the fold point, given that the amplitude of its oscillations is sufficient to cross the Hopf bifurcation point, for example see Fig. 3.3(f).

Similar to the experiments, the model produces bursts of high amplitude periodic oscillations amidst nearly quiescent state [Figs. 3.3(f-g)] and modulated limit cycle oscillations [Fig. 3.3(h)]. We also notice that, such bursting behaviour occurs only when the control parameter value crosses both the Hopf and the fold points in every cycle of the oscillation. Further, for the bursts induced by slow parameter oscillations (as shown in Fig. 3.3), we note that the transition from the rest to the active state (growth) and from the active to the rest state (decay) is asymmetric. A similar asymmetry in the growth and decay of the bursts of acoustic pressure signal has been recently reported in a Rijke-type burner by Weng *et al.* (2016). They observed that the asymmetry associated with bursting oscillations changes with the change in the equivalence ratio in the system; however, the cause of such asymmetry in a burst is not clear. In the next Sec. 3.4.3, we try to explain this asymmetry of growth and decay of bursts with the help of the model discussed in Sec. 3.3.

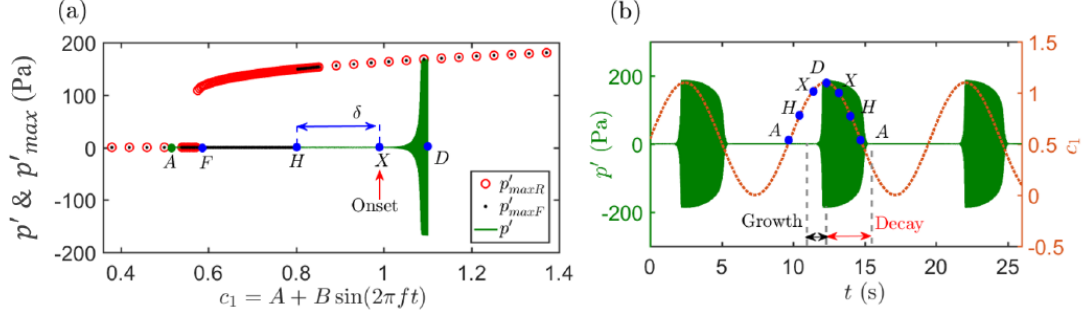


Fig. 3.4: (a) Transformed phase portrait of acoustic pressure oscillations (p') obtained from the standard model superposed on the bifurcation diagram of acoustic pressure (p'_{max}) obtained from quasi-static variation of c_1 . (b) The overlapped time series of the control parameter oscillations (c_1) and the acoustic pressure oscillations (p') during a state of bursting in the system, obtained from the model. Here, p'_{maxR} and p'_{maxF} refer to the reverse and the forward paths of quasi-static variation of c_1 . The point demarcated as A represents the mean value of c_1 .

3.4.3 Delayed bifurcation due to slow oscillations across a subcritical Hopf bifurcation

In this section, we discuss the reason for asymmetry in the growth and the decay pattern in the bursts induced by slow-fast dynamics in the experiments and the model [Fig. 3.3]. We believe that such asymmetry occurs due to the disproportionate time duration for which the system dynamics is restricted to the stable limit cycle branch during the forward and the reverse oscillation paths of the control parameter. Such unequal durations arise due to two reasons: (I) delayed bifurcation caused by the slow scale oscillations of the control parameter and (II) the existence of a hysteresis zone in the bifurcation diagram of the system. The effect of delayed bifurcation is explained with the help of the model in Fig. 3.4.

Delayed bifurcation effect or memory effect associated with the slow passage of control parameter through Hopf bifurcation point is widely studied in the literature (Baer and Gaekel (2008); Han *et al.* (2014, 2016); Premraj *et al.* (2016)). When the control parameter is varied across the Hopf bifurcation point in a rate-dependent manner, the transition of the system dynamics from steady state to limit cycle oscillations gets delayed and occurs at a control parameter value greater than that at the Hopf bi-

furcation point. Such a delay in the transition of the system behaviour is referred to as delayed bifurcation.

For our model involving a slow-fast system, the delayed bifurcation due to slow parameter oscillations can be depicted using a ‘transformed phase portrait’ (Han *et al.* (2016)). The transformed phase portrait is a plot of the time evolution of the acoustic pressure oscillations (the fast subsystem variable) with respect to the time-varying control parameter c_1 (the slow subsystem variable), as shown in Fig. 3.4(a). For clarity, we plot the acoustic pressure oscillations on the transformed phase diagram starting from the point A [Fig. 3.4(a)] where the pressure fluctuations are in the rest state [Fig. 3.4(a)] to the point where the pressure fluctuations achieve the maximum amplitude of periodic oscillations (at point D), observed during the onset of burst in a signal [Fig. 3.4(b)]. We then superimpose this transformed phase portrait on the bifurcation diagram which is obtained by plotting the variation of the maximum amplitude of the acoustic pressure oscillations with respect to the quasi-static variation of the control parameter [Fig. 3.4(a)].

We note that the delay associated with the occurrence of the first burst depends on the initial conditions (i.e., $\eta(0)$) of the acoustic pressure fluctuations. However, the delay associated with the subsequent bursts in the same signal is independent of initial conditions for fixed values of A , B and f [in Eq. (3.9)] for the oscillating parameter c_1 (Han *et al.* (2014)). Hence, the transformed phase portrait is obtained from any subsequent burst after disregarding the first burst as a transient. In Fig. 3.4(a), we show the transformed phase portrait for the case when the control parameter oscillates with an amplitude of $B = 0.55$ with a frequency $f = 0.102$ Hz about a mean value $A = 0.55$. Furthermore, we show the overlapped time series of slow control parameter oscillations and fast acoustic pressure oscillations during the state of bursting in the system, in Fig. 3.4(b). Points A , F , H , X , and D are the reference points of c_1 on the bifurcation diagram in Fig. 3.4(a) corresponding to the demarcations on the time series in Fig. 3.4(b). Consider the oscillation of the control parameter starting from the mean value, indicated by the point A in Figs. 3.4(a,b). We define the forward oscillation from point A to point D and the reverse oscillation from point D to point A in half a cycle of the

control parameter oscillation [Fig. 3.4(b)].

Even as the control parameter oscillations cross the Hopf bifurcation point H , we observe steady state dynamics in acoustic pressure (p'), i.e., the transition of p' from the rest to the active state does not occur immediately at H [Fig. 3.4(a)]. Such transition occurs only at a value of c_1 that is greater than that at H , i.e., at point X . The identification of the exact point of the onset of the growth of oscillations (i.e., point X) is non-trivial and is described in detail in Appendix A.1. We qualitatively indicate the delayed bifurcation in the system by what we define as the ‘delay-value’ (in terms of c_1), henceforth referred to as δ . The delay-value (δ) represents the difference in the values of c_1 at point H (the Hopf point) and at point X (where the onset of a burst of periodic oscillations occurs in the acoustic pressure signal).

In the forward direction, when the value of c_1 grows from point A to D [Fig. 3.4(b)], we obtain periodic oscillations in the p' signal only when the value of c_1 traverses from point X to D on the bifurcation plot [Fig. 3.4(a)]. In the reverse path of c_1 (i.e., from point D to A), the value of p'_{max} continuously decreases from point D to F [Fig. 3.4(a)] corresponding to which the amplitude of the p' oscillations in the burst also decreases. Once the control parameter crosses the fold point F , the periodic oscillations of p' in the burst decay rapidly to the rest state. Hence, the dynamics of p' is sustained on a longer stretch of the stable limit cycle branch in the reverse direction of the control parameter oscillation as compared to the forward direction. As a result, the growth and the decay pattern of the bursts are asymmetric.

In addition, we investigate the effect of slow parameter oscillations across a supercritical Hopf bifurcation, which does not have a hysteresis zone, using a similar model. The corresponding equations and results are discussed in Sec. 3.5. In a supercritical Hopf bifurcation, the amplitude of limit cycle oscillations increases gradually from the rest state and there is no sudden jump in the value of p'_{max} . We find that the slow parameter oscillations across the supercritical Hopf bifurcation induce bursts of periodic oscillations amidst nearly quiescent state with distinct growth and decay pattern. Since there is a delay associated with the transition of dynamics from steady state to periodic oscillations, there is a steep rise in the amplitude of the acoustic pressure signal, that

is, a sudden growth of high amplitude periodic oscillations (refer Fig. 3.6). During the reverse oscillation, the amplitude of periodic oscillations decreases gradually to the rest state.

3.4.4 Factors effecting the delayed bifurcation

In this section, we present the effect of the change in the mean value, amplitude, and frequency of the control parameter oscillations on the delay value (represented as δ in Fig. 3.4) and also on the characteristics of bursting oscillations, using the model, through Fig. 3.5.

In the transformed phase diagrams in Fig. 3.5, points F and H indicate the fold and the Hopf points, respectively. We consider two cases in Figs. 3.5(a,b) where for case I, $A_I = 0.55$, and for case II, $A_{II} = 0.85$, while $B = 0.55$, $f = 0.102$ Hz in both cases. From the transformed phase diagram in Fig. 3.5(a), we observe that an increase in A leads to a corresponding increase in the delay value (δ), i.e., if $A_I < A_{II}$ then $\delta_I < \delta_{II}$. The time series of the acoustic pressure for both the cases are overlapped and plotted in Fig. 3.5(b) for the ease of comparison. From Fig. 3.5(b), we infer that as A increases, the epochs of high amplitude periodic oscillations (i.e., burst) increase and the epochs of low amplitude aperiodic fluctuations correspondingly decrease in the p' signal. The maximum amplitude of the periodic oscillations in the p' signal also increases with an increase of A . This is expected from the bifurcation diagram, where we see an increase in the amplitude of limit cycle oscillation with the increase in the value of the control parameter. Since the value of A_I is lesser than A_{II} , for the same amplitude B , the maximum amplitude achieved along the limit cycle branch is greater for case II.

Next, we inspect the effect of variation in the frequency (f) of the control parameter oscillations whilst its amplitude (B) and mean value (A) are kept constant in Figs. 3.5(c,d). Two cases are considered as before, case I: $f_I = 0.102$ Hz and case II: $f_{II} = 0.238$ Hz, while the amplitude and mean value of c_1 for both cases are fixed at $B = 0.55$ and $A = 0.85$, respectively. We note that as f increases, the number of bursts occurring in the signal in a fixed duration also increases [Fig. 3.5(d)]. Furthermore,

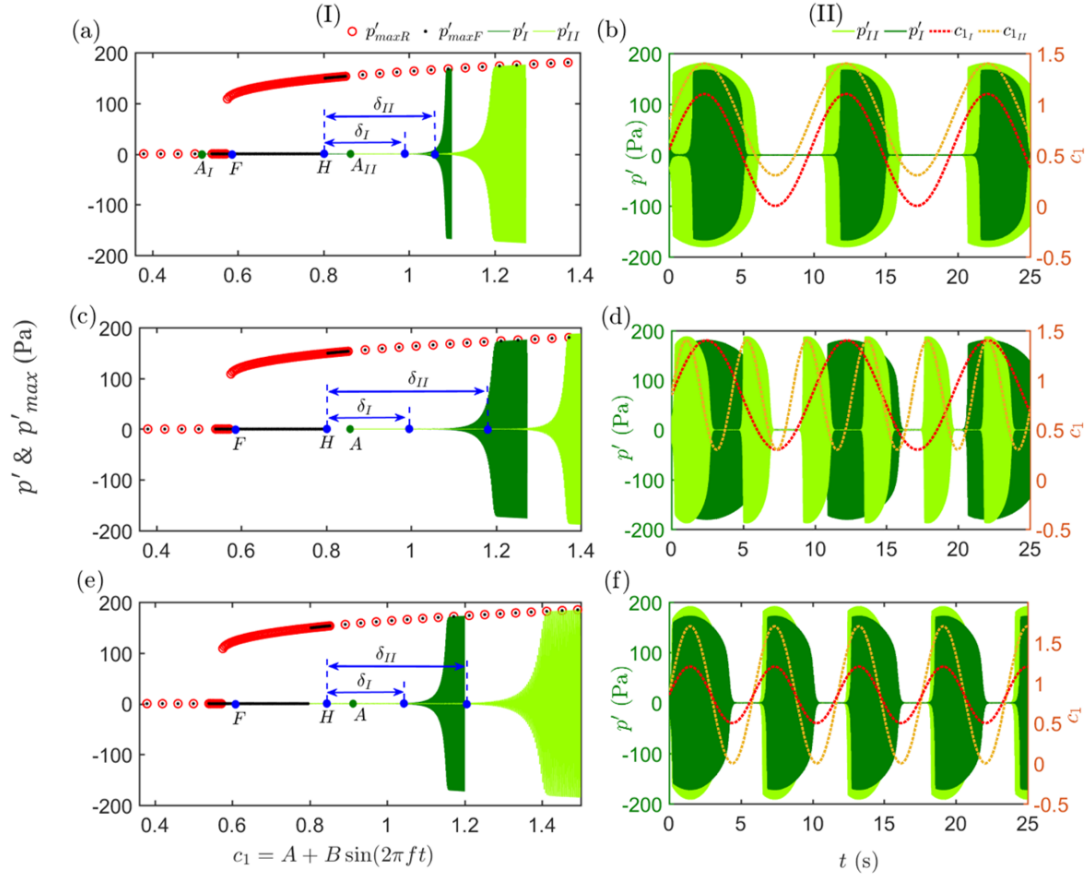


Fig. 3.5: (I) Transformed phase diagrams and (II) the corresponding overlapped time series of the control parameter oscillations and the acoustic pressure oscillations obtained from the model, for the cases shown in (a), (b) with different mean values A_I and A_{II} while B and f are fixed, (c), (d) with different frequencies f_I and f_{II} , while A and B are fixed, and (e), (f) with different amplitudes B_I and B_{II} while A and f are fixed. The point demarcated as A represents the mean value of c_1 .

from the transformed phase portrait in Fig. 3.5(c), it is clear that the delay value (δ) associated with the onset of bursts increases corresponding to the increase in f . This means, if $f_I < f_{II}$ then $\delta_I < \delta_{II}$. We also note that the maximum amplitude of the burst remains nearly the same with an increase in f at fixed values of A and B .

Finally in Figs. 3.5(e,f), we study the effect of variation of the amplitude (B) of the control parameter oscillations while keeping A and f constant. Again, we consider two cases, case I: $B_I = 0.35$ and case II: $B_{II} = 0.85$ for fixed values of $A = 0.85$ and $f = 0.17$ Hz. We find that the maximum amplitude of acoustic pressure oscillations in the burst is directly proportional to the amplitude of the control parameter oscillations. We also note that an increase in B does not affect the epoch of a burst observed in the signal, i.e., the duration of bursts remains the same [Fig. 3.5(f)]. Further, from the transformed phase portrait in Fig. 3.5(e), we note that the delay value (δ) is higher for case II, i.e., if $B_I < B_{II}$ then $\delta_I < \delta_{II}$.

3.5 Delayed bifurcation due to slow oscillations across a supercritical Hopf bifurcation

In Fig. 3.6, we show the effect of slow oscillations in the control parameter across a supercritical Hopf bifurcation. The bifurcation diagram is obtained from quasi-static variation of the control parameter c_1 , when the coherent heat release term is modelled by the canonical form of supercritical Hopf bifurcation, as given in Eq. (3.11) in the standard model, [instead of Eq. (3.8)].

$$\dot{q}'_c = -c_1(\eta - \tau\dot{\eta}) + c_3(\eta - \tau\dot{\eta})^3. \quad (3.11)$$

Figure 3.6(a) shows the transformed phase portrait for the case when the control parameter oscillates with an amplitude of $B = 0.65$, and frequency $f = 0.17$ Hz about a mean value $A = 0.7$. Figure 3.6(b) shows the overlapped time series of oscillations of c_1 and p' during the bursting state in the system. Reference point A demarcates the starting

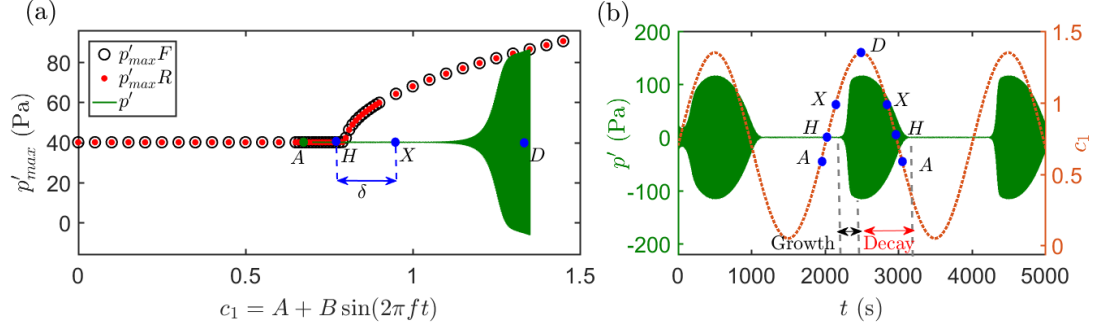


Fig. 3.6: (a) Transformed phase portrait of acoustic pressure oscillations obtained from the standard model for supercritical bifurcation superposed on the bifurcation diagram of acoustic pressure (p'_{max}) obtained from quasi-static variation of c_1 . (b) The overlapped time series of the control parameter oscillations (c_1) and the acoustic pressure oscillations (p') during a state of bursting in the system.

point of oscillation of c_1 , H demarcates the Hopf bifurcation point of the supercritical bifurcation which occurs at $c_1 = 0.79$, X demarcates the onset point of the burst and D demarcates the point at which c_1 achieves a maximum value in an oscillation cycle. Clearly, slow oscillations of the control parameter across the supercritical Hopf bifurcation point introduce a delayed bifurcation as observed for subcritical Hopf bifurcation earlier in Fig. 3.4.

As compared to subcritical Hopf bifurcation, a supercritical bifurcation does not have a hysteresis zone and the amplitude of the limit cycle oscillations increases gradually from the steady state [Fig. 3.6(a)]. The dynamics of the system transitions from the steady state to limit cycle oscillations after a delayed bifurcation, and therefore there is a sudden jump in the amplitude of the pressure oscillations during the onset of a burst. In the reverse path, the amplitude of periodic oscillations decreases gradually along the limit cycle branch and the pressure oscillations eventually attain a rest state. The growth and decay patterns are thus different, even when the system undergoes a supercritical bifurcation. The effect of varying the amplitude, the frequency and the mean value of the oscillating parameter across a supercritical Hopf bifurcation is similar to that is discussed for the case of subcritical Hopf bifurcation in Sec. 3.4.4.

We note a subtle difference between the decay pattern of the bursts that occur in the case of a subcritical and a supercritical bifurcation. The decay of the oscillations in a burst caused in a system having subcritical bifurcation is initially gradual, as the

control parameter oscillations move along the limit cycle branch. However as the control parameter crosses the fold point, there is a sharp decay in the pressure oscillations in the burst. For a system exhibiting supercritical bifurcation, the decay in pressure oscillations in a burst is always gradual as the control parameter oscillations trace the continuous limit cycle branch into the steady state regime.

3.6 Investigating the interdependence of slow and fast subsystems using model

In the previous section, Sec. 3.4, we discussed the case where the externally introduced slow scale oscillations in the control parameter are independent of the dynamics of the fast scale oscillations observed in the acoustic pressure. However, in practical thermoacoustic systems, the acoustic, hydrodynamic, and flame fluctuations, which ensue at distinct timescales, are non-linearly coupled (Lieuwen (2012)) and the quantification of the effect of each subsystem on the other is difficult. For instance, there is an inevitable dependence between the evolution of the acoustic pressure fluctuations and various control parameters viz., equivalence ratio, mixing and burning rates, temperature, etc., inherent to the governing system. In addition, there is a possible interdependence between the underlying turbulence intensity and the dynamics of acoustic variables (as discussed in Fig. 1.1 in Sec. 1.1). The dynamics arising in the system due to the interaction between the subsystems with multiple timescales is highly complex. Therefore, in this section, we intend to probe the occurrence of bursting dynamics in the acoustic field due to such interdependence of the slow and fast subsystems through the model. To model the interaction between the various subsystems of a thermoacoustic system, we present two approaches: (I) by coupling the slow and fast subsystems in the presence of low-intensity noise and (II) by introducing noise (additive and multiplicative) in the absence of slow oscillations in the control parameter.

3.6.1 Effect of coupling the slow and fast subsystems

From our experiments in the Rijke tube, we understand that bursts of periodic oscillations arise in the acoustic pressure fluctuations (fast subsystem) as a result of slow oscillations of a control parameter (slow subsystem). Further, we notice that when the slow and the fast oscillations are uncoupled, the bursts occur at equal intervals in the acoustic pressure signal. However, in practical combustors, such bursts occur at random intervals in the signal. Sometimes, such bursts also possess a peculiar feature of periodic modulation in the amplitude envelope of the active state in the acoustic pressure signal (Boudy *et al.* (2013); Pawar *et al.* (2016)) (as shown in Fig. 3.8(a)), known as amplitude modulated bursting.

‘Amplitude modulated bursting’ is a known phenomenon in the studies pertaining to slow-fast systems Vo *et al.* (2016); Han *et al.* (2018). As discussed by Han *et al.* (2018), amplitude modulated bursting is characterized by modulations in the envelope of the active phase of bursting. They show that amplitude modulated bursting can occur in the system dynamics due to ‘multi-frequency slow parametric modulation’, that is, if there exist multiple slow frequencies in the parameter modulations when the system undergoes a Hopf bifurcation or any other type of bifurcation. In our approach using the modified model, the system has only one frequency that is a function of time, which introduces amplitude modulated bursting.

We speculate that amplitude modulated bursting in the acoustic pressure signal may arise as a result of interactions between the slow and the fast subsystems in a combustor. Therefore, to study the interdependence of these two subsystems, we modify the standard model by making the frequency of the control parameter oscillations dependent on the amplitude of the fast oscillations in the acoustic pressure. Due to such interdependence, we assume that the frequency of the control parameter oscillations increases to a higher value during the active state of the burst as compared to that during the rest state. We subsequently show that such an assumption models the amplitude modulated bursting observed in laboratory-scaled combustors. In order to realise this altering frequency in the model, we numerically capture the amplitude envelope of the acoustic pressure fluctuations as and when the system evolves [see Fig. 3.7]. Then, we choose a thresh-

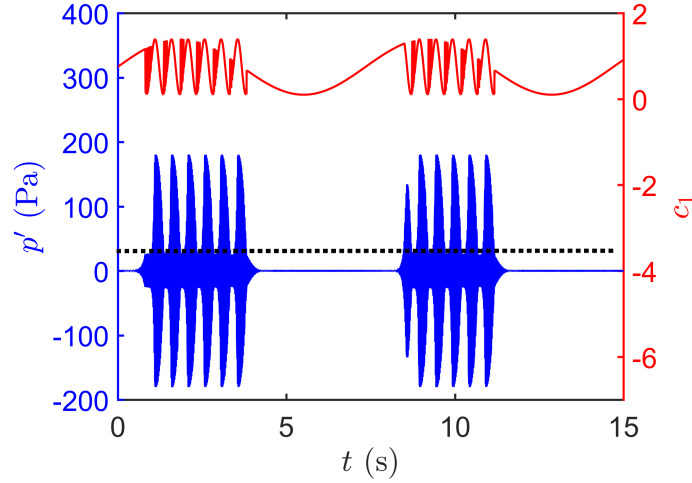


Fig. 3.7: Schematic representation of the simultaneous evolution of the acoustic pressure (p' , in blue) and the control parameter (c_1 , in red) oscillations obtained through the modified model. The dotted line represents the chosen threshold of $p'_{th} = 25$ Pa (which is around 15% of the maximum amplitude); if $p'_{env} < p'_{th}$, frequency of the control parameter (c_1) oscillation is $f = 0.17$ Hz; if $p'_{env} > p'_{th}$, then $f = 15 \times 0.17$ Hz. The frequency of the acoustic pressure oscillations is 170 Hz. The noise intensities are $\sigma_a = 0.0001$, $\sigma_m = 0$.

old of acoustic pressure amplitude, p'_{th} , which is a suitable fraction of the amplitude of the limit cycle oscillations. The choice of p'_{th} is based on examining several threshold values in the model and is restricted to be around 10-30% of the maximum amplitude of acoustic pressure oscillations (depending on the level of noise used in the system). If the value of the threshold is higher than 30%, we observe bursting dynamics only for a very small range of the control parameter. If the amplitude envelope of the acoustic pressure oscillations is below p'_{th} , the frequency of c_1 is chosen to be f ; whereas, if the amplitude envelope of acoustic pressure oscillations is above p'_{th} , the frequency of c_1 is chosen to be a multiple of f . Figure 3.7 represents the simultaneous evolution of c_1 and p' when the frequency of c_1 is allowed to vary according to the amplitude of p' as described. We, henceforth, refer to the model with such interdependence between the slow and the fast subsystems as the ‘modified model’.

In a thermoacoustic system, the evolution of dynamics of each subsystem is dependent on that of the other subsystems. As a result, the interaction of some slow subsystems with the fast subsystem may give rise to perturbations in various other slow subsystems. Thus, there may be frequency variations in parameters associated with

different subsystems other than the control parameter originally oscillating at a slow timescale. However, the cumulative effect of the interaction of all these slow subsystems will be reflected in the heat release rate fluctuations. Hence, in the modified model, we account for the interactions between the various slow and fast subsystems through the frequency variation of a single parameter c_1 , which eventually affects the heat release rate oscillations according to Eq. (3.8).

3.6.2 Effect of additive and multiplicative noise

To model the interactions between the various subsystems (hydrodynamics, acoustics and flame dynamics), a completely different approach may be identified, in which we disregard the approach using slow timescale oscillations of the control parameter. In this second approach, we model such interactions using a combination of additive and multiplicative noise. According to Eq. (3.9), the multiplicative noise introduces dependence between the non-coherent heat release rate (\dot{q}_{nc}) and the instantaneous value of the acoustic pressure oscillations in the system. Thus, the multiplicative noise aids in capturing the nonlinear interaction between the acoustic subsystem (pressure oscillations) and the heat release rate oscillations in the combustor. Further, the additive noise term in Eq. (3.9) helps to model the effect of turbulence (hydrodynamic subsystem) on the heat release rate fluctuations (Lieuwen and Banaszuk (2005)). Thus, a combination of additive and multiplicative noise is used to model the interaction between the various subsystems of a combustor. When such a combination of additive and multiplicative noise is introduced in the model, we observe bursting behaviour when the control parameter is in the vicinity of the Hopf bifurcation point.

First, we show the intermittency signals and the corresponding amplitude spectra observed prior to thermoacoustic instability in two laboratory-scaled combustors which have been discussed earlier by Pawar *et al.* (2016) [Fig. 3.8(a)] and Nair *et al.* (2014) [Fig. 3.8(b)]. Next, we compare the time series and the amplitude spectra of the intermittent oscillations in the acoustic pressure signals obtained from the model using the two approaches, namely (i) the modified model [Fig. 3.9(a)] and (ii) the introduction of additive and multiplicative noise in the model [Fig. 3.9(b)]. Finally, we compare

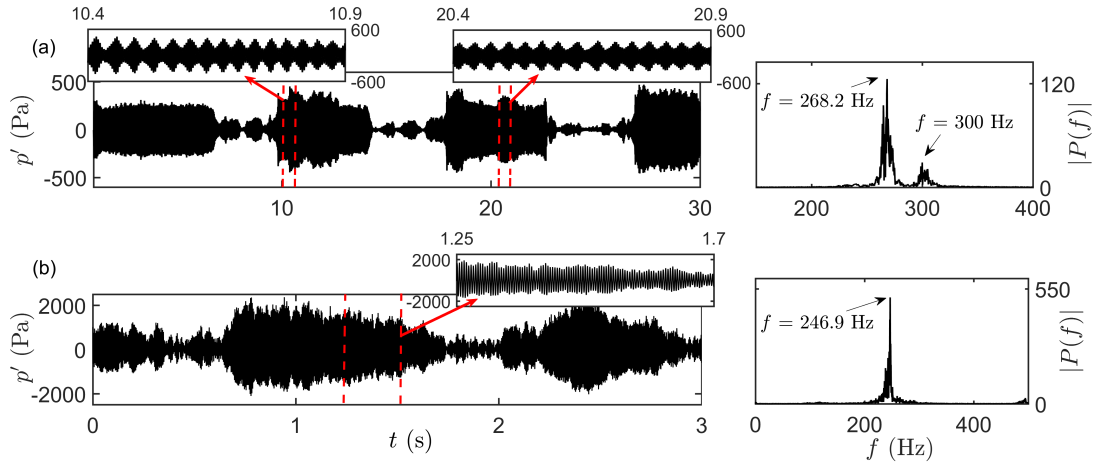


Fig. 3.8: Time series of the acoustic pressure oscillations and corresponding amplitude spectrum observed during the state of intermittency prior to thermoacoustic instability in (a) spray combustor (Pawar *et al.* (2016)) ($Re \approx 2.6 \times 10^3$) and (b) turbulent combustor (Nair *et al.* (2014)) ($Re \approx 1.4 \times 10^4$). The insets show small epochs of periodic oscillations during bursts where the inset of (a) shows regular amplitude modulations in the envelope and the inset of (b) highlights irregularly modulated envelope of the acoustic pressure oscillations

the features of intermittent bursts obtained from model [Fig. 3.9] with that observed through experiments [Fig. 3.8].

Figure 3.8(a) delineates the intermittency signal from a low-turbulence spray combustor where we observe distinct amplitude modulated bursting in the signal and also the occurrence of a sideband frequency in the amplitude spectrum of the acoustic pressure oscillations (Pawar *et al.* (2016)). The corresponding amplitude spectrum has a dominant frequency peak at 268.2 Hz and a sideband frequency at 300 Hz. These features, in turn, indicate the presence of multiple frequencies in the slow subsystems of the combustor.

Similarly, Fig. 3.8(b) illustrates the intermittent oscillations in the acoustic pressure signal obtained prior to thermoacoustic instability in a laboratory-scale bluff-body stabilized turbulent combustor (Nair *et al.* (2014)). The amplitude envelope of the pressure signal has very small and irregular modulations during the high amplitude bursts of periodic oscillations. The amplitude spectrum of this signal shows a single dominant peak around a frequency of 246.9 Hz. This could happen if the nonlinear interaction of the slow and the fast subsystems is incapable of introducing multiple slow frequencies

in the system in the presence of dominant turbulent flow fluctuations.

In order to replicate the feature of amplitude modulated bursting as observed in a laboratory-scale spray combustor [Fig. 3.8(a)], we use the modified model described in Sec. V-A. Figure 3.9(a) shows the intermittent oscillations obtained from the modified model when the value of p'_{th} is approximately 15% of the maximum amplitude of the acoustic pressure oscillations. It is assumed that the control parameter oscillates at a base frequency of 0.17 Hz when the pressure amplitude is below the threshold, while the frequency of the control parameter increases to 8.5 Hz otherwise. Here, we use additive noise alone, i.e., $\sigma_m = 0$ and $\sigma_a = 0.1$. With this approach, we obtain an intermittency signal where the acoustic pressure oscillations switch between high amplitude periodic oscillations and low amplitude aperiodic fluctuations [Fig. 3.9(a)]. Moreover, the occurrence of bursts is not periodic, owing to the fact that the frequency of the slowly oscillating control parameter varies as per the acoustic pressure oscillations which is influenced by the presence of noise in the acoustic field. This is different from the periodically occurring bursts we observed in Fig. 3.3, when the slow and the fast subsystems were not coupled.

The inset of Fig. 3.9(a) shows regular modulations in the amplitude envelope of the acoustic pressure oscillations, which is known as amplitude modulated bursting. The corresponding amplitude spectrum has one dominant peak at the natural frequency of the acoustic field (176.7 Hz) and two sideband frequency peaks at 168.2 Hz and 185.2 Hz. Here, the frequency difference of 8.5 Hz between the dominant frequency and the sideband frequencies is equal to the value of the frequency of the slow oscillations (i.e., 8.5 Hz) introduced in the control parameter, when the amplitude envelope of pressure oscillations is above the designated threshold. This is also the frequency of the modulations in the amplitude envelope of the pressure oscillations during bursts of periodic oscillations. This behaviour reasserts that the presence of multiple slow frequencies of control parameter oscillations is responsible for amplitude modulated bursting, and the higher of these multiple slow frequencies is reflected in the modulations of the amplitude envelope of acoustic pressure during bursts. Such a signal closely replicates the features of the amplitude-modulated limit cycle oscillations observed by Boudy *et al.*

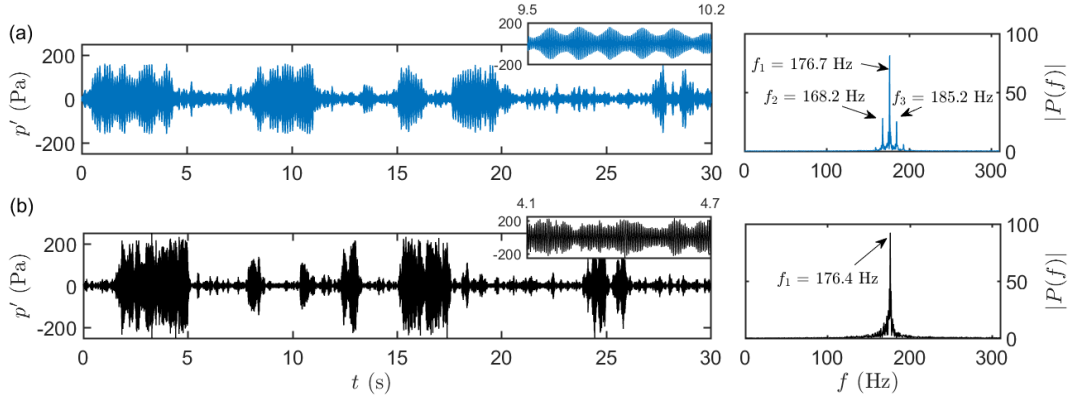


Fig. 3.9: (a) The intermittency signal obtained from the modified model when the pressure threshold is set at $p'_{th} = 25$ Pa. If $p'_{env} < p'_{th}$, frequency of oscillating control parameter c_1 is $f = 0.17$ Hz, while if $p'_{env} > p'_{th}$, then $f = 8.5$ Hz with noise strengths $\sigma_a = 0.1$ and $\sigma_m = 0$. (b) The intermittency signal obtained from introducing additive and multiplicative noise of strengths $\sigma_a = 0.05$ and $\sigma_m = 0.2$, respectively, in the model. The amplitude spectrums corresponding to periodic oscillations of each time series shown in the insets are plotted in the right column.

(2013) in a multiple-flame premixed burner and the amplitude-modulated intermittent oscillations seen in a low-turbulence laboratory-scale spray combustor (Pawar *et al.* (2016)), as shown in Fig. 3.8(a).

On the other hand, Fig. 3.9(b) shows the intermittency signal obtained from the combination of additive and multiplicative noise alone (i.e. without the slow oscillations in the control parameter) in the model [refer to Eq. (3.9)]. Here, we choose the noise intensities such that $\sigma_a < \sigma_m$, since we expect that in low-turbulence systems, the acoustic pressure dynamics would be more strongly influenced by the interaction of the heat release rate and the acoustic pressure oscillations as compared to the effect of turbulent fluctuations. Switching of the acoustic pressure oscillations between periodic and aperiodic oscillations in the presence of noise is obtained when the control parameter value is close to the Hopf bifurcation point. Similar to the previous approach using the modified model, this approach also produces bursts of periodic oscillations at irregular intervals. Furthermore, we observe that the amplitude envelope of the acoustic pressure oscillations has small and irregular amplitude modulations during bursts. The amplitude spectrum corresponding to periodic oscillations in the burst shows only

a single dominant peak at 176.4 Hz and no sideband frequencies. Moreover, if we use $\sigma_a > \sigma_m$, this approach can also produce intermittent bursting similar to that observed experimentally in the intermittency signals obtained from a highly turbulent combustor (Nair *et al.* (2014)) such as that shown in Fig. 3.8(b). Thus, the introduction of additive and multiplicative noise alone in the model aids in capturing the occurrence of bursts in the acoustic field of the combustor. However, unlike the modified model, this approach does not capture the feature of regular amplitude modulated bursting as shown in Fig. 3.9(a).

From comparing our results discussed in Fig. 3.9(a,b), we can postulate to some extent the physical cause of the bursting behaviour observed during intermittency in different combustors. Thermoacoustic systems which show amplitude modulated bursting, i.e., regular modulations in the limit cycle oscillations or the existence of sideband frequencies along with a dominant peak at the natural frequency in the amplitude spectrum are likely to have strongly interacting slow and fast subsystems. On the other hand, if the bursting dynamics portrays irregular modulations in the amplitude of bursts or the envelope of limit cycles or a single dominant frequency peak in the amplitude spectrum, then the system dynamics might be predominantly controlled by the underlying flow fluctuations (background turbulence) and its influence on other various subsystems.

3.7 Summary

In this work, we investigated experimentally and theoretically the role of multiple timescales in the occurrence of bursting dynamics during intermittency in a thermoacoustic system. We conduct experiments on a horizontal Rijke tube and theoretical investigations through a model, both exhibiting subcritical Hopf bifurcation. Bursting dynamics is obtained when the control parameter oscillates at low frequencies about a mean value in the bistable zone of subcritical Hopf bifurcation. In order for sustained bursting dynamics to occur, the amplitude of the control parameter oscillations must be such that these oscillations necessarily cross the Hopf bifurcation point to overcome delayed bifurcation. When the slow and fast subsystems are independent of each other, we

obtain bursting at regular intervals and the bursts are asymmetric. Through model, we explain that the growth and decay patterns are different due to the delayed bifurcation associated with slow oscillations of the control parameter around the Hopf bifurcation point. We showed that the delayed bifurcation of the acoustic pressure fluctuations with respect to the oscillating control parameter is dependent on the frequency, the amplitude and the mean value of the oscillating control parameter.

Further, we present two approaches to model the interaction between the various subsystems. In the first approach, we introduce a coupling between the frequency of the slowly oscillating control parameter and the amplitude envelope of the fast oscillating acoustic pressure in the system. In the second approach, we model the interactions of various subsystems using noise which produces bursts of periodic oscillations with irregular amplitude modulations. The interactions between the subsystems of a thermoacoustic system may be influenced more by either multiple timescales or the underlying flow fluctuations, depending on the experimental conditions. We, thus, provide a possible explanation to various features of bursting oscillations observed during intermittency in thermoacoustic systems.

CHAPTER 4

Preliminary concepts: Complex networks

A brief discussion is presented in this chapter on the importance of using complex networks to analyse complex systems. We also summarise some basic concepts and definitions of measures derived from networks.

4.1 History: Complex networks as a tool to analyse real-world systems

The concept of graphs or networks have been employed since the 1700s to analyse challenging problems. The foundations of graph theory were laid in 1735 by Leonhard Euler who solved the famous Königsberg Bridge problem. The aim of this problem was to find the number of single-pass paths possible through a network of seven bridges (Euler (1956); Gribkovskaia *et al.* (2007)). Graph theory has been developed thereafter and applied to various fields to study interconnected systems. The concepts of path optimization, flow control of computations in computer science, analysis of social interactions in a country are heavily dependent on graph theory. One of the first network models were developed by Paul Erdős and Alfred Rényi in 1959, referred to as random or ER networks today (Erdős and Rényi (2011)). They introduced a model for the evolution of connections in a graph where the connections between nodes are established based on a probability $p \in (0, 1]$. Graphs produced using this model spanned a wide range of network-types starting from fully connected network (at $p = 1$) to random networks with low-density of connections. Their model was based on the assumption that any two nodes are equally likely to be connected. However, nodes in real-world networks do not connect randomly. Rather, there are underlying physical phenomena (such as in fluid systems) or human preferences (such as in social networks) that influence the

possibility of connection between any two nodes. Moreover, ER networks failed to produce high clustering together of a subset of nodes in the network, or the existence of central nodes such as that observed in real networks. For example, in a social network there may be one or two highly influential individuals that connect smaller clusters of the network across each other.

Only in the 1990s, did the concept of complex networks catch the attention of the physics community. Several real-world networks such as airport networks, brain-networks, network of hyperlinks between web-pages were studied. Researchers from disparate fields showed that real world networks exhibit heterogeneous distribution of connections, and some nodes appear to be more important than others. This discovery called for new models to understand real world networks. In the late 1990s, Watts and Strogatz (1998) proposed a network model which now famous as the Watts-Strogatz model. In their model, a network was produced by randomly perturbing and reconnecting a certain number of links in a regular network. This model was able to capture the occurrence of high local clustering and short average path length as observed in real networks, which came to be known as the ‘small-world’ property. However, their model produced non-growing networks that did not have realistic degree distribution (distribution of number of nodes having certain number of connections).

Most real-world network delineate scale-free degree distribution, that is, there are several nodes with low number of connections while a few nodes which have very high connectivity (Barabási and Bonabeau (2003)). In other words, the probability distribution of the degree of connectivity of nodes does not fall into any particular scale and follows a power law. A new model for growing networks was proposed by Albert Barabasi and Reka Albert. Their model, referred to as the BA model (Albert and Barabási (2002)), allowed newly added nodes to build connections with a certain probability which was proportional to the degree of the old nodes. Thus, the nodes developed links based on preferential attachment to high-degree nodes. This model was able to successfully capture the scale-invariance in the degree distribution as observed in real systems; however, it could not capture the high local clustering as achieved by the Watts-Strogatz model. Therefore, there is no perfect network model but a variety of

models to choose from depending the system at hand. Further, several new models are being developed to explain the topology and evolution of connectivity in real networks (Bianconi and Barabási (2001); Krapivsky *et al.* (2000)).

For complex systems such as fluid flows and thermoacoustic systems, the physical interaction between different modes of oscillations cannot be easily identified. Rather, such interactions need to be quantified by either using time series analysis or phase space reconstruction. Several methods of network construction have been employed in literature (Gao *et al.* (2017)). The choice of the method depends on and dictates the information we extract from the dynamics of the system. For example, a network of oscillators may be developed where connections are established based on the extent of synchronization of these oscillators. Then the centrality measures derived from such a network will reflect the local and global picture of synchronization amongst various oscillators. Similarly, networks constructed from the phase space trajectory reflect the topology of the phase space. In Chapter 5, we use cycle networks to analyse the dynamics observed in thermoacoustic systems.

4.2 Basic definitions

A complex network consists of nodes representing the components of a system. These nodes are connected based on physical or abstract connections derived from the interaction between various components of the specific system. Let G represent the graph (network), such that $G \equiv \{V, E\}$ where V represents the set of vertices (nodes) and E represents the set of edges (connections) in the network G . The number of nodes is represented by $N = |V|$ Here, we summarise definitions of some basic properties of complex networks.

Degree Distribution

The number of connections a node has in a network is known as its degree, K . The topology of a network is usually understood through its degree distribution. Let $P(K)$

is the probability that a node has a degree K in the network. Assuming enough number of nodes in the network, one can find $P(K)$ as the percentage of nodes having degree K in the network.

$$P(K) = \frac{1}{N}N(K) = \frac{1}{N} \sum_{i=1}^N \delta(K, k_i) \quad (4.1)$$

where k_i is the degree of node i , and $\delta(x, y)$ is the Kronecker delta function. The plot of $P(K)$ vs K represents the degree distribution of the network. A power law in the degree distribution, as observed in most real networks, indicates the presence of central or hub nodes that are few in number but have very high connectivity.

4.2.1 Centrality measures

Various centrality measures have been developed to quantify the importance of nodes in a complex network (Boccaletti *et al.* (2002)). While these centrality measures are used widely across all type of networks irrespective of how the network is connected, their interpretation is closely tied to the method of construction of the network. Thus, here we summarize the definition of three such measures which will be used to analyse the topology of cycle networks in Chapter 5. Later, in section 5.3, we assign meaning to these centrality measures derived from cycle networks in order to interpret the topology of the phase space.

Closeness centrality

Closeness centrality is a measure that quantifies the distance between nodes. A node having high closeness centrality is at a shorter distance from most nodes in the network. The local closeness centrality of a node is calculated as:

$$C_{close_i} = \frac{1}{\frac{1}{N-1} \sum_j d_{ij}} \quad (4.2)$$

The averaged closeness centrality helps estimate how closely connected are nodes in a network on an average. High average closeness centrality would indicate dense connections and an intricate structure of the network. It is essentially the mean of the closeness

centrality of all nodes in the network, and is calculated as follows:

$$\langle C_{close} \rangle = \frac{1}{N} \sum_{i=1}^N C_{close_i} \quad (4.3)$$

If the complex network is derived from the phase space cycles, we show in Chapter 5 that the average closeness centrality reflects the average correlation of phase space cycles.

Betweenness centrality

Betweenness centrality attributes more significance to nodes that act as a bridge between two otherwise disconnected nodes. A high betweenness centrality indicates the importance of the node in forming a pathway for flow of information or influence between disconnected or unrelated components of the network. Local betweenness centrality is calculated according to Eq. 4.4, where n_{rs}^i represents the number of only those shortest paths between nodes r and s that pass via node i , and g_{rs} represents the total number of shortest paths between the nodes r and s .

$$b_i = \sum_{r,s} \frac{n_{rs}^i}{g_{rs}} \quad (4.4)$$

Averaged betweenness centrality (Eq. 4.5) quantifies the overall capacity of flow of information/ influence in a network. For cycle networks, betweenness centrality helps to quantify the stability of periodic orbits in the phase space as discussed in detail in Chapter 5.

$$\langle C_{BC} \rangle = \frac{1}{N} \sum_{i=1}^N b_i \quad (4.5)$$

Clustering coefficient

Clustering coefficient quantifies how many neighbours of a node are also neighbors of each other. Clustering coefficient thus characterizes the existence of clusters of a subset of nodes in the network which are highly interconnected and provide an important struc-

ture to the network. The local clustering coefficient C_i of node i refers to the density of triangular closures of connections including that node. Local clustering coefficient is zero if the degree of a node is ≤ 1 , else it is calculated as described by Eq. 4.6.

$$C_i = \frac{\text{number of triangles passing via node } i}{k_i(k_i - 1)/2} \quad (4.6)$$

To estimate the overall inter-connectedness of the network, we can find the global clustering coefficient as the average of local clustering coefficient of all the nodes in the network. For cycle networks, we show in Chapter 5 that, average clustering coefficient quantifies the number of periodic orbits in the phase space.

$$\langle CC \rangle = \frac{1}{N} \sum_{i=1}^N C_i \quad (4.7)$$

CHAPTER 5

The onset of thermoacoustic instability via the route of intermittency as a phase transition similar to Bose-Einstein Condensation

5.1 Introduction

5.1.1 Emergence of order from chaos in various turbulent systems

The transition from chaos to order through the route of intermittency is not unique to thermoacoustic systems alone. Emergence of order from chaos has been widely reported in several turbulent systems such as turbulent thermoacoustic (Nair *et al.* (2013); Murugesan and Sujith (2015)), aero-acoustic (Nair and Sujith (2016)) and aeroelastic systems (Venkatramani *et al.* (2017)). These systems initially exhibit low-amplitude aperiodic fluctuations in flow quantities such as acoustic pressure in combustors and aero-acoustic chambers, or in the oscillations of flexible structures. With change in the control parameter of the turbulent system (such as the flow Reynolds number), the dynamics exhibits intermittent oscillations comprising short epochs of periodic oscillations interspersed with aperiodic fluctuations. Such a state of intermittency en route to oscillatory instability in turbulent systems have been reported in thermoacoustic systems such as turbulent combustors (Nair *et al.* (2014)), in aero-acoustic systems (Nair and Sujith (2016)), as well as in aeroelastic systems (Venkatramani *et al.* (2016)). With further increase in the control parameter, order begins to emerge and the system dynamics transitions to self-sustained high-amplitude periodic oscillations, called limit cycle oscillations (LCO).

The occurrence of such high-amplitude periodic oscillations are referred to as oscillatory instabilities, and often adversely affects the health of the system in question. For

example, thermoacoustic instability, which comprises high-amplitude periodic oscillations of acoustic pressure inside a combustion chamber, can lead to structural failure, or overwhelm the thermal protection system (Culick (2006); Sujith and Unni (2020b); Lieuwen and Yang (2005)) and also affect the guidance system of rockets causing mission failures (Fisher and Rahman (2009)). In aero-acoustic systems, such oscillatory instabilities are known to have detrimental effects in systems such as gas-transport pipe networks (Kriesels *et al.* (1995)), and in turbulent cavity flows (Chatellier *et al.* (2004)). Further, aeroelastic flutter observed in flexible structures such as an aircraft wing results in fatigue in the material of the structure and can be disastrous (Garrick and Reed III (1981)). Another classic example of failure due to aeroelastic instability is the catastrophic collapse of the Tacoma bridge (Larsen and Walther (1997)). It is, therefore, essential to characterize the transition from chaos to order and predict the onset of oscillatory instabilities in such turbulent systems.

Several efforts have been made to identify the transitions between different dynamical states of a system. Synchronization theory (Pawar *et al.* (2017)), fractal analysis (Nair and Sujith (2014)), recurrence based techniques (Marwan *et al.* (2008)), complex networks analysis (Murugesan and Sujith (2015); Godavarthi *et al.* (2017); Okuno *et al.* (2015)) and phase space reconstruction methods (Bradley and Kantz (2015)) are some of the many approaches employed to classify the different dynamical states observed in a complex system. Using synchronization theory Pawar *et al.* (2017, 2019) have discussed how the acoustic pressure and heat release rate signals begin to synchronize with each other as order emerges in the dynamics of turbulent combustors. In another study, Raaj *et al.* (2019) have shown that the transition of structural oscillations in an aeroelastic system from a state of aperiodic fluctuations to aeroelastic flutter (high amplitude periodic oscillations) can be viewed as a mutual phase-synchronization between the pitch (torsion) and plunge (bending) motions of the flexible structure.

Some recent efforts have used complex networks approach to characterize the various dynamical states observed in turbulent systems (Iacobello *et al.* (2020)). The transition from chaos to order in turbulent thermoacoustic systems has been discussed using visibility networks. Murugesan and Sujith (2015) showed that the topology of the net-

works derived using visibility algorithm exhibits scale free degree distribution during chaotic dynamics, while this scale free nature is lost as order emerges in the combustor dynamics. Similarly using recurrence networks Godavarthi *et al.* (2017) showed that the topology of the networks derived from the acoustic pressure dynamics of the combustor becomes more orderly as the system transitions from chaos to order. Further, using weighted complex networks derived from phase space cycles, Okuno *et al.* (2015) have studied the pseudo-periodic dynamics obtained during the occurrence of thermoacoustic instability. They show that the distribution of node strengths of such a network follows a power law, and hence the state of thermoacoustic instability corresponds to scale-free weighted network.

5.1.2 A new perspective: Emergence of order from chaos in the phase space as a condensation transition

While the above-mentioned perspectives have proven to be successful in identifying various dynamical states in the system, the understanding of the transition from chaos to order in turbulent systems is far from complete. Some approaches such as visibility algorithm rely on using the information from fluctuations and location of peaks in a time series obtained from experiments, and do not account for the governing structure of the phase space. While recurrence networks do preserve the information about the phase space dynamics, their rich geometric structure makes it hard to interpret and visualize the topology of the phase space. Further, it is difficult to interpret the influence of invariant dynamical attractors in the phase space on the evolution of the trajectory during the transition between various dynamical states.

During the occurrence of chaos, the phase space is characterized by the presence of an infinite number of UPOs, of which some dominant ones may be detected (Auerbach *et al.* (1987); Lathrop and Kostelich (1989); Pawelzik and Schuster (1991)). The phase space trajectory jumps between these UPOs often, as it gets ejected from one UPO and is attracted by a neighboring UPO. As shown in Fig. 5.1, a trajectory may approach a UPO along its stable manifold and get ejected after some time along the unstable

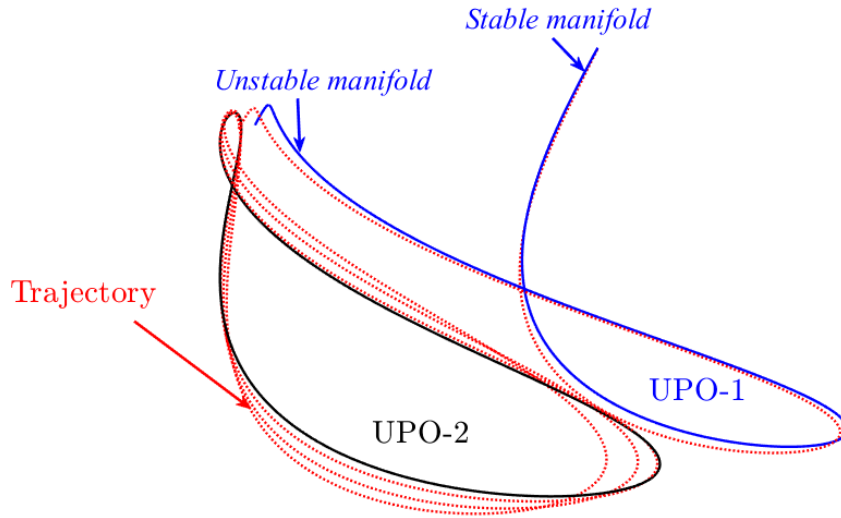


Fig. 5.1: Schematic diagram showing a sample realization of the trajectory around two unstable periodic orbits (UPOs) in the phase space.

manifold. Further, the trajectory gets trapped for a larger number of cycles around a relatively more stable periodic orbit, such as UPO-2, as compared to a relatively less stable periodic orbit, such as UPO-1 in Fig. 5.1, and hence spends a longer duration around the more stable orbits.

Unstable periodic orbits (UPOs) are dynamical invariants (Gunaratne *et al.* (1989)). For, multiple realizations of a chaotic system at the same operating condition, the phase space trajectory can trace distinct paths in each realization. The order in which the trajectory visits the various UPOs in the phase space may differ in each realization. However, the set of UPOs which attract or repel this trajectory in every realization remains the same. On the other hand, during the occurrence of limit cycle oscillations, the phase space consists typically of several cycles located around a single stable orbit in the phase space. It is essential to consider how these structures consisting of periodic orbits in the phase space morph during the transition from chaos to order. Through this study, we introduce a new perspective, that identifies the various dynamical states in a turbulent system based on the structure of the corresponding phase space. Also, we note that while the phase space cycles are associated with several UPOs during chaotic dynamics, these cycles ‘condense’ to a single stable orbit during periodic dynamics. Thus, we intend to cast the emergence of order from chaos in turbulent systems as a “condensation transition” using the phase space cycles and the dynamically invariant

periodic orbits in the phase space.

Condensation transition was first discussed in quantum mechanical systems consisting of indistinguishable particles called Bosons (Bose (1924)), which at room temperature occupy several higher energy states. The temperature of the system is reduced using advanced techniques such as laser cooling, and brought closer to 0 K (practically to 10 μ K). After a certain critical temperature is reached, a large fraction of Bosons begin occupying the lowest energy state of the system (Reif (2009)). The sudden occupancy of the lowest energy state by almost all Bosons in the system below a critical temperature is referred to as Bose-Einstein condensation (Einstein (1924)). In statistical physics, condensation transition means that a large fraction of the ‘particles’ in the system occupy a single ‘energy level’, referred to as the ground state.

Condensation transition has also been discussed in the context of classical systems such as random lasers (Conti *et al.* (2008)), light pulses in a laser cavity (Oren *et al.* (2014)), vehicular traffic systems (Evans (1996); Chowdhury *et al.* (2000)), epidemic spreading (Tang *et al.* (2009)), and many others. Such analogy with the condensation observed in a system of Bosons is made possible by defining ‘particles’ and ‘energy levels’ appropriately for the concerned system. For example, to study the spread of epidemics in analogy to condensation transition, Tang *et al.* (2009) define public places as energy levels, while the people occupying these places are referred to as particles. Using mean-field approximations, they develop a model and prove that the condensation of several people in one place enhances the infection rate and sustains the epidemic for longer duration.

Further, such condensation transition has been discussed for complex networks (Krapivsky *et al.* (2000); Bianconi and Barabási (2001); Su *et al.* (2012)) where despite the non-equilibrium nature of the networks, the ‘particles’ follow Bose statistics and can exhibit Bose-Einstein condensation. Bianconi and Barabási (2001) draw an analogy between networks and a system of Bosons where the nodes of the network are equivalent to energy levels and the links between nodes are considered to be particles. They consider a growing network in which links are added according to a fitness model which assigns a certain fitness parameter to each of the nodes. The energy of a node is

defined through the fitness parameter associated with that node. Using such a model, the authors show that a complex network, initially in the scale-free phase, evolves into a network with a few dominant hubs due to higher fitness and connectivity. Finally, further evolution of the network leads to Bose-Einstein like condensation, where the node with the largest fitness emerges as the ‘ground state’, and a finite fraction of links always connects to this hub-node.

5.1.3 Potential contributions of the new perspective

We ask some intriguing questions in this study that are summarized here. We noted earlier that the number and the stability of phase space orbits differ during chaotic and ordered dynamics. Here, we ask, what is the phase space topology during the intermediate states when the system dynamics transitions from chaos to order, such as the state of intermittency? Moreover, can we characterize the transition of dynamics from chaos to order using measures associated with the the topological transformations in the phase space as order emerges in the system dynamics?

Also, as stated earlier, the occurrence of oscillatory instabilities in turbulent systems can be catastrophic, and it is desirable to identify the onset of such dynamical states. We, therefore, ask if it is feasible to identify the onset of oscillatory instabilities in turbulent systems by studying the topological transformations in the phase space. Finally, we understand that in the purview of statistical physics, condensation transition is associated with the emergence of order in a system of disordered particles. We then ask, is it possible to relate such condensation transition to the emergence of order from chaos in complex systems?

To answer these questions, we analyze the transition from chaotic dynamics to self-sustained periodic oscillations in two types of turbulent systems, namely, a swirl-stabilized (Pawar *et al.* (2019)) and a bluff-body stabilized (Pawar *et al.* (2017)) turbulent combustor. We choose to analyze such thermoacoustic systems since they exhibit transition from chaotic to periodic dynamics, through the route of intermittency, with variation in the control parameter of the system. Further, turbulent combustors are prac-

tically relevant systems, since the onset of thermoacoustic instability in combustors is a major concern in the aviation and the power industries. The various dynamical states observed during experiments in turbulent combustors are discussed in Sec. 2.2.

For the analysis presented in this chapter, we consider the time series of acoustic pressure (p') obtained from turbulent combustors to study the various dynamical states observed in the system. Note that we do not consider the time series of \dot{q}' in our analysis, and therefore do not comment on the occurrence of PS and GS states obtained in these combustors. Instead, we refer to the two types of dynamics obtained in p' during thermoacoustic instability in bluff-body stabilized combustor as weakly and strongly correlated limit cycle oscillations as proposed by Pawar *et al.* (2017). Further, we discuss the transition from chaotic dynamics to limit cycle oscillations via the route of intermittency and identify the onset of thermoacoustic instability in these combustors. For the current study, we use the same data set as reported by Pawar *et al.* (2017) and Godavarthi *et al.* (2018) for the analysis of dynamics in a bluff-body stabilized turbulent combustor, and the data set reported by Pawar *et al.* (2019) for the analysis of dynamics in a swirl-stabilized turbulent combustor.

Here, we use unweighted cycle networks (Zhang and Small (2006)) constructed from acoustic pressure oscillations obtained from these combustors, as discussed in Sec. 5.2. Using the centrality measures and the degree distribution derived from cycle networks, we interpret the phase space structure during various dynamical states and identify the onset of the oscillatory instabilities in these combustors, as discussed in Sec. 5.3 and Sec. 5.4, respectively. Finally, in Sec. 5.5, we conjecture that the emergence of order from chaos in turbulent systems can be viewed as a ‘condensation phenomenon’ in the phase space. We draw an analogy with Bose-Einstein condensation by defining the nodes in the network, i.e., the phase space cycles as particles and the periodic attractors as energy levels whose energy is defined by the connectivity of nodes associated with it. Such a definition is apt, since, higher the stability of a UPO, larger the number of cycles associated with it (Auerbach *et al.* (1987); Lathrop and Kostelich (1989)), and larger the connectivity of the corresponding nodes in the derived network. We also note that such analogy between networks and system of Bosons is different from that defined by

Bianconi and Barabási (2001), and is a novel perspective to condensation in complex networks as well as for the emergence of order from chaos.

5.2 Converting time series of acoustic pressure to cycle network

Zhang and Small (2006) suggested the use of phase space cycles derived from time series obtained from experiments to characterize the dynamics of complex systems that show pseudo-periodic behaviour. They proposed constructing complex networks where the phase space cycles are the nodes in the network, and the correlation between the phase space cycles is associated with the connectivity between nodes. We extend their method, here, to study the transition of the dynamics from chaos to order in a turbulent thermoacoustic system, considering the example of a bluff-body stabilized turbulent combustor. Such phase space visualization of the dynamical states for a swirl-stabilized turbulent combustor reveals similar results, but is not presented here in order to stay concise. The method to build cycle networks from time series, as proposed by Zhang and Small (2006), is described briefly here for the sake of completion.

First, the time series of acoustic pressure fluctuations (p') obtained from experiments in a bluff-body stabilized turbulent combustor (Pawar *et al.* (2017)) is divided into cycles between consecutive local maxima. These cycles in the time series also correspond to cycles in the phase space, which can be reconstructed from the time series by using delay-embedding method (Takens (1981)). The average correlation between any two cycles is calculated using Eq. (5.1) as proposed by Zhang and Small (2006); Zhang *et al.* (2006).

$$\rho_{ij} = \max_{l=0,1,\dots,l_j-l_i} \frac{\text{Cov}(C_i(1:l_i), C_j(1+l:l_i+l))}{\sqrt{\text{var}(C_i(1:l_i))\text{var}(C_j(1+l:l_i+l))}} \quad (5.1)$$

Here, C_i and C_j denote the time series of p' corresponding to the i^{th} and j^{th} cycles respectively, while l_i and l_j (assuming $l_i < l_j$) denote the peak-to-peak lengths of cycles

C_i and C_j , respectively. Also, Cov stands for covariance and var stands for variance. The average correlation between two cycles in the time series is inversely proportional to the average phase space distance between the two cycles in the reconstructed phase space (Zhang *et al.* (2006)). So, the closer the two cycles are in the phase space, the higher is their correlation.

To derive the adjacency matrix $A = [a_{ij}]$ of the unweighted cycle network, we set a correlation threshold ρ_{th} . If the correlation between two cycles i and j is such that $\rho_{ij} > \rho_{th}$, then these cycles are assumed to be connected and $a_{ij} = 1$, else $a_{ij} = 0$. The choice of this correlation threshold ρ_{th} is non-trivial. We may vary this threshold ρ_{th} to reveal several features of the phase space structure during each dynamical state of the combustor, which we discuss in Sec. 5.4. Further, by fixing the threshold, we can differentiate the topology of the derived complex networks for the various dynamical states observed in a turbulent combustor, as discussed in this section and Sec. 5.3.

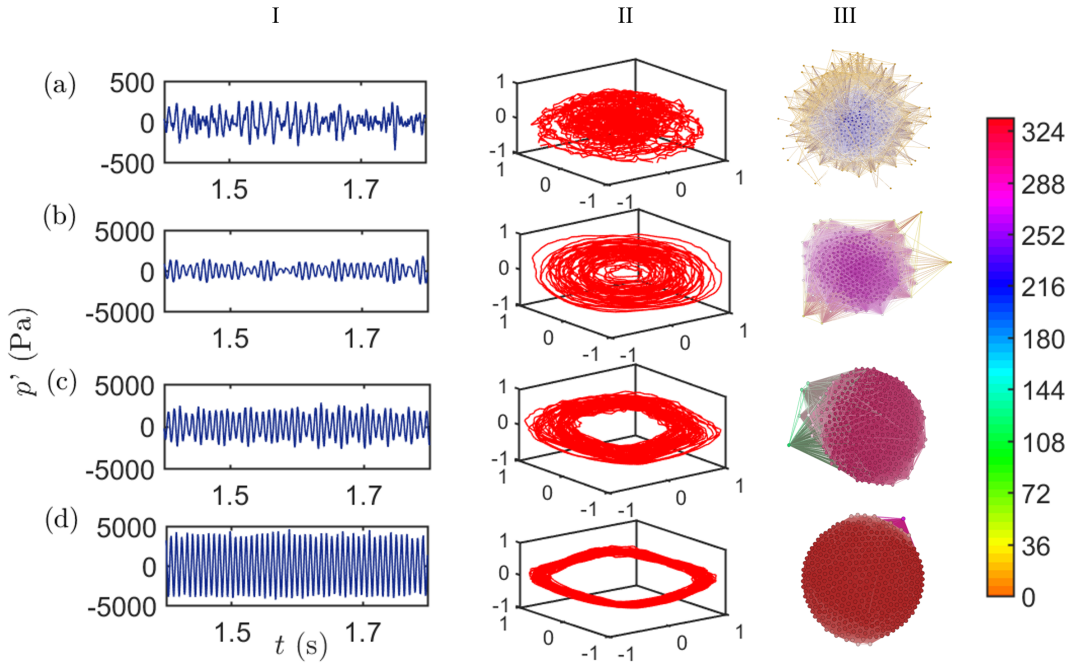


Fig. 5.2: The time series of acoustic pressure fluctuations (I), the corresponding normalised phase space (II) and cycle network (III) during distinct dynamical states namely, (a) combustion noise, (b) intermittency, and (c) weakly correlated and (d) strongly correlated limit cycle oscillations during thermoacoustic instability observed in a bluff-body stabilized turbulent combustor. The adjacent colorbar indicates the degree of nodes across the various dynamical states. The network is derived by setting $\rho_{th} = 0.92$.

Here, we illustrate the topology of the phase space and the cycle networks corresponding to the dynamics of the combustor during the states of combustion noise, intermittency, and thermoacoustic instability (Pawar *et al.* (2017)), through Fig. 5.2(a)-(d). Though we obtain time series of p' for 3 seconds at each value of the control parameter in experiments, we show shorter interval of the time series in Fig. 5.2 for clarity. The phase space is reconstructed from the time series of acoustic pressure fluctuations normalised by their maximum (i.e., $p'/\max(p')$), by using the Takens' delay-embedding method (Takens (1981); Nair and Sujith (2013)). We find the optimum delay time to be 2 ms and the least embedding dimension to be 7 for the state of combustion noise observed in the experiments. For illustration purpose, we plot only three dimensions of the 7-dimensional phase space in column-II of Fig. 5.2. Further, in order to derive and differentiate the unweighted cycle networks during various dynamical states, we set $\rho_{th} = 0.92$. This choice of the correlation threshold is made after examining the connectivity of networks corresponding to the various dynamical states and comparing with that during the state of thermoacoustic instability. In order to obtain maximum variability between the network metrics (in Sec. 5.3) and the topology of the network during various dynamical states, we choose the correlation threshold as the maximum value of ρ_{th} such that the network obtained during the occurrence of strongly correlated LCO (Fig. 5.2(d)) is fully connected. The network is visualized via the Force-Atlas algorithm in Gephi software (Bastian *et al.* (2009)), where nodes having higher connectivity are repelled from all directions and pushed to the center while those with lower degree are repelled to the boundaries. Moreover, the networks are color-coded across the various dynamical states to help differentiate the degree distribution during each state.

The time series of acoustic pressure fluctuations (p') obtained during the state of combustion noise (Fig. 5.2(a) column-I) consists of low-amplitude chaotic fluctuations, and the cycles obtained from such time series are weakly correlated with each other. Hence, most of the nodes in the network in Fig. 5.2(a) column-III are concentrated on the periphery and have very low degrees (≈ 10), while the nodes in the centre mostly correspond to degrees between 100 and 200.

During intermittency, the time series of p' (Fig. 5.2(b) column-I) comprises epochs of periodic oscillations interspersed with epochs of chaotic fluctuations. Further, the phase space diagram (Fig. 5.2(b) column-II) shows that a few of the cycles are oriented in concentric rings spread throughout the phase space indicating significant correlation between these cycles. The trajectory also portrays chaotic motion in the central region of the phase space, and the cycles in this region are very weakly correlated. As a result, the corresponding network (Fig. 5.2(b) column-III) has a lesser fraction of low-degree nodes (degree ≈ 10) protruding outwards as compared to the network in Fig. 5.2(a), while most of the nodes appear to be arranged in a globular structure with their degree around 250. We, therefore, infer that the complex network obtained during the state of intermittency comprises nodes of both high and low degrees.

Further, during thermoacoustic instability, we initially observe amplitude-modulated limit cycle oscillations (LCO), as shown in Fig. 5.2(c) column-I, which may be a signature of pseudo-periodicity. As a result, we obtain several closely spaced concentric rings in the corresponding phase space diagram of this state (Fig. 5.2(c) column-II). Note that, unlike the state of intermittency, there is an absence of chaotic behaviour in the dynamics obtained during this state. In the network derived from the amplitude-modulated LCO (Fig. 5.2(c) column-III), almost all nodes lump together due to their high inter-connectivity (degree around 300), while very few nodes are pushed to the periphery due to low connectivity (with a degree around 100). With further increase in the mass flow rate, we observe high-amplitude periodic oscillations with irregular and negligible amplitude modulation, as shown in Fig. 5.2(d), column-I. As a result, all the cycles are highly correlated to each other, and the corresponding network is fully connected (degree ≈ 350) and forms a globular structure with no outliers.

5.3 Identifying the onset of thermoacoustic instability via network centrality measures

In this section, we wish to investigate the topological transformation in the phase space by studying the variation in the network properties during the transition from chaos to order in turbulent systems. In order to do so, we obtain a complex network corresponding to each time series of acoustic pressure oscillations obtained during the transition from combustion noise to thermoacoustic instability in turbulent combustors. We fix the correlation threshold (as justified earlier for Fig. 1) at $\rho_{th} = 0.92$ for the bluff-body stabilized combustor, and similarly at $\rho_{th} = 0.94$ for a swirl-stabilized combustor to derive these networks. We calculate average network centrality measures (Boccaletti *et al.* (2006)), such as average closeness centrality $\langle C_{close} \rangle$, betweenness centrality $\langle C_{BC} \rangle$ and clustering coefficient $\langle CC \rangle$ of each of the networks, as \bar{u} is varied in the combustor, where $\langle \rangle$ denotes average over all the nodes in the network. Here, we introduce how these centrality measures can help interpret the number and the stability of periodic orbits in the phase space. We also identify the onset of thermoacoustic instability in the combustors. In Appendix B.1, we show that the choice of the point of onset of oscillatory instabilities using network centrality measures is largely unaffected by small variations in the choice of ρ_{th} .

Closeness centrality, C_{close} , is the reciprocal of farness between nodes (Sabidussi (1966); Boccaletti *et al.* (2006)), i.e., a network which is fully connected will have very short average path lengths and will thus have a very high value of $\langle C_{close} \rangle$. For cycle networks, $\langle C_{close} \rangle$ gives a direct measure for the average correlation between phase space cycles. For example, high values of $\langle C_{close} \rangle$ indicate that any two nodes in the network are likely to be linked by a short path length, and thus the distance between the corresponding cycles in the phase space is likely to be small. When cycles of the trajectory are more closely spaced, one can infer that the trajectory jumps between lesser number of UPOs thus delineating periodic dynamics.

Next, we consider the betweenness centrality of nodes, C_{BC} , that characterizes the importance of a node in forming a connection between other nodes of the network

(Freeman (1977); Boccaletti *et al.* (2006)). For cycle networks, $\langle C_{BC} \rangle$ helps quantify the stability of periodic orbits in the phase space. If we assume a phase space consisting of just two neighbouring UPOs, say UPO-1 and UPO-2, of comparable stability, the trajectory would switch often between these two UPOs. Then, a few cycles of the trajectory will be associated with UPO-1 and a few with UPO-2. However, a few cycles which form the transition cycles between UPO-1 and UPO-2 will most probably be correlated to some cycles around both of these UPOs. These transition cycles correspond to nodes with high betweenness centrality in the cycle network. A high value of $\langle C_{BC} \rangle$ thus indicates that the phase space consists of neighboring periodic orbits, and the trajectory often switches between these orbits indicating that these orbits must be highly unstable. Further, a very low value of $\langle C_{BC} \rangle$ indicates the absence of numerous transition cycles, and hence, signifies the presence of highly stable periodic orbit in the phase space.

Another useful measure is the clustering coefficient, CC , which helps quantify how many neighbours of node i are also neighbours of each other in a network (Watts and Strogatz (1998); Boccaletti *et al.* (2006)). For cycle networks, $\langle CC \rangle$ implies a measure of the number of UPOs in the phase space and the connectedness between cycles around these UPOs. In a phase space consisting of a single periodic orbit, all the cycles of the trajectory associated with that orbit are highly correlated, and all the corresponding nodes in the network form a single cluster; thus, $\langle CC \rangle$ is expected to be nearly one. However, in a phase space consisting of numerous UPOs, cycles form small clusters around distinct UPOs leading to multiple small clusters in the network. As a result, the average clustering coefficient of the network is expected to be small.

Figure 5.3 shows the variation of the centrality measures with the increase in the mean flow velocity (\bar{u}) for a bluff-body stabilized turbulent combustor. We observe that $\langle C_{close} \rangle$ and $\langle CC \rangle$ increase gradually for low values of \bar{u} , but show a sharp increase in value at $\bar{u} = 11.1$ m/s, indicating a change in the dynamics. Similarly, $\langle C_{BC} \rangle$ is comparatively high and increases gradually for low values of \bar{u} , but shows a decrease in value after $\bar{u} = 11.1$ m/s. We attribute such a sudden change at $\bar{u} = 11.1$ m/s to the onset of the state of intermittency, while the dynamics observed for $\bar{u} < 11.1$ m/s

is ascribed to the state of combustion noise. Since the value of $\langle CC \rangle$ is small during the state of combustion noise ($\bar{u} < 11.1$ m/s), we infer that the phase space comprises numerous UPOs and the phase space cycles form several small clusters around these numerous UPOs. As a result, these cycles are less correlated on an average and the value of $\langle C_{close} \rangle$ is low during the state of combustion noise. Also, since $\langle C_{BC} \rangle$ is high for $\bar{u} < 11.1$ m/s, we infer that the numerous UPOs in the phase space are highly unstable eventually leading to chaotic switching of the trajectory between various UPOs during the state of combustion noise.

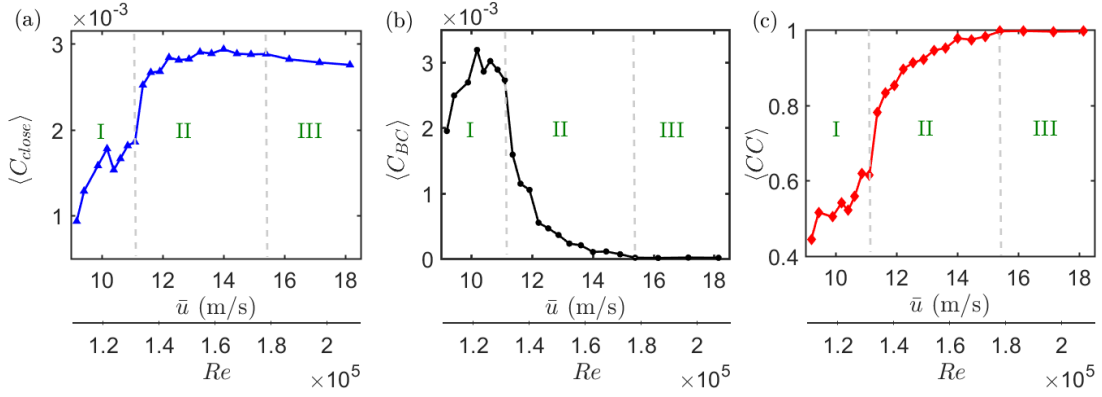


Fig. 5.3: The variation in the average (a) closeness centrality ($\langle C_{close} \rangle$), (b) betweenness centrality ($\langle C_{BC} \rangle$) and (c) clustering coefficient ($\langle CC \rangle$) with the variation in the control parameter (\bar{u} and corresponding Re) of the bluff-body stabilized turbulent combustor, for the derived cycle networks with $\rho_{th} = 0.92$. The regions (I), (II) and (III) correspond to the different dynamical states observed that are combustion noise, intermittency and thermoacoustic instability, respectively (Pawar *et al.* (2017)).

Further, the sharp increase in the values of $\langle C_{close} \rangle$ and $\langle CC \rangle$ at $\bar{u} = 11.1$ m/s in Fig. 5.3 indicates that the number of UPOs decreases and the average correlation of cycles in the phase space increases remarkably at the onset of the state of intermittency. Also, the sharp decrease in the value of $\langle C_{BC} \rangle$ after $\bar{u} = 11.1$ m/s indicates the significant increase in the stability of the UPOs in the phase space during the occurrence of intermittency. We thus infer that, during this state, the phase space consists of some weakly unstable (or moderately stable) periodic orbits along with highly unstable periodic orbits. These weakly unstable periodic orbits attract the trajectory for comparatively longer epochs, due to which more number of cycles of the trajectory become closely spaced and the average correlation of cycles starts increasing. Thus, we obtain epochs of periodic oscil-

lations amidst aperiodic fluctuations in the acoustic pressure dynamics of the combustor during the state of intermittency (Fig. 5.2(b) column-I).

In Fig. 5.3(a), we observe that $\langle C_{close} \rangle$ attains a maximum value and its growth is negligible after $\bar{u} = 14.45$ m/s. Such saturation of the value of $\langle C_{close} \rangle$ indicates the onset of periodic dynamics. Further, the value of $\langle C_{BC} \rangle = 0$ (Fig. 5.3(b)) and $\langle CC \rangle = 1$ (Fig. 5.3(c)) at $\bar{u} = 15.4$ m/s. We thus associate the point $\bar{u} = 15.4$ m/s as the onset of thermoacoustic instability in the bluff-body stabilized turbulent combustor. Note that, $\langle C_{BC} \rangle$ and $\langle CC \rangle$ do not change very rapidly after $\bar{u} = 14.45$ m/s, indicating the possibility of pseudo-periodic dynamics in the regime $14.45 \leq \bar{u} \leq 15.4$ m/s (as shown in Fig. 5.2(c)). Moreover, since we find $\langle C_{BC} \rangle = 0$ during thermoacoustic instability, we infer that no transition cycles exist in the phase space. Thus, a highly stable periodic orbit governs the phase space dynamics during the occurrence of thermoacoustic instability. As a result, we observe almost constant amplitude limit cycle oscillations in the time series of p' (refer column-I of Fig. 5.2(d)).

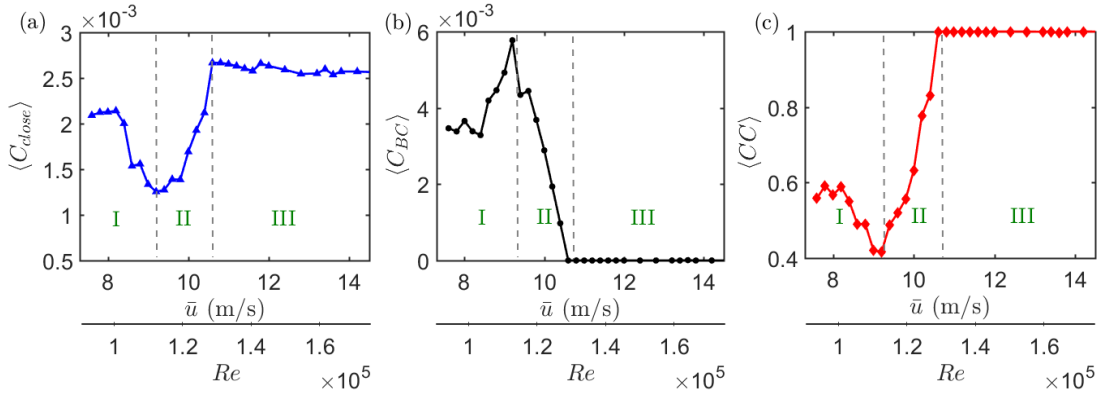


Fig. 5.4: The variation in the average (a) closeness centrality (C_{close}), (b) betweenness centrality (C_{BC}) and (c) clustering coefficient (CC) with the variation in \bar{u} (and corresponding Re) of a swirl-stabilized turbulent combustor for the derived cycle networks with $\rho_{th} = 0.94$. The regions (I), (II) and (III) correspond to the different dynamical states observed that are combustion noise, intermittency and thermoacoustic instability, respectively (Pawar *et al.* (2019)).

Similarly, we plot the variation of average network centrality measures during the transition of the dynamics from chaotic to periodic in a swirl-stabilized turbulent combustor in Fig. 5.4. We observe that the values of $\langle C_{close} \rangle$ and $\langle CC \rangle$ initially decrease for $\bar{u} < 9.2$ m/s and then increase after $\bar{u} = 9.2$ m/s, indicating that the number of UPOs

which influence the phase space trajectory first increases and then decreases. Moreover, the value of $\langle C_{BC} \rangle$ initially increases and then decreases, indicating that the stability of these UPOs declines for $\bar{u} < 9.2$ m/s but increases after $\bar{u} = 9.2$ m/s. We identify the point $\bar{u} = 9.2$ m/s, at which all the three centrality measures reverse their trends, as the point of onset of the state of intermittency. Also, we infer that the phase space dynamics becomes significantly more chaotic with \bar{u} during the occurrence of combustion noise, while a notable transition occurs at the onset of the state of intermittency. Such reversal in the variation of these centrality measures also implies that the flow dynamics changes drastically at the onset of the state of intermittency in a swirl-stabilized combustor.

We understand that in a swirl combustor, the turbulent fluctuations are very significant as compared to the mean, and the intense turbulent fluctuations that exist downstream of the center-body disrupt the formation of organized coherent structures (Reddy *et al.* (2006); Huang and Yang (2009)). Here, we conjecture that as the mean flow velocity \bar{u} (and hence the Reynolds number) increases, the flow becomes more turbulent and chaotic dynamics becomes more significant during the occurrence of combustion noise. However, after a critical Reynolds number, the flow dynamics becomes more orderly due to the occurrence of large periodic coherent structures. As a result, periodicity emerges amidst chaos and we see a reversal in the trend of the network centrality measures (Fig. 5.4). Furthermore, $\langle C_{close} \rangle$ saturates to a maximum, $\langle C_{BC} \rangle = 0$ and $\langle CC \rangle = 1$ after $\bar{u} = 10.6$ m/s, which we identify as the point of onset of thermoacoustic instability, in the swirl-stabilized combustor (Pawar *et al.* (2019)).

In summary, we propose a new method to visualize the topology of the phase space and interpret the number and stability of periodic orbits in the phase space using network centrality measures such as clustering coefficient, closeness centrality and betweenness centrality. Also, we differentiate the various dynamical states and identify the point of onset of oscillatory instability in two distinct turbulent combustors. Further, we note that the variation of network centrality measures helps conjecture the transitions in the flow dynamics of these combustors with variation of the control parameter \bar{u} .

5.4 Deriving the phase space topology from the degree distribution of cycle networks

In the previous sections, we examined the topology of the phase space and the corresponding topology of cycle networks during the various dynamical states observed in turbulent combustors. To do so, we had justifiably chosen and fixed the correlation threshold at some ρ_{th} . However, there is no accurate choice for the value of ρ_{th} and different choices of this threshold reveal significant features of the structure of the phase space. We can exploit this fact to our benefit and acquire qualitative information about the number and the stability of the UPOs in the phase space by varying ρ_{th} . An easy way to do so is using the two-dimensional (2D) degree distribution as proposed by Zhang and Small (2006).

Towards this purpose, during each dynamical state observed in the turbulent combustors, we obtain the degree distribution of the cycle networks derived from the acoustic pressure oscillations while the correlation threshold is varied in the range $0.5 < \rho_{th} < 0.99$. We then plot a series of degree distributions with variation in ρ_{th} referred to as the two-dimensional (2D) degree distribution (Zhang and Small (2006)) in Sec. 5.4.1. We then quantify the variation of these peaks in the 2D degree distribution using a quantity called the variance of the normalized derivative (*VND*) in Sec. 5.4.2

5.4.1 2D Degree Distribution

Peaks in the degree distribution of cycle networks indicate the existence of periodic orbits in the phase space (Zhang and Small (2006)). A trajectory which approaches a UPO along its stable manifold can last for several cycles around that UPO depending on the stability properties of such an orbit (see Fig. 5.1). All the cycles associated with a particular UPO will be spatially adjacent, and thus highly correlated. As a result, all these cycles will be connected to each other in the corresponding network and will have almost the same degree, thus leading to a peak in the degree distribution. Further, a small value of the correlation threshold, ρ_{th} , corresponds to a large value of a phase

space distance threshold, D_{th} , in the cycle networks since correlation and phase space distance of cycles are inversely related (Zhang *et al.* (2006)). If the value of ρ_{th} is high, i.e., the value of D_{th} is small, then only those nodes in the network are connected which correspond to very closely spaced cycles in the phase space and have distance $D < D_{th}$. However, if we decrease the correlation threshold (or correspondingly increase D_{th}), then even those phase space cycles, which are probably on different but neighboring UPOs may be close enough such that their phase space distance is lesser than the specified threshold D_{th} , and the corresponding nodes in the network will be connected. As a result, cycles associated with distinct but neighboring UPOs will be represented by the same peak, and the number of peaks in the degree distribution shall decrease with increase in D_{th} . In other words, if we increase the correlation threshold, we expect that the number of peaks in the degree distribution will increase, if the phase space comprises several UPOs.

Also, depending on where these peaks occur in the degree distribution as the correlation threshold is increased, we can infer the stability of the periodic orbits in the phase space. A highly unstable periodic orbit will attract the trajectory rarely, and the number of cycles of the trajectory around this orbit will also be lesser as compared to a periodic orbit with higher stability. As a result, the cycles associated with a highly unstable periodic orbit will correspond to low-degree nodes in the cycle network. Thus, in the degree distribution of a cycle network, a peak around low-degrees indicates the presence of highly unstable periodic orbits that lead to chaotic dynamics. However, a peak around comparatively higher degrees in the degree distribution indicates the presence of weakly unstable periodic orbits that trap the trajectory for longer epochs, and thus cause periodic dynamics. Further, if there exists a highly stable periodic orbit, then for low as well as high values of the correlation threshold, the degree distribution would comprise a single dominant peak.

The 2D degree distribution obtained by varying the correlation threshold reveals the number and the relative stability of the periodic orbits in the phase space. With this in mind, we examine the 2D degree distribution of the various dynamical states in a bluff-body stabilized turbulent combustor, as the dynamics transitions from chaos to order in

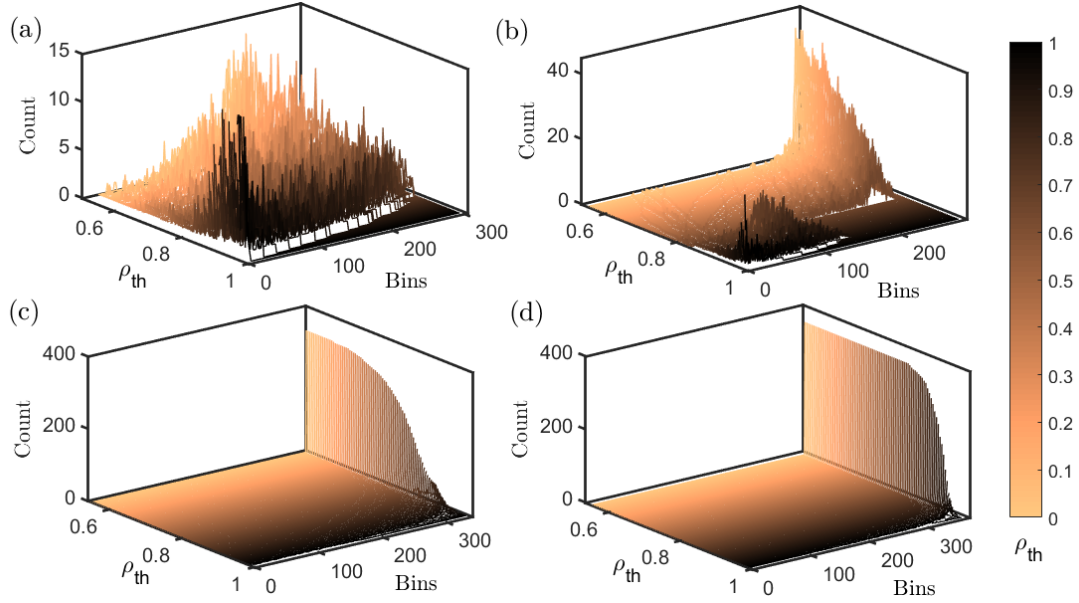


Fig. 5.5: 2D degree distribution showing the variation of the degree distribution of cycle networks obtained from the time series of acoustic pressure oscillations with the correlation threshold, during the states of (a) combustion noise, (b) intermittency, (c) weakly correlated and (d) strongly correlated limit cycle oscillations observed in a bluff-body stabilized turbulent combustor. Here, ρ_{th} is varied from 0.55 to 0.99 in steps of 0.001. Bins refer to degrees and count refers to the number of nodes having certain degree.

Fig. 5.5. A similar visualization may be done, and similar inferences may be drawn for the dynamics observed in a swirl-stabilized combustor as well.

Figure 5.5(a) shows the 2D degree distribution during the state of combustion noise, which is known to consist of chaotic fluctuations of moderately high dimensions (Nair *et al.* (2013); Tony *et al.* (2015)). For low as well as high values of ρ_{th} , we obtain several peaks in the degree distribution spread in the range of 100 to 200 degree, which indicate the presence of multiple UPOs in the phase space. Chaotic dynamics is known to have infinitely many UPOs, of which only a few dominant ones can be detected, and we detect these dominant UPOs through the peaks in the degree distribution. As the correlation threshold (ρ_{th}) increases, we find that the number of peaks in the degree distribution increases and more peaks occur at lower degrees (≈ 40). As a result, we infer that the phase space of chaotic dynamics obtained during the state of combustion noise consists of several closely-spaced highly-unstable periodic orbits.

Figure 5.5(b) shows the 2D degree distribution for the state of intermittency ob-

tained prior to thermoacoustic instability. For low values of ρ_{th} we obtain a few dominant peaks at degrees around 250 which remain significant for a certain range of the correlation threshold ($0.55 < \rho_{th} < 0.75$). We note that these peaks occur at slightly higher degrees as compared to those in Fig. 5.5(a). Due to such peaks around high degree values, we infer that the phase space consists of a few weakly unstable (or moderately stable) periodic orbits, as compared to the highly unstable periodic orbits during the state of combustion noise. When the trajectory approaches these weakly unstable periodic orbits, it is trapped for a greater number of cycles which manifests as short epochs of periodicity in the time series of acoustic pressure oscillations. However, with further increase in the threshold value ($\rho_{th} > 0.75$), such dominant peaks decline and multiple peaks appear near the low-degrees in the degree distribution (around ≈ 50). Such low-degree peaks show that the phase space also consists of several closely-spaced highly unstable periodic orbits which cause chaotic fluctuations for short epochs. In summary, during the state of intermittency, isolated and moderately stable periodic orbits co-exists with multiple closely-spaced highly unstable periodic orbits in the phase space.

The 2D degree distribution during weakly correlated LCO (see Fig. 5.5(c)) shows a dominant peak at very high degree (around 300) which remains dominant despite the increase of the correlation threshold. Such 2D degree distribution clearly delineates that during this state, the phase space consists of a dominant periodic orbit with very high stability. However, for very high values of ρ_{th} (when $\rho_{th} > 0.8$), the dominant peak declines and a few high-degree peaks arise in the degree distribution. These multiple high-degree peaks indicate that two or more closely spaced sub-period orbits may exist in the phase space and these orbits are of comparable stability. As a result, the trajectory delineates periodic motion even while switching between these orbits, and the acoustic pressure dynamics delineates pseudo-periodic behaviour.

A similar distribution is obtained during the state of strongly correlated LCO as well, as shown in Fig. 5.5(d). The peak at very high degree (≈ 350) in Fig. 5.5(d) remains dominant for a larger range of ρ_{th} ($0.55 < \rho_{th} < 0.92$), as compared to Fig. 5.5(c). Clearly, the phase space consists of a periodic orbit of much higher stability during the occurrence of thermoacoustic instability. Note that $\rho_{th} = 0.92$ is the max-

imum ρ_{th} for which the network during the occurrence of strongly correlated LCO is fully connected. However, we extend the analysis of degree distribution to $\rho_{th} > 0.92$ to check for the stability of the periodic orbit obtained during this state. We find that the peak corresponding to the periodic orbit remains dominant even for higher correlation threshold (for $\rho_{th} > 0.92$) indicating that the periodic orbit detected during thermoacoustic instability is indeed highly stable and no other periodic orbits are detected.

To summarize, we find that several low-degree peaks occur with varying correlation threshold during combustion noise, indicating the presence of several highly unstable periodic orbits in the phase space. During intermittency, we obtain high-degree peaks for low values of ρ_{th} , as well as low-degree peaks for high values of ρ_{th} . Such 2D degree distribution indicates the coexistence of weakly unstable periodic orbits and highly unstable periodic orbits in the phase space. Finally, during thermoacoustic instability, we obtain a single dominant peak for all values of ρ_{th} , indicating the presence of a stable periodic orbit in the phase space.

5.4.2 Quantifying the peaks in the 2D degree distribution: VND

A quantity that can differentiate the stability and the number of periodic orbits during each dynamical state of the turbulent combustors is clearly desirable. We, use a measure called the variance of the normalized derivative (VND) obtained from the 2D degree distribution (Zhang and Small (2006)) to characterize the number of peaks in the distribution. Let DD denote the 2D degree distribution, which is essentially a two-dimensional matrix, where a row (denoted by index i) consists of the degree distribution corresponding to a particular ρ_{th} , and the column index j indicates the degrees. Now, DD' denotes the normalized derivative of the 2D degree distribution DD , and the variance of DD' gives VND , i.e., $VND = var(DD')$. The normalized derivative DD' is calculated as given by Eq. (5.2). Note that the normalization of the derivative of the 2D degree distribution we have introduced is different from what was originally proposed by Zhang and Small (2006). To calculate VND for each dynamical state, we vary the correlation threshold in the range $0.55 < \rho_{th} < 0.99$ in steps of 0.001. If we vary ρ_{th} with steps smaller than 0.001 (say 0.0005), we obtain the same results, that is, VND

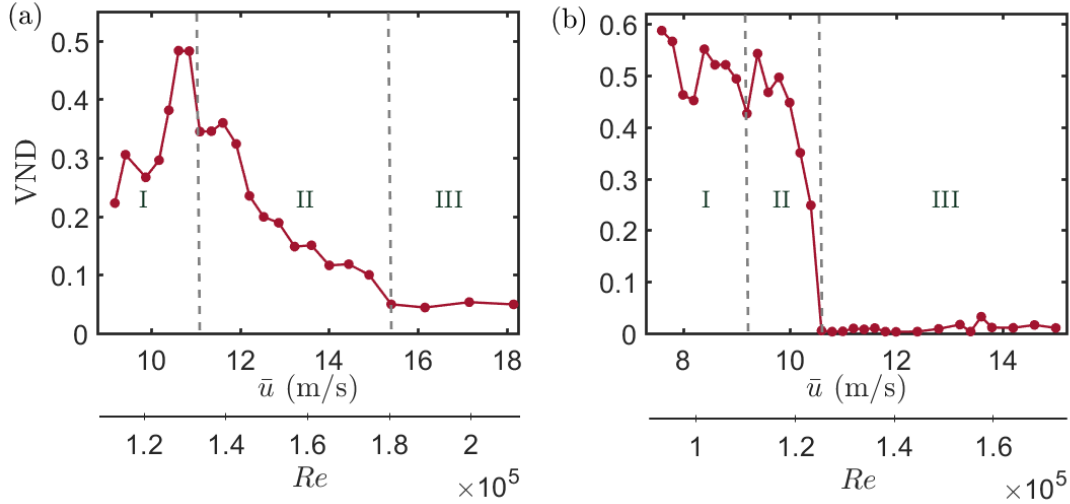


Fig. 5.6: Variation of VND (variance of the normalized derivative) of the 2D degree distribution with the control parameter (\bar{u} and corresponding Re) for (a) bluff-body and (b) swirl stabilized turbulent combustors. The dynamical states of the combustor are demarcated by I-combustion noise, II-intermittency and III-thermoacoustic instability. Here, ρ_{th} is varied from 0.55 to 0.99 in steps of 0.001.

converges when ρ_{th} is varied in steps of 0.001. Further, we have justified the choice of the range of ρ_{th} for the calculation of VND in Appendix B.2.

$$DD'(i, j) = \frac{DD(i, j+1) - DD(i, j)}{DD(i, j+1) + DD(i, j)} \quad (5.2)$$

The VND measure characterizes the fluctuations in the 2D degree distribution. At the location of a peak, the local derivative of the degree distribution will be high in value. Larger the number of peaks and larger the variation in the heights of these peaks, larger the variance in the local derivative values throughout the 2D degree distribution. Further, we understand that for dynamics involving greater number of UPOs, the number of peaks in the 2D degree distribution will be higher (Zhang and Small (2006)). As a result, high value of VND implies the presence of greater number of UPOs in the phase space, and hence implies more chaotic dynamics. In Fig. 5.6(a,b) we plot VND as a function of the control parameter \bar{u} , as the combustor dynamics transitions from combustion noise (chaos) to thermoacoustic instability (order) via intermittency in bluff-body and swirl stabilized combustors, respectively. We also demarcate the regions

corresponding to the states of combustion noise (I), intermittency (II) and thermoacoustic instability (III) based on the classification that we introduced earlier in Sec. 5.3.

In Fig. 5.6(a), we observe that, during the state of combustion noise in a bluff-body stabilized combustor, the value of VND increases and attains a maximum value of $VND \approx 0.5$. Such an increase in the value of VND with \bar{u} during the state of combustion noise indicates increase in the number and decrease in the stability of unstable periodic orbits in the phase space. Also, the increase in $\langle C_{BC} \rangle$ in Fig. 5.3(b) (in Sec. 5.3) indicates a decline in the stability of periodic orbits during the occurrence of combustion noise. On the other hand, increase of $\langle C_{close} \rangle$ and $\langle CC \rangle$ in Fig. 5.3 delineates an increase in the correlation between phase space cycles, and thus increase in periodic dynamics. We therefore infer that the occurrence of both chaotic and periodic dynamics increases in a bluff-body stabilized turbulent combustor with increase in \bar{u} , where chaotic dynamics dominates during the occurrence of combustion noise.

Moreover, the value of VND declines significantly and monotonically during the state of intermittency (region-II), and then saturates to a very low value (≈ 0.05) at the onset of thermoacoustic instability. We then infer that the number of UPOs in the phase space decreases, while their stability increases with \bar{u} . Further, the saturation of VND to a very low value indicates the onset of oscillatory dynamics in the bluff-body stabilized turbulent combustor.

For a swirl-stabilized combustor (Fig. 5.6(b)), $VND \approx 0.6$ during the state of combustion noise. We infer that, with increase in \bar{u} , the number of UPOs in the phase space increases, while their stability decreases slightly during the state of combustion noise, as also inferred earlier from Fig. 5.4. With further increase in \bar{u} , VND declines monotonically during the state of intermittency and saturates to almost zero after the onset of thermoacoustic instability in the combustor. Thus, again, we infer that the dynamics becomes significantly more chaotic with increasing \bar{u} during the state of combustion noise, while order begins to emerge at the onset of the state of intermittency. Also, the saturation of VND to zero helps identify the onset of thermoacoustic instability in a swirl-stabilized turbulent combustor.

Therefore, the variation of VND and centrality measures with the control param-

eter (\bar{u}) of the combustors delineate the transformation of the phase space from (i) a set of several closely-located highly unstable periodic orbits during the occurrence of combustion noise, to (ii) a set of isolated moderately stable periodic orbits in coexistence with highly unstable periodic orbits during the state of intermittency, and finally to (iii) a highly stable periodic orbit during thermoacoustic instability. The saturation of VND at the onset of oscillatory dynamics indicates that the phase space has morphed completely into a stable limit cycle oscillator.

5.5 Analogy with Bose-Einstein Condensation

Using network centrality measures in Sec. 5.3, and also by studying the variation of network degree distribution with the correlation threshold in Sec. 5.4, we have elucidated the topological transformation of the phase space during the emergence of order from chaos in turbulent combustors. We observed that cycles are initially associated with different UPOs of varying stability during the state of combustion noise. However, with increasing control parameter, the cycles of the trajectory form clusters around more stable UPOs during the state of intermittency and finally “condense” to the most stable periodic orbit at the onset of thermoacoustic instability.

With this observation in mind, we now draw an analogy between the topological transformation of the phase space structure during the transition from chaos to order in a turbulent system and the well-known Bose-Einstein condensation observed for Bosons (Bose (1924); Einstein (1924)). In order to do so, we define the phase space cycles as particles and the periodic orbits as energy levels such that a more stable periodic orbit will have lower energy. The immediate concern then is, with what measure do we define the energy of these UPOs? As noted earlier, higher the stability of a UPO, higher is the number of cycles associated with that UPO, and higher is the degree of the corresponding nodes in the cycle network. Thus, a convenient measure to quantify the energy of phase space orbits is the degree of the nodes corresponding to the cycles associated with these orbits. Note that the total number of nodes (N) varies from one network to another due to the varying time series structure obtained during different dynamical

states. Thus, in order to compare across various dynamical states, we normalize the degree of nodes in a network with the maximum possible degree in that network, i.e. $k_{max} = N - 1$. We then treat nodes (cycles) as particles and define energy levels such that energy $\varepsilon = 1 - k/k_{max}$, where k is the degree of a node in the network.

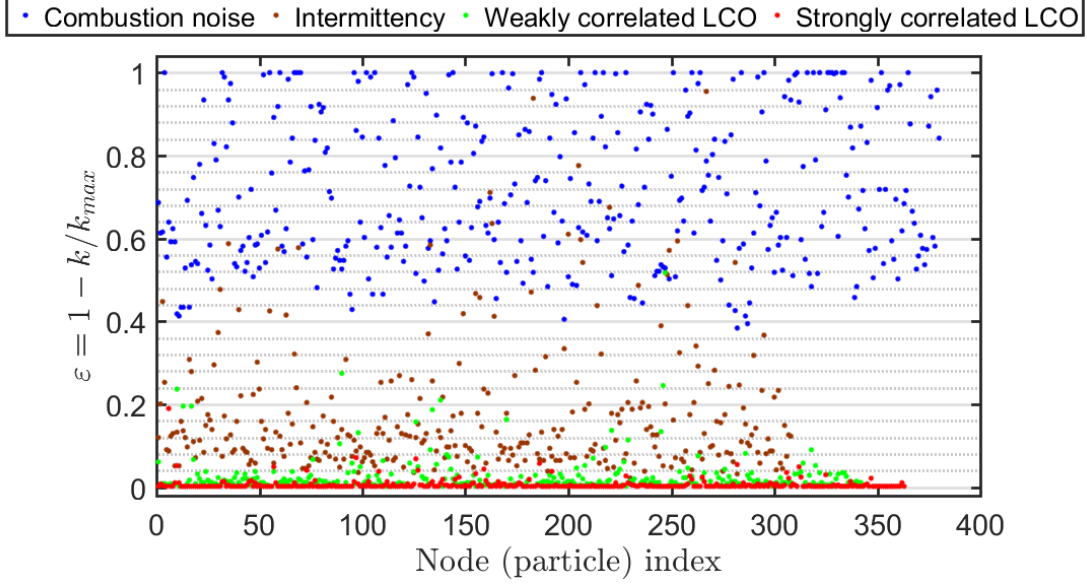


Fig. 5.7: Distribution of nodes (particles) in energy levels whose energy is defined as $\varepsilon = 1 - k/k_{max}$ (where $k_{max} = N - 1$ and N is the number of nodes in the network), during different dynamical states of operation in a bluff-body stabilized turbulent combustor ($\rho_{th} = 0.92$). The dynamical states shown are combustion noise (blue), intermittency (brown), weakly correlated (green) and strongly correlated (red) limit cycle oscillations (LCO) during thermoacoustic instability.

We derive the cycle networks for each state during the transition from chaos to order in the bluff-body stabilized turbulent combustor, with $\rho_{th} = 0.92$ (as justified in Sec. 5.2). Figure 5.7 shows the typical distribution of particles in different energy levels during the different dynamical states observed in a turbulent combustor. We observe that during the occurrence of combustion noise, the particles are distributed across a large number of high energy levels, which shows the presence of numerous highly unstable periodic orbits in the phase space. Further, during the state of intermittency, the particles move to slightly lower energy levels and are distributed across a smaller range of such energy levels. Since the range of energy levels across which particles are spread reduces, we infer that with further increase in \bar{u} , the number of UPOs in the phase space decreases. Moreover, since the particles occupy lower energy levels, we understand that

the stability of the UPOs in the phase space increases during the state of intermittency. Further, during the occurrence of weakly correlated LCO (as shown in Fig. 5.2(c)), we find that a significant fraction of particles occupy very low energy levels over a very small range, which characterizes the condensation process. Finally, during the occurrence of strongly correlated LCO (as shown in Fig. 5.2(d)), a large fraction of particles condense to the lowest possible energy level.

Such comparison between the transformation of network topology and particle distribution in energy levels through Fig. 5.7 immediately establishes a visual understanding about the change in the distribution of phase space cycles around the periodic orbits in the phase space, as the system dynamics transitions to order from chaos. Due to the definition of the energy of periodic orbits being $\varepsilon = 1 - k/k_{max}$, we are able to simultaneously capture the variation in the number of periodic orbits in the phase space, as well as compare their stability during various dynamical states observed in the combustor. To further examine the distribution of particles in the energy levels during the various dynamical states, we plot (in Fig. 5.8) the variation of the fraction of particles that occupy very low energy levels (i.e., ground state) with variation of the control parameter \bar{u} , for both the bluff-body and the swirl stabilized turbulent combustors. The energy-band of the ground state is assumed to be $\varepsilon \leq \varepsilon_0$, where the order of magnitude of $\varepsilon_0 \approx 10^{-2}$ or lower. (Here, we choose the lowest possible value of ε_0 , such that condensation to the lowest energy state is observed in the system.)

When either of the turbulent combustors operate in the state of combustion noise or intermittency, we observe from Fig. 5.8 that the percentage of particles in the energy levels below ε_0 is negligible (≈ 0). All the particles are distributed in energy levels higher than ε_0 . Further, for our experiments in the bluff-body stabilized combustor (Fig. 5.8(a)), we observe that the percentage of particles in energy levels having $\varepsilon \leq \varepsilon_0$ becomes significant at the onset of thermoacoustic instability (at $\bar{u} = 14.45$ m/s) demarcating the onset of ‘condensation’. We find that this percentage saturates at a maximum value of 68% for $\bar{u} \geq 14.45$ m/s indicating that not all phase space cycles condense to the same phase space orbit and may be attracted by closely located but less dominant periodic orbits (or sub-periods), which further implies the possibility of

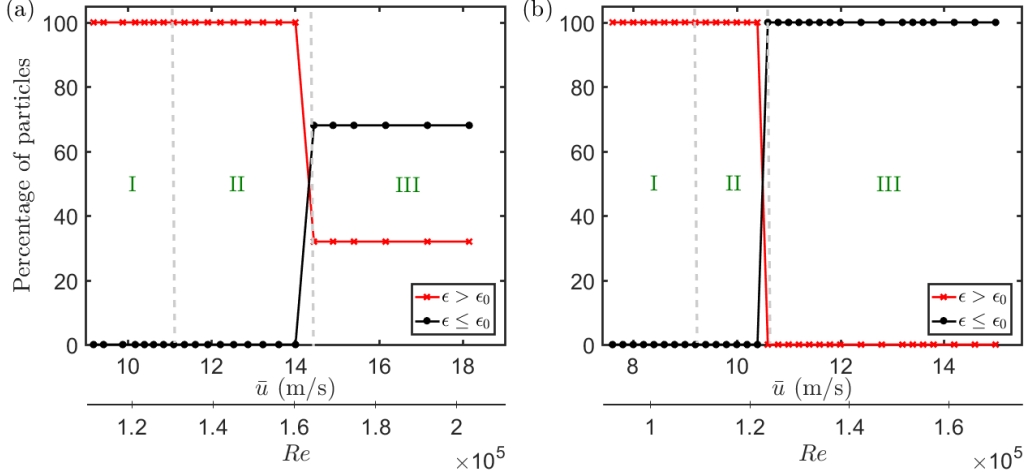


Fig. 5.8: The variation in the percentage of particles (nodes) which occupy energy levels less than (black) and more than (red) ϵ_0 with variation in \bar{u} (and corresponding Re) for (a) bluff-body and (b) swirl stabilized combustors, where $\epsilon_0 = 0.003$ in both cases. The regions (I), (II) and (III) correspond to the different dynamical states observed in these combustors namely combustion noise, intermittency and thermoacoustic instability respectively.

occurrence of pseudo-periodic dynamics in the system. Further, in our experiments in the swirl combustor (Fig. 5.8(b)), this percentage reaches a maximum of 100% at the onset of thermoacoustic instability (at $\bar{u} = 10.6$ m/s) characterizing the occurrence of constant-amplitude LCO in the dynamics. Thus, we identify the onset of thermoacoustic instability in a turbulent combustor as the point when a significant fraction of particles occupy energy levels equal to or below ϵ_0 . Also, we differentiate the occurrence of pseudo-periodic limit cycle oscillations as a state of partial condensation, i.e., the percentage of particles occupying the ground state is significant but $< 100\%$, while constant-amplitude limit cycle oscillations as a state of complete condensation.

Thus, the transition of the combustor dynamics from chaos (combustion noise) to order (thermoacoustic instability) can be viewed as a condensation phenomenon similar to that observed in a system of Bosons. We claim that such analogy between the transition from chaos to order and condensation transition can be used to identify the onset of oscillatory instabilities in turbulent systems as shown here for a thermoacoustic system. Finally, such an analogy also provides a clear understanding about the topological transformation in the structure of the phase space during the emergence of order from chaos. It may be possible to infer the implications of such transition in the physical flow field

of the turbulent systems by investigating the spatio-temporal dynamics of these systems. Further, we believe that such analogy with the condensation phenomenon can potentially provide quantitative measures to study the transition from chaos to order in turbulent systems such as turbulent thermoacoustic, aeroelastic and aero-acoustic systems.

5.6 Summary

In this chapter, we consider the problem of transition from chaotic dynamics to ordered oscillatory dynamics observed in turbulent thermoacoustic systems. We consider the examples of bluff-body and swirl stabilized turbulent combustors, in which we observe transition from combustion noise (chaos) to thermoacoustic instability (order) via the route of intermittency. We construct unweighted cycle networks from the time series of acoustic pressure oscillations during various dynamical states observed in these thermoacoustic systems. We show that transition from combustion noise to thermoacoustic instability in a combustor can be viewed as the transformation of a random network to a fully connected network. We also study the 2D degree distribution of cycle networks during various dynamical states of the combustor, obtained by varying the correlation threshold. The variation in the number of peaks in the degree distribution with the correlation threshold helps reveal the underlying structure of the phase space. We identify the onset of thermoacoustic instability by studying the variation of peaks using variance of the normalized derivative (VND) of the 2D degree distribution.

Further, we use network centrality measures to characterize the transformation in network topology and relate it to the transformation in the phase space with variation in the system control parameter (\bar{u}). Using average closeness centrality, we are able to comment on the increasing correlation between cycles of the phase space with \bar{u} . Using average betweenness centrality, we discuss the increasing stability of UPOs in the phase space with \bar{u} and explain the occurrence of pseudo-periodicity in the acoustic pressure dynamics during thermoacoustic instability. Finally using average clustering coefficient, we illustrate that the number of dominant UPOs in the phase space decreases

with \bar{u} . Also, these average centrality measures are used as a means to identify the onset of thermoacoustic instability.

Finally, we draw a parallel between condensation of Bosons into the lowest energy level and condensation of cycles into the most stable periodic orbit in the phase space. Using this formulation, we provide a measure of stability of the UPOs in the phase space, in terms of the degree of nodes corresponding to the cycles associated with that UPO. Thus, an immediate helpfulness of the complex network framework and statistical physics analogy is established.

CHAPTER 6

Conclusions and Scope of the study

6.1 Conclusions

The aim of this thesis is to investigate and understand the occurrence of intermittency state prior to the onset of thermoacoustic instability in laminar and turbulent combustors. Intermittency observed prior to the onset of thermoacoustic instability is characterized by the occurrence of bursts of high amplitude periodic oscillations amidst low amplitude aperiodic fluctuations. It is desirable to analyse as well as understand the phenomena leading to such intermittent dynamics. In Chapter 2, we describe the experimental set-ups referred to in this thesis.

First, we develop a physical intuition of how intermittency occurs in the acoustic pressure dynamics of laminar and turbulent thermoacoustic system. In Chapter 3, we assert that the bursting behaviour obtained during the occurrence of intermittency is predominantly caused by either turbulence or multiple timescales (slow-fast system) or their combined presence, depending on the features of the system. To prove our conjecture, we perform experiments in a horizontal Rijke tube and also construct a theoretical model for the same. Slow-fast dynamics is investigated by externally introducing oscillations in the control parameter (i.e. heater power) with a frequency which is orders of magnitude lesser than the frequency of acoustic fluctuations.

We observe that turbulence-induced bursting has no clear demarcation of transition from periodic to aperiodic oscillations and the amplitude envelope of the pressure oscillations are very noisy. Bursting behaviour caused by slow-fast dynamics, on the other hand, has distinct transitions from high amplitude periodic to low amplitude aperiodic fluctuations. The induced bursts display an abrupt transition between the rest and the active states. We show, using our model, that the growth and decay patterns of such

bursts exhibit asymmetry due to delayed-bifurcation caused by slow oscillations of the control parameter about the Hopf bifurcation point. We also present a novel analysis of the effect of amplitude, frequency and the mean position of the control parameter oscillations on the growth and decay pattern of the bursting dynamics.

We observe modulations in the amplitude of the high amplitude periodic bursts during intermittency obtained from practical low-turbulence combustors. We show that this peculiar feature of bursts, referred to as amplitude-modulated bursting, arises as a result of interaction and interdependence between the slow and fast timescales. To do so we introduce a coupling between the frequency of the slow subsystem and amplitude envelope of the fast subsystem. Finally, we apply the model to study the intermittency route to thermoacoustic instability for lab-scale turbulent and spray combustors having high and low levels of turbulence respectively. We show that for most thermoacoustic systems, the cause of intermittent bursts can be explained by the two broad concepts, turbulence-induced bursting and bursting induced by slow-fast dynamics; however, the level of turbulence decides the dominance of either mechanism.

After having developed the intuition of the physical phenomena causing intermittent dynamics in laminar and turbulent combustors, we move on to analysing the transition from chaos to order via the route of intermittency in thermoacoustic systems. In Chapter 5, employing unweighted cycle networks derived from the time series of acoustic pressure oscillations, we differentiate between the various dynamical states observed in these thermoacoustic systems. Using network centrality measures derived from these cycle networks, we provide a novel method to characterize the number and the stability of dynamically invariant periodic orbits in the phase space. We show that the average closeness centrality ($\langle C_{close} \rangle$) is a direct measure of the average correlation between the phase space cycles, and the average betweenness centrality ($\langle C_{BC} \rangle$) quantifies the stability, while the average clustering coefficient ($\langle CC \rangle$) quantifies the number of periodic orbits in the phase space. We thus propose the use of network centrality measures derived from cycle networks as a novel means to study the topology of the phase space for distinct dynamical states in diverse applications.

Further, using VND measure we characterize the variation of the number of peaks

in the 2D degree distribution derived from cycle networks. We then study the variation of VND and averaged network centrality measures with the system control parameter to elucidate the topological transformation of the phase space with the transition of system dynamics. We show that the phase space topology corresponding to the state of combustion noise (chaos) consists of multiple highly unstable periodic orbits. While during the state of intermittency (transitional state), the phase space consists of periodic orbits of moderate stability in co-existence with other highly unstable periodic orbits. Further, the pseudo-periodic (weakly correlated) oscillatory dynamics consists of a stable periodic orbit with sub-periods that morph into a highly stable limit cycle oscillator at the onset of the strongly correlated limit cycle oscillations (order).

Also, using network centrality measures, we identify the onset of thermoacoustic instability in turbulent combustors as the point after which average closeness centrality saturates to a maximum value, average betweenness centrality tends to zero and average clustering coefficient tends to unity. We thus suggest that the saturation of these network centrality measures can be potentially used to identify the onset of periodic dynamics in turbulent systems. Moreover, centrality measures derived from cycle networks can serve as reliable early warning indicators since they show significant variations much prior to the onset of thermoacoustic instability in turbulent combustors.

Finally, we conjecture that the transition from chaos to order in turbulent systems may be viewed as a condensation phenomenon in the phase space. Here, we define the phase space cycles as particles and the periodic orbits in the phase space as analogous to energy levels. Using such an analogy, we present the distribution of particles in the energy levels, and are able to simultaneously visualize the decrease in the number of periodic orbits as well as the increase in their stability with variation in the control parameter of the system. We conjecture that such an analogy can promote the use of tools from statistical physics to characterize the topological transformation in the phase space during the emergence of order from chaos. Further, we identify the onset of thermoacoustic instability as the onset of condensation transition where almost all the phase space cycles condense to the most stable periodic orbit in the phase space.

6.2 Scope for future work

We have opened many new avenues for research on the emergence of order from chaos in laminar and turbulent thermoacoustic systems. We believe future work in this direction can lead to important applications in the understanding and mitigation of thermoacoustic instability in distinct combustors.

The phenomenological model developed in Chapter 3 can prove to be useful in developing system-specific models for laminar and low-turbulence systems. Using the model, we also developed an understanding of the similarities and differences between features of intermittency dynamics observed prior to the onset of thermoacoustic instability in laminar and turbulent combustors. Thus, future work can exploit this understanding when analysing either laminar or turbulent systems and develop models accordingly. For example, for low-turbulence systems, the new models must avoid using high-intensity white noise but may use coupling between different variables of the system along with multiplicative or colored noise for modelling the dynamics in the system. Another possible direction for future work is to investigate the variation in the delay time (δ) of the bifurcation with the maximum of root mean squared amplitude of the system dynamics. Such variation could yield certain scaling measures or prediction schemes to identify and differentiate the onset of thermoacoustic instability.

We introduced the idea that the interplay between slow and fast timescales leads to the occurrence of intermittency prior to the onset of thermoacoustic instability in low-turbulence combustors. This idea can be probed further and can have implications on active control design for mitigating thermoacoustic system. Active control strategies can be developed by identifying the slow and fast subsystems of any particular thermoacoustic system and disrupting their interaction at specific locations in the combustor as soon as amplitude modulated bursting is evident in the acoustic pressure signal. Moreover, since we understand that slow oscillations of a control parameter can delay the bifurcation and occurrence of bursting behavior, one may introduce slow parameter oscillations probably as a means of delaying the onset of combustion instability.

In Chapter 5, we have cast the emergence of order from chaos as a phase transition

similar to Bose-Einstein condensation. While we have investigated the transition from chaos to order using time series analysis, future work can study the transformations in the spatio-temporal dynamics of a turbulent combustor in analogy with condensation phenomenon. This approach may help infer the dynamics in the physical flow field during the various dynamical states of the combustor. It may be desirable to develop a phenomenological model to demonstrate that the emergence of order from chaos is indeed a phase transition such as the condensation phenomenon. Further efforts in this direction can probably help quantify the emergence of order from chaos and predict the occurrence of oscillatory instabilities in various turbulent systems such as turbulent aeroelastic, aero-acoustic and thermoacoustic systems.

Moreover, the analogy between cycle networks and a system of Bosons, as proposed here, is a new perspective to study condensation in complex networks. We note that, we obtain condensation of nodes in the network, while all previous works have discussed condensation of edges in a network. Thus, our work proposes a new kind of condensation in complex networks in analogy to emergence of order from chaos. Such an analogy may be of interest in complex network theory as well, and may be worth pursuing through a model.

Thus, we have opened up a new perspective to study the transition from chaos to order, as well as developed an understanding of the physical phenomena involved during such a transition. We believe that the scope of this study is vast and diverse.

APPENDIX A

Appendix for Chapter 3

A.1 Detection of the onset of the active state of burst in the parameter space

In Sec. 3.4.3, we discussed the delayed bifurcation effect caused by the slow passage of control parameter via Hopf bifurcation. As noted earlier, the choice of the onset point (X) corresponding to the onset of periodic oscillations from the steady state is non-trivial. Here, we describe the manner in which we detect the point X with the help of an example. Consider control parameter (c_1) oscillations about a mean value of $A = 0.8$ with an amplitude $B = 0.4$ and frequency $f = 0.17$ Hz. Figure A.1(a) shows the pressure oscillations while Fig. A.1(b) shows the amplitude envelope of the corresponding pressure oscillations plotted on a log scale as a function of the control parameter oscillations. Despite minute oscillations, we see a sudden change in the slope of the log of the envelope of pressure fluctuations in Fig. A.1(b). Such sudden change of the pressure amplitude in the log-scale delineates the starting of exponential growth of amplitude, which thus demarcates the point of the onset of a burst of periodic oscillations in the signal and we choose this point as X in our analysis. Thus, the plot of pressure amplitude on a log-scale helps in identifying the onset of burst in the signal, which is otherwise not evident from the plot of pressure oscillations in Fig. A.1(a).

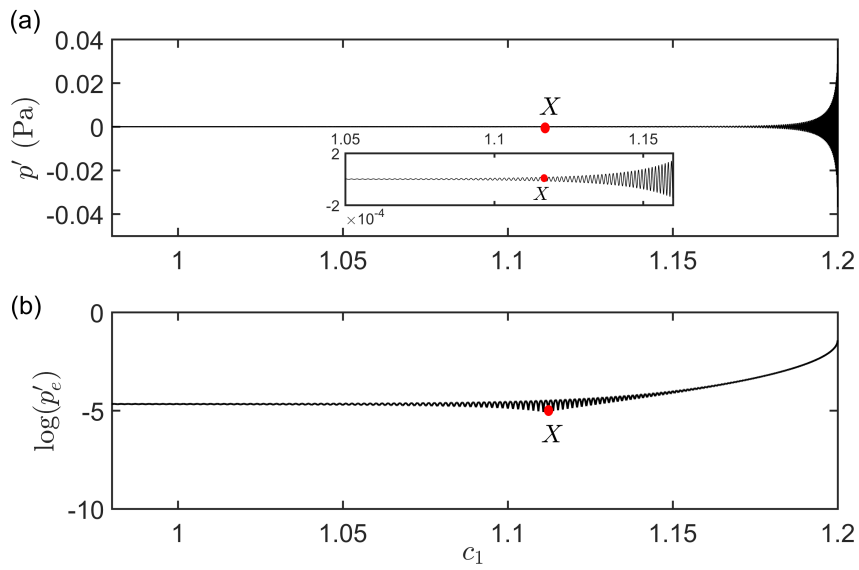


Fig. A.1: (a) The variation of acoustic pressure oscillations (p') and (b) log of the amplitude envelope of these pressure oscillations (p'_e) as a function of the time-varying control parameter (c_1) during the growth of amplitude of the burst. The values of parameters are: $A = 0.8$, $B = 0.4$, $f = 0.17$ Hz and $\sigma_a = 0.0001$ while $\sigma_m = 0$.

APPENDIX B

Appendix for Chapter 5

B.1 Variation of centrality measures as a function of \bar{u} for different correlation thresholds

Figures B.1 and B.2 show the variation of average network centrality measures with \bar{u} for three different correlation thresholds ($\rho_{th} = 0.9, 0.92, \text{ and } 0.94$) for the bluff-body and the swirl stabilized turbulent combustors, respectively. We observe that for certain \bar{u} in the dynamical regimes corresponding to combustion noise (I) and intermittency (II), the values of $\langle C_{close} \rangle$ and $\langle CC \rangle$ decrease while the value of $\langle C_{BC} \rangle$ increases if we increase ρ_{th} .

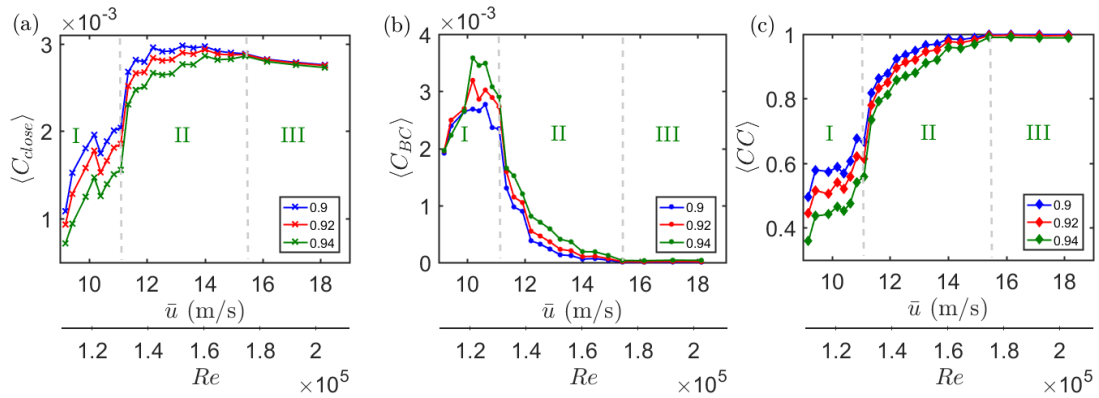


Fig. B.1: The variation in the average (a) closeness centrality ($\langle C_{close} \rangle$), (b) betweenness centrality ($\langle C_{BC} \rangle$) and (c) clustering coefficient ($\langle CC \rangle$) with the variation in the control parameter (\bar{u}) of a bluff-body stabilized turbulent combustor for the derived cycle networks with $\rho_{th} = 0.9, 0.92, \text{ and } 0.94$. The regions (I), (II) and (III) correspond to the different dynamical states observed that are combustion noise, intermittency and thermoacoustic instability, respectively (Pawar *et al.* (2017)).

However, for distinct values of ρ_{th} , these centrality measures saturate to the same value simultaneously (at the same value of \bar{u}). Thus, the saturation point which we

identify as the point of onset of thermoacoustic instability in Sec. 5.3 remains largely unaffected by the change in the value of ρ_{th} used to construct the cycle networks.

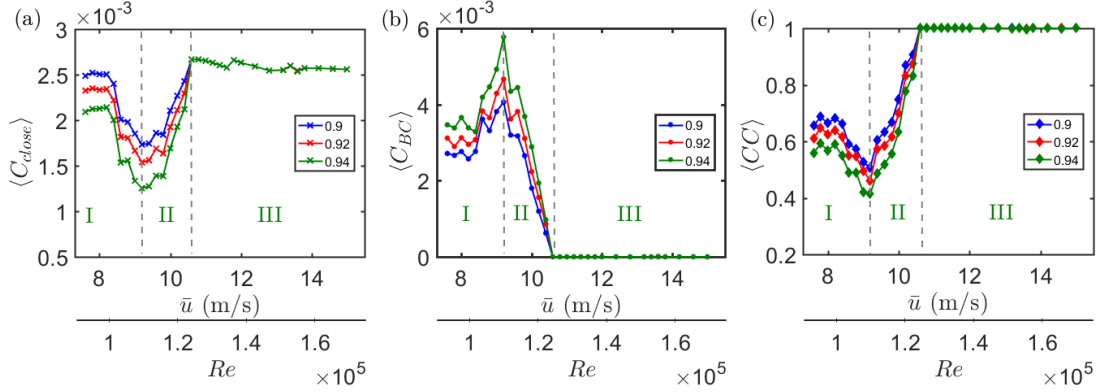


Fig. B.2: The variation in the average (a) closeness centrality ($\langle C_{close} \rangle$), (b) betweenness centrality ($\langle C_{BC} \rangle$) and (c) clustering coefficient ($\langle CC \rangle$) with the variation in the control parameter (\bar{u}) of a swirl-stabilized turbulent combustor for the derived cycle networks with $\rho_{th} = 0.9, 0.92,$ and 0.94 . The regions (I), (II) and (III) correspond to the different dynamical states observed that are combustion noise, intermittency and thermoacoustic instability, respectively (Pawar *et al.* (2017)).

B.2 Effect of the range of correlation threshold on the 2D degree distribution

In Sec. 5.4, we introduced the use VND to quantify the variation in the number and stability of periodic orbits in the phase space. We note that the range of correlation threshold chosen for the calculation of VND in Sec. 5.4 was $[0.55, 0.99]$. Here, we examine the effect of different choices of this range on the calculation of VND in Fig. B.3. Firstly, we note that the calculation of VND measure is not very sensitive to the upper bound, as evident from comparing the blue and crimson graph lines in Fig. B.3(a, b). Further, the identification of the point of onset of thermoacoustic instability does not change when we expand the range of ρ_{th} to $[0.2, 0.992]$.

If we choose a range of ρ_{th} where the lower bound being < 0.5 , we will also obtain peaks in the 2D degree distribution due to very weakly correlated cycles. As mentioned earlier, correlation between the time series of cycles is inversely proportional to distance

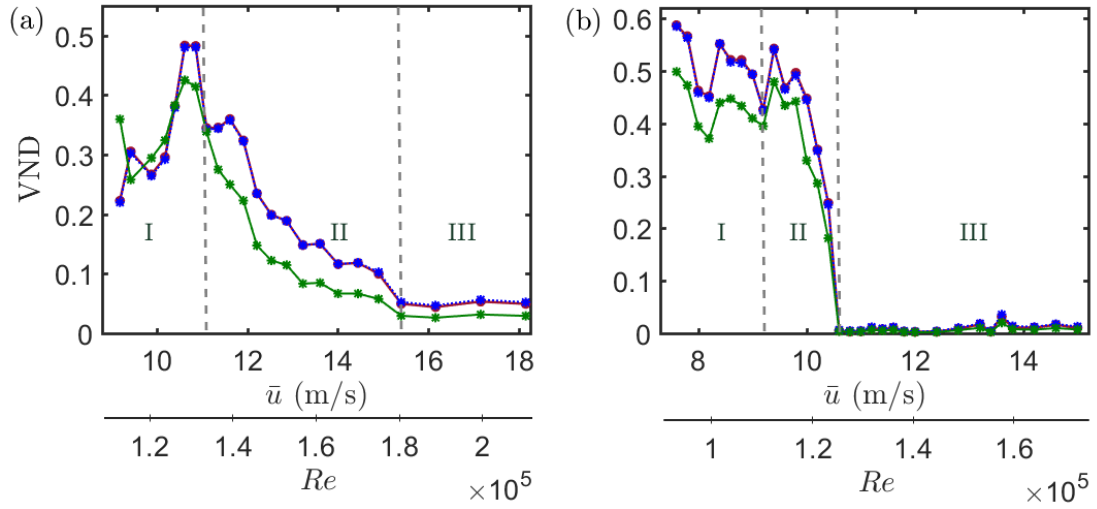


Fig. B.3: The variation of VND with the control parameter for (a) bluff body stabilized and (b) swirl stabilized turbulent combustor for different choices of the range of ρ_{th} . Note that the crimson and the blue graphs overlap.

between these cycles in the phase space. Then, a very low ρ_{th} essentially allows even those cycles to be linked in the cycle network which have a large phase space distance and may be associated with distant UPOs, which must be clearly avoided. Note that during combustion noise and intermittency such weakly correlated cycles exist in the phase space and will alter the calculation of VND . Thus we observe a remarkable difference in the calculation of VND in regions I and II of Fig. B.3(a,b). Therefore, the lower bound of the range of correlation threshold must be > 0.5 .

REFERENCES

1. **Albert, R.** and **A.-L. Barabási** (2002). Statistical mechanics of complex networks. *Reviews of modern physics*, **74**(1), 47.
2. **Ananthkrishnan, N.**, **S. Deo**, and **F. E. Culick** (2005). Reduced-order modeling and dynamics of nonlinear acoustic waves in a combustion chamber. *Combust. Sci. Technol.*, **177**(2), 221–248.
3. **Auerbach, D.**, **P. Cvitanović**, **J.-P. Eckmann**, **G. Gunaratne**, and **I. Procaccia** (1987). Exploring chaotic motion through periodic orbits. *Phys. Rev. Lett.*, **58**(23), 2387.
4. **Baer, S. M.** and **E. M. Gaekel** (2008). Slow acceleration and deceleration through a hopf bifurcation: Power ramps, target nucleation, and elliptic bursting. *Phys. Rev. E*, **78**(3), 036205.
5. **Balasubramanian, K.** and **R. I. Sujith** (2008). Thermoacoustic instability in a Rijke tube: Non-normality and nonlinearity. *Phys. Fluids*, **20**(4), 044103.
6. **Barabási, A.-L.** and **E. Bonabeau** (2003). Scale-free networks. *Scientific american*, **288**(5), 60–69.
7. **Bastian, M.**, **S. Heymann**, and **M. Jacomy** (2009). Gephi: an open source software for exploring and manipulating networks. *ICWSM*, **8**(2009), 361–362.
8. **Bi, Q.** (2010). The mechanism of bursting phenomena in Belousov-Zhabotinsky (bz) chemical reaction with multiple time scales. *Sci. China Technol. Sci.*, **53**(3), 748–760.
9. **Bianconi, G.** and **A.-L. Barabási** (2001). Bose-einstein condensation in complex networks. *Phys. Rev. Lett.*, **86**(24), 5632.
10. **Boccaletti, S.**, **J. Kurths**, **G. Osipov**, **D. Valladares**, and **C. Zhou** (2002). The synchronization of chaotic systems. *Phys. Rep.*, **366**(1-2), 1–101.
11. **Boccaletti, S.**, **V. Latora**, **Y. Moreno**, **M. Chavez**, and **D.-U. Hwang** (2006). Complex networks: Structure and dynamics. *Phys. Rep.*, **424**(4-5), 175–308.
12. **Bose, S. N.** (1924). Plancks gesetz und lichtquantenhypothese. *Z. Phys.*, **26**, 178–181.
13. **Boudy, F.**, **D. Durox**, **T. Schuller**, and **S. Candel** (2013). Analysis of limit cycles sustained by two modes in the flame describing function framework. *Comptes Rendus Mécanique*, **341**(1-2), 181–190.
14. **Bradley, E.** and **H. Kantz** (2015). Nonlinear time-series analysis revisited. *Chaos*, **25**(9), 097610.

15. **Burrage, P. M.** (1999). Runge-Kutta methods for stochastic differential equations. Ph.D. thesis.
16. **Chatellier, L., J. Laumonier, and Y. Gervais** (2004). Theoretical and experimental investigations of low mach number turbulent cavity flows. *Exp. Fluids*, **36**(5), 728–740.
17. **Chowdhury, D., L. Santen, and A. Schadschneider** (2000). Statistical physics of vehicular traffic and some related systems. *Phys. Rep.*, **329**(4-6), 199–329.
18. **Conti, C., M. Leonetti, A. Fratalocchi, L. Angelani, and G. Ruocco** (2008). Condensation in disordered lasers: Theory, 3 d+ 1 simulations, and experiments. *Phys. Rev. Lett.*, **101**(14), 143901.
19. **Culick, F.** (1994). Some recent results for nonlinear acoustics in combustion chambers. *AIAA J.*, **32**(1), 146–169.
20. **Culick, F.** (2006). *Unsteady motions in combustion chambers for propulsion systems*. Technical report, NATO Research and Technology Organization Neuilly-Sur-Seine (France).
21. **Delage, R., Y. Takayama, and T. Biwa** (2017). On–off intermittency in coupled chaotic thermoacoustic oscillations. *Chaos*, **27**(4), 043111.
22. **Domen, S., H. Gotoda, T. Kuriyama, Y. Okuno, and S. Tachibana** (2015). Detection and prevention of blowout in a lean premixed gas-turbine model combustor using the concept of dynamical system theory. *Proc. Combust. Inst.*, **35**(3), 3245–3253.
23. **Ebi, D., A. Denisov, G. Bonciolini, E. Boujo, and N. Noiray** (2018). Flame dynamics intermittency in the bistable region near a subcritical Hopf bifurcation. *J. Eng. Gas Turb. Power*, **140**(6), 061504.
24. **Einstein, A.** (1924). Quantum theory of the monatomic ideal gas. *Sitzungsberichte der Preussischen Akademie der Wissenschaften, Physikalisch-mathematische Klasse*, 261–267.
25. **Erdős, P. and A. Rényi** (2011). On the evolution of random graphs. *In The Structure and Dynamics of Networks*, 38–82. Princeton University Press.
26. **Euler, L.** (1956). The seven bridges of königsberg. *The world of mathematics*, **1**, 573–580.
27. **Evans, M.** (1996). Bose-Einstein condensation in disordered exclusion models and relation to traffic flow. *EPL*, **36**(1), 13.
28. **Fisher, S. C. and S. A. Rahman** (2009). *Remembering The Giants: Apollo Rocket Propulsion Development*.
29. **Freeman, L. C.** (1977). A set of measures of centrality based on betweenness. *Sociometry*, 35–41.
30. **Gao, Z.-K., M. Small, and J. Kurths** (2017). Complex network analysis of time series. *EPL*, **116**(5), 50001.

31. **Garrick, I. and W. H. Reed III** (1981). Historical development of aircraft flutter. *J. Aircr.*, **18**(11), 897–912.
32. **George, N. B., V. R. Unni, M. Raghunathan, and R. Sujith** (2018). Pattern formation during transition from combustion noise to thermoacoustic instability via intermittency. *Journal of Fluid Mechanics*, **849**, 615–644.
33. **Godavarthi, V., S. A. Pawar, V. R. Unni, R. I. Sujith, N. Marwan, and J. Kurths** (2018). Coupled interaction between unsteady flame dynamics and acoustic field in a turbulent combustor. *Chaos*, **28**(11), 113111.
34. **Godavarthi, V., V. Unni, E. A. Gopalakrishnan, and R. I. Sujith** (2017). Recurrence networks to study dynamical transitions in a turbulent combustor. *Chaos*, **27**(6), 063113.
35. **Gopalakrishnan, E. and R. I. Sujith** (2014). Influence of system parameters on the hysteresis characteristics of a horizontal Rijke tube. *Int. J. Spray Combust.*, **6**(3), 293–316.
36. **Gopalakrishnan, E., J. Tony, E. Sreelekha, and R. I. Sujith** (2016). Stochastic bifurcations in a prototypical thermoacoustic system. *Phys. Rev. E*, **94**(2), 022203.
37. **Gotoda, H., H. Kinugawa, R. Tsujimoto, S. Domen, and Y. Okuno** (2017). Characterization of combustion dynamics, detection, and prevention of an unstable combustion state based on a complex-network theory. *Phys. Rev. Appl.*, **7**(4), 044027.
38. **Gotoda, H., Y. Shinoda, M. Kobayashi, Y. Okuno, and S. Tachibana** (2014). Detection and control of combustion instability based on the concept of dynamical system theory. *Phys. Rev. E*, **89**(2), 022910.
39. **Gribkovskaia, I., Ø. Halskau Sr, and G. Laporte** (2007). The bridges of Königsberg—a historical perspective. *Networks: An International Journal*, **49**(3), 199–203.
40. **Gunaratne, G. H., P. S. Linsay, and M. J. Vinson** (1989). Chaos beyond onset: A comparison of theory and experiment. *Phys. Rev. Lett.*, **63**(1), 1.
41. **Hachijo, T., H. Gotoda, T. Nishizawa, and J. Kazawa** (2020). Early detection of cascade flutter in a model aircraft turbine using a methodology combining complex networks and synchronization. *Phys. Rev. Appl.*, **14**(1), 014093.
42. **Han, X., Q. Bi, C. Zhang, and Y. Yu** (2014). Study of mixed-mode oscillations in a parametrically excited Van der Pol system. *Nonlinear Dyn.*, **77**(4), 1285–1296.
43. **Han, X., M. Wei, Q. Bi, and J. Kurths** (2018). Obtaining amplitude-modulated bursting by multiple-frequency slow parametric modulation. *Phys. Rev. E*, **97**(1), 012202.
44. **Han, X., F. Xia, P. Ji, Q. Bi, and J. Kurths** (2016). Hopf-bifurcation-delay-induced bursting patterns in a modified circuit system. *Commun. Nonlinear Sci. Numer. Simul.*, **36**, 517–527.

45. **Heckl, M. A.** (1988). Active control of the noise from a Rijke tube. *J. Sound Vib.*, **124**(1), 117–133.
46. **Hong, J. G., K. C. Oh, U. D. Lee, and H. D. Shin** (2008). Generation of low-frequency alternative flame behaviors in a lean premixed combustor. *Energ. Fuel*, **22**(5), 3016–3021.
47. **Huang, Y. and V. Yang** (2009). Dynamics and stability of lean-premixed swirl-stabilized combustion. *Progress in Energy and Combustion Science*, **35**(4), 293–364.
48. **Iacobello, G., L. Ridolfi, and S. Scarsoglio** (2020). A review on turbulent and vortical flow analyses via complex networks. *Physica A: Statistical Mechanics and its Applications*, 125476.
49. **Izhikevich, E. M.** (2000). Neural excitability, spiking and bursting. *Int. J. Bifurcat. Chaos*, **10**(06), 1171–1266.
50. **Juniper, M. P.** (2012). Triggering in thermoacoustics. *Int. J. Spray Combust.*, **4**(3), 217–237.
51. **Juniper, M. P. and R. I. Sujith** (2018). Sensitivity and nonlinearity of thermoacoustic oscillations. *Annu. Rev. Fluid Mech.*, **50**, 661–689.
52. **Kasthuri, P., I. Pavithran, S. A. Pawar, R. I. Sujith, R. Gejji, and W. Anderson** (2019a). Dynamical systems approach to study thermoacoustic transitions in a liquid rocket combustor. *Chaos: An Interdisciplinary Journal of Nonlinear Science*, **29**(10), 103115.
53. **Kasthuri, P., V. R. Unni, and R. I. Sujith** (2019b). Bursting and mixed mode oscillations during the transition to limit cycle oscillations in a matrix burner. *Chaos*, **29**(4), 043117.
54. **Kheirkhah, S., J. M. Cirtwill, P. Saini, K. Venkatesan, and A. M. Steinberg** (2017). Dynamics and mechanisms of pressure, heat release rate, and fuel spray coupling during intermittent thermoacoustic oscillations in a model aeronautical combustor at elevated pressure. *Combust. Flame*, **185**, 319–334.
55. **King, L. V.** (1914). XII. on the convection of heat from small cylinders in a stream of fluid: Determination of the convection constants of small platinum wires with applications to hot-wire anemometry. *Philos. Trans. A Math. Phys. Eng. Sci.*, **214**(509-522), 373–432.
56. **Kobayashi, T., S. Murayama, T. Hachijo, and H. Gotoda** (2019). Early detection of thermoacoustic combustion instability using a methodology combining complex networks and machine learning. *Phys. Rev. Appl.*, **11**(6), 064034.
57. **Krapivsky, P. L., S. Redner, and F. Leyvraz** (2000). Connectivity of growing random networks. *Phys. Rev. Lett.*, **85**(21), 4629.

58. **Kriesels, P., M. Peters, A. Hirschberg, A. Wijnands, A. Iafrati, G. Riccardi, R. Piva, and J. Bruggeman** (1995). High amplitude vortex-induced pulsations in a gas transport system. *J. Sound Vib.*, **184**(2), 343–368.
59. **Krishnan, A., R. Manikandan, P. Midhun, K. Reeja, V. Unni, R. Sujith, N. Marwan, and J. Kurths** (2019). Mitigation of oscillatory instability in turbulent reactive flows: A novel approach using complex networks. *EPL (Europhysics Letters)*, **128**(1), 14003.
60. **Larsen, A. and J. H. Walther** (1997). Aeroelastic analysis of bridge girder sections based on discrete vortex simulations. *J. Wind. Eng. Ind. Aerodyn.*, **67**, 253–265.
61. **Lathrop, D. P. and E. J. Kostelich** (1989). Characterization of an experimental strange attractor by periodic orbits. *Phys. Rev. A*, **40**(7), 4028.
62. **Lieuwen, T. and A. Banaszuk** (2005). Background noise effects on combustor stability. *Journal of Propulsion and Power*, **21**(1), 25–31.
63. **Lieuwen, T. C.** (2002). Experimental investigation of limit-cycle oscillations in an unstable gas turbine combustor. *J. Propuls. Power*, **18**(1), 61–67.
64. **Lieuwen, T. C.** (2012). *Unsteady combustor physics*. Cambridge University Press.
65. **Lieuwen, T. C. and V. Yang** (2005). *Combustion instabilities in gas turbine engines: operational experience, fundamental mechanisms, and modeling*. American Institute of Aeronautics and Astronautics.
66. **Mariappan, S. and R. I. Sujith** (2011). Modelling nonlinear thermoacoustic instability in an electrically heated Rijke tube. *J. Fluid Mech.*, **680**, 511–533.
67. **Marwan, N., S. Schinkel, and J. Kurths** (2008). Significance for a recurrence based transition analysis. In *Proceedings of the 2008 International Symposium on Nonlinear Theory and its Applications NOLTA08, Budapest, Hungary*.
68. **Matveev, K. I.** (2003). *Thermoacoustic instabilities in the Rijke tube: Experiments and modeling*. Doctoral thesis, California Institute of Technology.
69. **Murugesan, M. and R. I. Sujith** (2015). Combustion noise is scale-free: transition from scale-free to order at the onset of thermoacoustic instability. *J. Fluid Mech.*, **772**, 225–245.
70. **Nair, V. and R. I. Sujith** (2013). Identifying homoclinic orbits in the dynamics of intermittent signals through recurrence quantification. *Chaos*, **23**(3), 033136.
71. **Nair, V. and R. I. Sujith** (2014). Multifractality in combustion noise: predicting an impending combustion instability. *Journal of Fluid Mechanics*, **747**, 635–655.
72. **Nair, V. and R. I. Sujith** (2015). A reduced-order model for the onset of combustion instability: Physical mechanisms for intermittency and precursors. *Proc. Combust. Inst.*, **35**(3), 3193–3200.

73. **Nair, V.** and **R. I. Sujith** (2016). Precursors to self-sustained oscillations in aeroacoustic systems. *Int. J. Aeroacoust.*, **15**(3), 312–323.
74. **Nair, V., G. Thampi, S. Karuppusamy, S. Gopalan,** and **R. I. Sujith** (2013). Loss of chaos in combustion noise as a precursor of impending combustion instability. *Int. J. Spray Combust. Dyn.*, **5**(4), 273–290.
75. **Nair, V., G. Thampi,** and **R. I. Sujith** (2014). Intermittency route to thermoacoustic instability in turbulent combustors. *J. Fluid Mech.*, **756**, 470.
76. **Nicoud, F.** and **K. Wieczorek** (2009). About the zero mach number assumption in the calculation of thermoacoustic instabilities. *Int. J. Spray Combust.*, **1**(1), 67–111.
77. **Noiray, N.** (2017). Linear growth rate estimation from dynamics and statistics of acoustic signal envelope in turbulent combustors. *J. Eng. Gas Turb. Power*, **139**(4), 041503.
78. **Noiray, N.** and **B. Schuermans** (2013). Deterministic quantities characterizing noise driven Hopf bifurcations in gas turbine combustors. *Int. J. Nonlin. Mech.*, **50**, 152–163.
79. **Okuno, Y., M. Small,** and **H. Gotoda** (2015). Dynamics of self-excited thermoacoustic instability in a combustion system: Pseudo-periodic and high-dimensional nature. *Chaos*, **25**(4), 043107.
80. **Oren, G., A. Bekker,** and **B. Fischer** (2014). Classical condensation of light pulses in a loss trap in a laser cavity. *Optica*, **1**(3), 145–148.
81. **Pawar, S. A.** (Indian Institute of Technology Madras, 2018). Studying thermoacoustic systems in the framework of synchronization theory. *Ph.D. thesis*.
82. **Pawar, S. A., S. Mondal, N. B. George,** and **R. I. Sujith** (2019). Temporal and spatiotemporal analyses of synchronization transition in a swirl-stabilized combustor. *AIAA J.*, **57**(2), 836–847.
83. **Pawar, S. A., A. Seshadri, V. R. Unni,** and **R. I. Sujith** (2017). Thermoacoustic instability as mutual synchronization between the acoustic field of the confinement and turbulent reactive flow. *J. Fluid Mech.*, **827**, 664–693.
84. **Pawar, S. A., R. Vishnu, M. Vadivukkarasan, M. Panchagnula,** and **R. I. Sujith** (2016). Intermittency route to combustion instability in a laboratory spray combustor. *J. Eng. Gas Turb. Power*, **138**(4), 041505.
85. **Pawelzik, K.** and **H. G. Schuster** (1991). Unstable periodic orbits and prediction. *Phys. Rev. A*, **43**(4), 1808.
86. **Premchand, C., N. B. George, M. Raghunathan, V. R. Unni, R. I. Sujith,** and **V. Nair** (2019). Lagrangian analysis of intermittent sound sources in the flow-field of a bluff-body stabilized combustor. *Phys. Fluids*, **31**(2), 025115.
87. **Premraj, D., K. Suresh, T. Banerjee,** and **K. Thamilmaran** (2016). An experimental study of slow passage through hopf and pitchfork bifurcations in a parametrically driven nonlinear oscillator. *Commun. Nonlinear Sci. Numer. Simul.*, **37**, 212–221.

88. **Raaj, A., J. Venkatramani, and S. Mondal** (2019). Synchronization of pitch and plunge motions during intermittency route to aeroelastic flutter. *Chaos*, **29**(4), 043129.
89. **Reddy, A. P., R. I. Sujith, and S. Chakravarthy** (2006). Swirler flow field characteristics in a sudden expansion combustor geometry. *Journal of Propulsion and Power*, **22**(4), 800–808.
90. **Reif, F.** (2009). *Fundamentals of statistical and thermal physics*. Waveland Press.
91. **Sabidussi, G.** (1966). The centrality index of a graph. *Psychometrika*, **31**(4), 581–603.
92. **Seshadri, A., V. Nair, and R. I. Sujith** (2016). A reduced-order deterministic model describing an intermittency route to combustion instability. *Combust. Theor. Model.*, **20**(3), 441–456.
93. **Sethares, W. A.** (2001). Repetition and pseudo-periodicity. *Tatra Mt. Math. Publ.*, **23**(1), 1–16.
94. **Sterling, J. D.** (1993). Nonlinear analysis and modelling of combustion instabilities in a laboratory combustor. *Combustion Science and Technology*, **89**(1-4), 167–179.
95. **Strutt, J. W. and B. Rayleigh** (1945). *The theory of sound*. Dover.
96. **Su, G., X. Zhang, and Y. Zhang** (2012). Condensation phase transition in nonlinear fitness networks. *EPL*, **100**(3), 38003.
97. **Sujith, R., M. Juniper, and P. Schmid** (2016). Non-normality and nonlinearity in thermoacoustic instabilities. *International Journal of Spray and Combustion Dynamics*, **8**(2), 119–146.
98. **Sujith, R. and V. R. Unni** (2020a). Complex system approach to investigate and mitigate thermoacoustic instability in turbulent combustors. *Physics of Fluids*, **32**(6), 061401.
99. **Sujith, R. I. and V. R. Unni** (2020b). Complex system approach to investigate and mitigate thermoacoustic instability in turbulent combustors. *Phys. Fluids*, **32**(6), 061401.
100. **Sujith, R. I. and V. R. Unni** (2020c). Dynamical systems and complex systems theory to study unsteady combustion. *Proceedings of the Combustion Institute*.
101. **Takens, F.** (1981). In dynamical systems of turbulence. *Lect. Notes Math.*, **898**, 366.
102. **Tang, M., L. Liu, and Z. Liu** (2009). Influence of dynamical condensation on epidemic spreading in scale-free networks. *Phys. Rev. E*, **79**(1), 016108.
103. **Tony, J., E. A. Gopalakrishnan, E. Sreelekha, and R. I. Sujith** (2015). Detecting deterministic nature of pressure measurements from a turbulent combustor. *Phys. Rev. E*, **92**(6), 062902.
104. **Unni, V. R., A. Krishnan, R. Manikandan, N. B. George, R. Sujith, N. Marwan, and J. Kurths** (2018). On the emergence of critical regions at the onset of thermoacoustic instability in a turbulent combustor. *Chaos: An Interdisciplinary Journal of Nonlinear Science*, **28**(6), 063125.

105. **Unni, V. R.** and **R. I. Sujith** (2017). Flame dynamics during intermittency in a turbulent combustor. *Proc. Combust. Inst.*, **36**(3), 3791–3798.
106. **Venkatramani, J., V. Nair, R. I. Sujith, S. Gupta,** and **S. Sarkar** (2016). Precursors to flutter instability by an intermittency route: a model free approach. *J. Fluids Struct.*, **61**, 376–391.
107. **Venkatramani, J., V. Nair, R. I. Sujith, S. Gupta,** and **S. Sarkar** (2017). Multi-fractality in aeroelastic response as a precursor to flutter. *J. Sound Vib.*, **386**, 390–406.
108. **Vo, T., M. A. Kramer,** and **T. J. Kaper** (2016). Amplitude-modulated bursting: A novel class of bursting rhythms. *Phys. Rev. Lett.*, **117**(26), 268101.
109. **Watts, D. J.** and **S. H. Strogatz** (1998). Collective dynamics of ‘small-world’ networks. *Nature*, **393**(6684), 440–442.
110. **Weng, F., S. Li, D. Zhong,** and **M. Zhu** (2016). Investigation of self-sustained beating oscillations in a Rijke burner. *Combust. Flame*, **166**, 181–191.
111. **Wong, H.** and **W. A. Sethares** (2004). Estimation of pseudo-periodic signals. In *2004 IEEE International Conference on Acoustics, Speech, and Signal Processing*, volume 2. IEEE.
112. **Yalin, M.** (1992). River mechanics.
113. **Zhang, J., X. Luo,** and **M. Small** (2006). Detecting chaos in pseudoperiodic time series without embedding. *Phys. Rev. E*, **73**(1), 016216.
114. **Zhang, J.** and **M. Small** (2006). Complex network from pseudoperiodic time series: Topology versus dynamics. *Phys. Rev. Lett.*, **96**(23), 238701.
115. **Zinn, B. T.** and **M. E. Lores** (1971). Application of the galerkin method in the solution of non-linear axial combustion instability problems in liquid rockets. *Combust. Sci. Technol.*, **4**(1), 269–278.

LIST OF PUBLICATIONS

I. PUBLICATIONS IN REFEREED JOURNALS BASED ON THE RESEARCH WORK

1. **Tandon, Shruti** and Pawar, Samadhan A and Banerjee, Subham and Varghese, Alan J and Durairaj, Premraj and Sujith, RI. Bursting during intermittency route to thermoacoustic instability: Effects of slow-fast dynamics *Chaos: An Interdisciplinary Journal of Nonlinear Science*, 30, 10, 103112, (2020).
2. **Tandon, Shruti** and Sujith, RI. Condensation in the phase space and network topology during transition from chaos to order in turbulent thermoacoustic systems *Chaos: An Interdisciplinary Journal of Nonlinear Science*, 31, 4, 043126, (2021).